January 2010

Roles Of Inhibitory Interneurons In Cerebellar Cortical Processing For Oculomotor Control

Shane Heiney
Washington University in St. Louis

WASHINGTON UNIVERSITY IN ST. LOUIS

Division of Biology and Biomedical Sciences
Neurosciences Program

Dissertation Examination Committee:
Pablo M. Blazquez, Chair
Dora E. Angelaki
Dennis L. Barbour
Stephen M. Highstein
Timothy E. Holy
Daniel W. Moran
Lawrence H. Snyder

ROLES OF INHIBITORY INTERNEURONS IN CEREBELLAR CORTICAL PROCESSING FOR OCULOMOTOR CONTROL

by

Shane A. Heiney

A dissertation presented to the
Graduate School of Arts and Sciences
of Washington University in
partial fulfillment of the
requirements for the degree
of Doctor of Philosophy

December, 2010
Saint Louis, Missouri

Abstract of the dissertation

The cerebellar cortex is usually offered up as the prime example of a well-worked out circuit; indeed, its basic neuronal composition and organization has been known for over one hundred years. Yet mysteries still abound about the computations that are performed within its layers, and how these computations contribute to sensation and behavior. This project was an effort to look inside the cerebellar cortical circuit during behavior to see if I could shed some light on the computations being performed. The dissertation is divided into three main sections. In the first, I present the results of preliminary work performed by myself and my colleagues to advance the aims of the project. This included writing software to train squirrel monkeys and control a variety of vestibulo-oculomotor tasks, characterizing the oculomotor behavioral repertoire of the squirrel monkey in comparison to that of the rhesus macaque, and developing two techniques for examining the roles of interneurons in cerebellar processing. In the second, I present the results of a study of one such interneuron, the Golgi cell, which is the main type of inhibitory interneuron that regulates information flow at the input stage of the cerebellar cortex. I recorded Golgi cells in the ventral paraflocculus (VPFL), a region of the cerebellum known to be involved in oculomotor behavior, while squirrel monkeys performed visual, vestibular, and eye movement tasks, and found that the VPFL Golgi cells only carry information from the eye movement pathways. Further, I found that this eye movement information is highly specific, with individual Golgi cells having relatively narrow directional tuning during saccades and pursuit, and only responding within a range of eye positions. This suggests that Golgi cells, through their powerful inhibition of the main path from the input stage to subsequent levels of processing, may serve as spatio-temporal filters of the

information arriving at the cerebellar cortex. I delve deeper into this problem in the third section of the dissertation, where I present results from my recordings of mossy fibers and Purkinje cells, the main input and sole output elements, respectively, of the cerebellar cortex. I recorded these elements while the monkeys performed the same tasks as with the Golgi cells, sometimes while simultaneously recording Golgi cells, and examined how their responses compared with the responses of Golgi cells. I found that mossy fibers as a population are more narrowly tuned than Golgi cells, though many individual Golgi cells share a similar tuning width as the mossy fibers, and have different temporal response properties. When individual mossy fibers were recorded near, or simultaneously with, a Golgi cell, the mossy fiber and Golgi cell responses were usually antiphasic. This suggests that the net effect of mossy fiber activity on Golgi cells is inhibitory. When I examined Purkinje cell responses with respect to mossy fibers and Golgi cells, I found that the Purkinje cells generally had broader tuning and more complex, multimodal responses than Golgi cells, consistent with a greater convergence of inputs to Purkinje cells. Finally, when I examined the potential role of Purkinje cell inhibitory inputs coming from molecular layer interneurons by blocking GABA-A receptors while recording Purkinje cells, I found that this inhibition may serve to suppress bursts that are present in the eye movement-related mossy fibers that provide a dominant input to the VPFL. At the end of that chapter I attempt to synthesize these results with the results on the Golgi cells, and in the concluding chapter I suggest additional experiments to further explore the roles of cerebellar cortical interneurons in sensorimotor processing.

Acknowledgements

I am indebted to many people, both professionally and personally, for their support throughout this project. First and foremost, I owe a great deal of gratitude to my mentor Pablo Blazquez, who has been a great source of both inspiration and distraction throughout my PhD. He has contributed by far the most of anyone to my growth as a scientist and a person over the past six years. The conversations we've had over the years have covered all ground, from science to love to crazy business plans, and have kept me from feeling stifled by the singular focus required to finish a PhD. I also want to thank my second mentor, Steve Highstein, for offering his wisdom and advice, especially in the early phases of the project.

In addition, I want to thank all members of the Blazquez and Highstein labs, past and present, including Gavin Perry, Pat Keller, Darryl Craig, Val Militchin, and Krystal Henderson, for all of their help and encouragement. I also wish to thank lab collaborators, such as Yutaka Hirata, Anglel Pastor, and Maya Davis for great discussions and advice over the years. Much appreciation also goes to the inhabitants of East McDonnell, particularly members of the Snyder, Padoa-Schioppa, and Angelaki labs, for sharing ideas and equipment, and the greater Wash U neuroscience community for providing an amazing atmosphere to pursue a PhD.

I also want to thank my friends and family, both in St Louis and around the world, especially Jennifer Sodini and Ryan Evans, and my brothers Brett and Josh. A special thanks goes to Krystal for being extremely understanding and supportive in my final push to complete the dissertation and for proof-reading the final draft. Lastly, and especially, I want to thank my parents for always supporting me in whatever I have attempted and allowing me to pursue my passions, no matter where they took me.

Table of Contents

List of figures

Chapter I
General Introduction

The cerebellum has been known to participate in the coordination of movement for over a century, when Florens found that animals with lesions or ablations of the cerebellum exhibit strange movements, awkward gait, and muscle weakness (Thach et al., 1992). General models of the cerebellum propose a role for the structure in sensorimotor processing, such that sensory information from the periphery is combined with central movement commands to achieve fine control of ongoing movements (Marr, 1969; Albus, 1971; Thach et al., 1992). Despite these general models however, the exact contribution of the cerebellum to motor control and a mechanistic explanation of its proposed role in sensorimotor processing remain unresolved.

The cerebellum and oculomotor control

A fruitful model for exploring questions of cerebellar function has been the oculomotor system, which presents a number of advantages over more complex motor systems. Namely, 1) in a control systems sense, the eye is relatively easy to control owing to its three degrees of freedom (compared to the seven of the arm), so the experimenter's task of identifying the relevant control signals is simplified; 2) the load experienced by the eye is relatively constant, minimizing the number of variables that must be taken into account; 3) the anatomy of the oculomotor system is well known and all motor and premotor nuclei are accessible by microelectrode; 4) movements of the eye are easy to measure and quantify with a high degree of precision; and 5) the cerebellum is known to

be involved in many oculomotor behaviors. Additionally, the oculomotor system is tightly coupled to the vestibular system, providing an avenue for exploring multimodal integration during vestibulo-oculomotor behaviors.

One area of the cerebellum known to be involved in combined vestibulo-oculomotor behaviors is the ventral paraflocculus (VPFL). Previous studies have implicated the VPFL in the control of pursuit (i.e., tracking) eye movements and adaptation of the vestibulo-ocular reflex (VOR) (Lisberger and Fuchs, 1978; Lisberger et al., 1994; Blazquez et al., 2003). Lesions of the floccular lobe, particularly the VPFL, severely impair pursuit behavior and abolish the ability to adapt the VOR (Zee et al., 1981; Rambold et al., 2002). Additionally, the VPFL receives sensory inputs from both the visual and vestibular systems, as well as a putative efference copy of oculomotor commands, and projects to premotor neurons in the vestibular nuclei (Langer et al., 1985), making it well positioned to influence oculomotor behavior (Fig 1.1). Indeed, microstimulation of the VPFL evokes eye movements at latencies of around 9 milliseconds (Belknap and Noda, 1987).

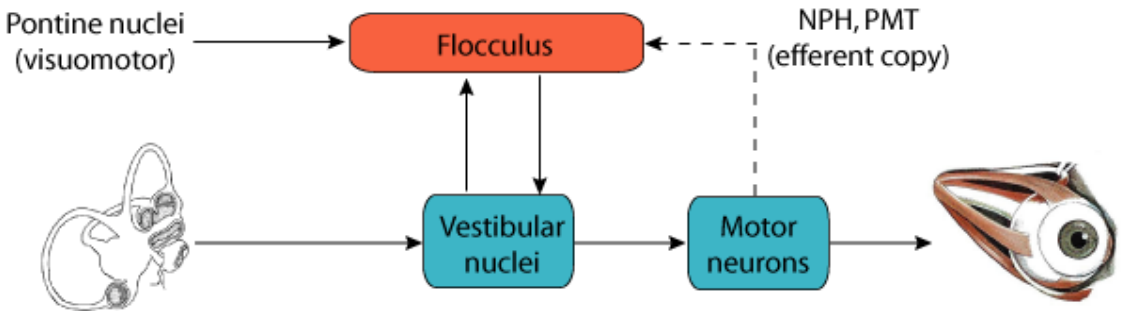

Figure 1.1. Simplified schematic of inputs and outputs of ventral paraflocculus (VPFL). Only the inputs conveyed by the mossy fiber system are shown. The three primary input modalities are visuomotor via the pontine nuclei, vestibular (semicircular canals) via the vestibular nuclei, and a putative efference copy of the oculomotor command via the nucleus of the prepositus hypoglossi (NPH) and paramedian tract (PMT).

The inputs and outputs of the VPFL have been relatively well characterized. In the monkey, mossy fiber inputs from the vestibular nucleus convey information about the velocity of head rotation; mossy fiber inputs from the dorsolateral pontine nuclei (DLPN) and nucleus reticularis tegmentis pontis (NRTP) convey visuomotor information from extrastriate cortex (Mustari et al., 1988; Ono et al., 2004; Ono et al., 2005); mossy fiber inputs from the nucleus of the prepositus hypoglossi (NPH) and paramedian tract (PMT) carry eye movement signals that may convey an efference copy of oculomotor commands (Nakamagoe et al., 2000; Green et al., 2007); and climbing fibers from the inferior olive provide a combined sensorimotor signal thought to convey information about movement error (Simpson and Alley, 1974; Winkelman and Frens, 2006). Purkinje cells, the sole output from the VPFL, represent various combinations of the input signals and are classically thought to provide a signal to the vestibular nuclei that is dominated by eye or gaze velocity (Lisberger and Fuchs, 1978; Miles et al., 1980; Lisberger et al., 1994), however recent experiments have indicated a more complex interplay than previously thought between velocity and position signals during two-dimensional pursuit tasks (Leung et al., 2000).

Past experiments have provided a seemingly solid framework for evaluating possible roles of the VPFL in oculomotor behavior, yet after over thirty years of active research and lively debate, a consensus on the function of the VPFL, and on a larger scale the cerebellum, has still not been reached (Highstein et al., 2005). Therefore it may be necessary to examine the processing that occurs *inside* the cortical layers of the VPFL to solve this stalemate. This dissertation is an attempt to contribute to that end.

General principles of cerebellar cortex organization and processing

Lines of research dating back to the time of Ramon y Cajal have identified the unique architecture of the cerebellar cortex (Eccles et al., 1967; Ramon y Cajal, 1911). Information from other parts of the brain and spinal cord enter the cortex via the mossy fiber system. Upon entering the granular layer, the mossy fibers diverge substantially and individual terminals form complex glomeruli, containing granule and Golgi cell dendrites and Golgi cell axons (Fig 1.2). The mossy fiber information is conveyed to the granule and descending Golgi cell dendrites through glutamatergic synapses. The granule cells in turn send ascending axons into the molecular layer, where they bifurcate as parallel fibers and provide the dominant excitatory input to Purkinje cells, as well as to Golgi cell ascending dendrites and molecular layer interneurons (basket and stellate cells). The only output of the cerebellar cortex is through Purkinje cells, which inhibit neurons in the deep cerebellar or vestibular nuclei.

The main path of information flow through the cerebellar cortex is the excitatory connection from mossy fibers, through granule cells, to Purkinje cells. However, there are substantial opportunities for this information to be shaped as it moves through the circuit. For instance, at the first synapse in the cerebellar cortex, mossy fiber to granule cell transmission is strongly regulated by Golgi cell inhibition (Eccles et al., 1964) through the unique axonal arborization of the Golgi cells. To wit, the axons of individual Golgi cells descend into the granular layer and repetitively branch such that the axon of a single Golgi cell participates in thousands of glomeruli. Granule cells are tonically inhibited at rest (Chadderton et al., 2004), suggesting that strong activation of them by mossy fibers is required to fire spikes. However, suppression of Golgi cell responses could also

increase granule cell activity through disinhibition. Because granule and Golgi cells both receive mossy fiber inputs, and granule cells provide the parallel fiber inputs to Golgi cells, there is a complex interplay between granule and Golgi cell activity that involves both feedforward and feedback inhibition. The role of this inhibition in cerebellar processing is still not clear.

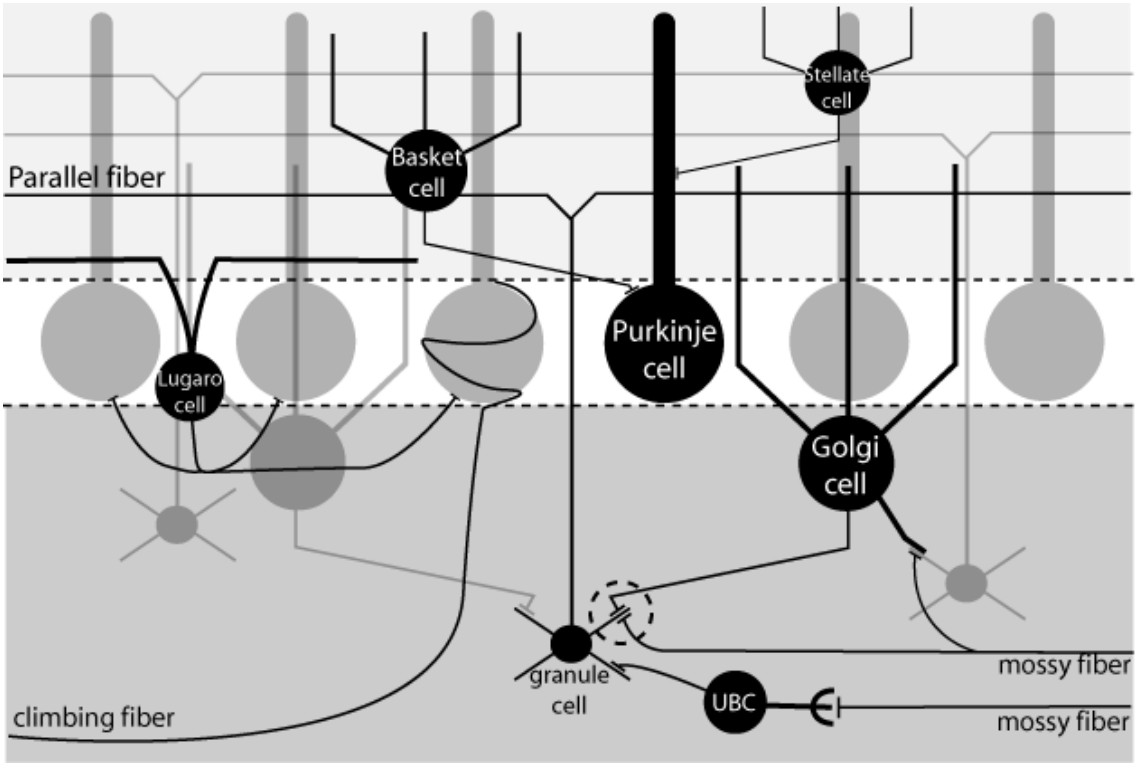

Figure 1.2. Schematic of basic synaptic organization of cerebellar cortex. Input to the cerebellar cortex arrives via two different fiber systems, the mossy and climbing fibers. Both are glutamatergic. The mossy fibers substantially diverge and contact granule cells in the granular layer. Granule cells in turn send their axons to the molecular layer, where they bifurcate as "parallel fibers" and provide glutamatergic input to a number of cell types, including Purkinje cells and the molecular layer interneurons (basket and stellate cells). Basket cells in turn form GABAergic synapses on Purkinje cell bodies and stellate cells form GABAergic synapses on Purkinje cell dendrites. The parallel fibers also contact Golgi cells through glutamatergic synapses. Golgi cells also receive glutamatergic input via mossy fibers and strongly inhibit granule cells through GABAergic synapses. Multiple other cell types that are less well understood populate the granular layer, including unipolar brush cells (UBCs) and Lugaro cells. Purkinje cells are the sole output of the cerebellar cortex.

The primary theoretical model of cerebellar processing that has dominated the field for the past 40 years proposes that the Golgi cells serve as gain control elements, keeping the

overall number of active parallel fibers relatively constant despite increases in mossy fiber activity (Marr, 1969; Albus, 1971) such that Purkinje cells can learn a large number of different patterns. The main assumption underlying this "gain control" hypothesis is that the glutamatergic inputs to Golgi cells (via mossy and parallel fibers) have a net excitatory effect, tending to increase the firing rates of Golgi cells—and thus their inhibition of granule cells—for increases in mossy fiber activity. But this theory has been hard to test because there have only been a few studies of Golgi cells in behaving animals, and these studies have provided heterogeneous data that make interpretation difficult (Miles et al., 1980; Edgley and Lidierth, 1987; Prsa et al., 2009). The most consistent finding in anesthetized preparations, however, is that the dominant response of Golgi cells to stimulation, both natural and artificial, is a pause in firing rate lasting hundreds of milliseconds (Vos et al., 1999; Tahon et al., 2005; Holtzman et al., 2006). If this is how Golgi cells respond in alert behaving animals, it would argue against the gain control hypothesis.

After the input stage in the granular layer, the next stage of significant processing likely occurs at the Purkinje cells, where excitation from ascending granule cell axons (Cohen and Yarom, 1998) and parallel fibers is balanced with inhibition from molecular layer interneurons, such as basket and stellate cells. Basket and stellate cells both receive their dominant input from the parallel fiber system so the primary distinguishing characteristics differentiating them are their location in the molecular layer and the mode of their inhibitory influence over Purkinje cells. Basket cell bodies are located deep in the molecular layer, lying just above the Purkinje cell layer. Their axons project along the cerebellar folia, perpendicular to the parallel fibers and form large "basket-like"

inhibitory synapses around Purkinje cell bodies. Stellate cell bodies sit higher in the molecular layer and their axons form inhibitory synapses on the dendrites of nearby Purkinje cells (Eccles et al., 1967). Though they may ultimately prove to serve different functions, the basket and stellate cells are often considered as a single processing unit ("molecular layer interneurons") because it is difficult to sort out their varied influences with existing experimental manipulations. Experiments carried out to date have suggested that the molecular layer interneurons provide rapid feedfoward inhibition of Purkinje cells operating within as little as 1 ms (Mittman et al., 2005), which may control the temporal characteristics of Purkinje cell responses. In addition, local application of GABA receptor blockers in the molecular layer removes lateral inhibition of Purkinje cells, suggesting that the inhibition from molecular layer interneurons curtails the spatial spread of parallel fiber activation of Purkinje cells (Santamaria et al., 2007). However, no studies of the molecular layer interneurons have been carried out in awake behaving animals.

Problems addressed and organization of the dissertation

This dissertation composed of three main components (Chapters 2-4). In the first, I present preliminary work that I performed to support the major experimental aims of the project, including software coding, behavioral characterization, and technique development and testing. In the second and third components, I examine the roles of inhibitory interneurons in cerebellar cortical processing.

Few investigators have attempted to address the roles of cerebellar interneurons using awake animals (Miles et al., 1980; Edgley and Lidierth, 1987; Prsa et al., 2009), mostly because until very recently there were no reliable criteria to distinguish them during *in vivo* recordings. Instead, investigators have focused on recording the readily identifiable Purkinje cells. Such an approach overlooks what are likely to be important components of the cerebellar circuit (Watanabe et al., 1998). However, a recent advance in methodology for neuronal tracing has finally made it feasible to provide a link between extracellularly recorded neuronal signals, including spike timing patterns and spike widths, and morphologically identified neuronal types (Pinault, 1996). Many labs are now attempting to sort through the various extracellular signals that make up the cerebellar cortical cacophony (Simpson et al., 2005; Holtzman et al., 2006; Barmack and Yakhinitsa, 2008), and the Golgi cell has emerged as the first interneuron type for which an identification consensus seems to have been reached (Holtzman et al., 2006; Prsa et al., 2009). We used these new criteria to record Golgi cells in the VPFL while squirrel monkeys performed vestibulo-oculomotor behaviors, and found strong evidence that the net effect of mossy and parallel fibers on Golgi cells is inhibitory (Chapters 3 and 4). Such an arrangement is inconsistent with a role of Golgi cells in gain control. We suggest a plausible mechanism to explain the origin of the inhibitory responses based on known synaptic properties of the mossy fiber and parallel fiber inputs to Golgi cells, and propose that changes in Golgi cell firing rate are primarily driven by a small number of specifically tuned mossy fibers. As an alternative to the gain control hypothesis, we argue that Golgi cells may operate as spatio-temporal filters at the input stage of the cerebellar cortex, regulating the spatial and temporal properties of relatively independent granule cell modules.

Because no consensus has been reached on the electrophysiological signatures of molecular layer interneurons, we needed to adopt a different strategy to examine the role of these neurons in cerebellar cortical processing. We exploited the knowledge that molecular layer interneurons are GABAergic, their primary targets are Purkinje cells, and the majority of Purkinje cell inhibition should be driven by the molecular layer interneurons, to unmask the effects of that inhibition with pharmacological manipulation (Chapter 4). We used multibarrel carbon fiber electrodes and tungsten electrode-multibarrel piggy back electrodes to record Purkinje cells while simultaneously injecting minute amounts of a potent GABA-A receptor blocker, SR-95531 (gabazine). We found that blockage of GABA-A receptors either reduced the amplitude of pauses in the Purkinje cell firing rate during saccadic eye movements or potentiated excitatory bursts during saccades. Our conclusion is that molecular layer interneurons in the VPFL act to suppress bursts in Purkinje cell firing rate that would otherwise occur due to parallel fiber inputs driven by burst-tonic mossy fibers.

References

Albus J (1971). A theory of cerebellar function. Math Biosci 10: 25-61.

Barmack NH, Yakhnitsa V (2008). Functions of interneurons in mouse cerebellum. J Neurosci 28: 1140-1152.

Belknap DB, Noda H (1987). Eye movements evoked by microstimulation in the flocculus of the alert macaque. Exp Brain Res 67(2):352-62.

Blazquez PM, Hirata Y, Heiney SA, Green AM, Highstein SM (2003). Cerebellar signatures of vestibulo-ocular reflex motor learning. J Neurosci 23: 9742-9751.

Chadderton P, Margrie TW, Häusser M (2004) Integration of quanta in cerebellar granule cells during sensory processing. Nature 428:856-60.

Cohen D, Yarom Y (1998). Patches of synchronized activity in the cerebellar cortex evoked by mossy-fiber stimulation: questioning the role of parallel fibers. Proc Natl Acad Sci U S A Dec 8;95(25):15032-6.

Eccles J, Ito M, Szentágothai J (1967). The Cerebellum as a Neuronal Machine (Heidelberg: Springer-Verlag).

Eccles J, Llinas R, Sasaki K (1964). Golgi cell inhibition in the cerebellar cortex. Nature 204: 1265-1266.

Edgley SA, Lidierth M (1987). The discharges of cerebellar Golgi cells during locomotion in the cat. J Physiol 392: 315-332.

Green AM, Meng H, Angelaki DE (2007). A reevaluation of the inverse dynamic model for eye movements. J Neurosci 27: 1346-1355.

Highstein SM, Porrill J, Dean P (2005). Report on a workshop concerning the cerebellum and motor learning, held in St Louis October 2004. Cerebellum 4(2):140-50.

Holtzman T, Rajapaksa T, Mostofi A, Edgley SA (2006). Different responses of rat cerebellar Purkinje cells and Golgi cells evoked by widespread convergent sensory inputs. J Physiol 574: 491-507.

Langer T, Fuchs AF, Scudder CA, Chubb MC (1985). Afferents to the flocculus of the cerebellum in the rhesus macaque as revealed by retrograde transport of horseradish peroxidase. J Comp Neurol 235: 1-25.

Leung HC, Suh M, Kettner RE (2000). Cerebellar flocculus and paraflocculus Purkinje cell activity during circular pursuit in monkey. J Neurophysiol 83:13-30.

Lisberger SG, Fuchs AF (1978). Role of primate flocculus during rapid behavioral modification of vestibuloocular reflex. I. Purkinje cell activity during visually guided horizontal smooth-pursuit eye movements and passive head rotation. J Neurophysiol 41: 733-763.

Lisberger SG, Pavelko Ta, Bronte-Stewart HM, Stone LS (1994). Neural basis for motor learning in the vestibuloocular reflex of primates. II. Changes in the responses of horizontal gaze velocity Purkinje cells in the cerebellar flocculus and ventral paraflocculus. J Neurophysiol 72: 954-73.

Marr D (1969). A theory of cerebellar cortex. J Physiol 202: 437-470.

Miles FA, Fuller JH, Braitman DJ, Dow BM (1980). Long-term adaptive changes in primate vestibuloocular reflex. III. Electrophysiological observations in flocculus of normal monkeys. J Neurophysiol 43: 1437-1476.

Mittmann W, Koch U, Häusser M (2005). Feed-forward inhibition shapes the spike output of cerebellar Purkinje cells. J Physiol 563: 369-78.

Mustari MJ, Fuchs AF, Wallman J (1988). Response properties of dorsolateral pontine units during smooth pursuit in the rhesus macaque. J Neurophysiol 60: 664-686.

Nakamagoe K, Iwamoto Y, Yoshida K (2000). Evidence for brainstem structures participating in oculomotor integration. Science 288: 857-859.

Ono S, Das VE, Mustari MJ (2004). Gaze-related response properties of DLPN and NRTP neurons in the rhesus macaque. J Neurophysiol 91(6):2484-500.

Ono S, Das VE, Economides JR, Mustari MJ (2005). Modeling of smooth pursuit-related neuronal responses in the DLPN and NRTP of the rhesus macaque. J Neurophysiol 93(1):108-16.

Pinault, D (1996). A novel single-cell staining procedure performed in vivo under electrophysiological control: morpho-functional features of juxtacellularly labeled thalamic cells and other central neurons with biocytin or Neurobiotin. J Neurosci Methods. 65(2): p. 113-36.

Prsa M, Dash S, Catz N, Dicke PW, Thier P (2009). Characteristics of responses of Golgi cells and mossy fibers to eye saccades and saccadic adaptation recorded from the posterior vermis of the cerebellum. J Neurosci 29: 250-262.

Rambold H, Churchland A, Selig Y, Jasmin L, Lisberger SG (2002). Partial ablations of the flocculus and ventral paraflocculus in monkeys cause linked deficits in smooth pursuit eye movements and adaptive modification of the VOR. J Neurophysiol 87(2): 912-924.

Ramon y Cajal S (1911). Histologie du Systeme Nerveux de L'Home et des Vertebres (Paris: Maloine).

Santamaria F, Tripp PG, Bower JM (2007). Feedforward inhibition controls the spread of granule cell-induced Purkinje cell activity in the cerebellar cortex. J Neurophysiol 97(1):248-63.

Simpson JI, Alley KE (1974). Visual climbing fiber input to rabbit vestibulo-cerebellum: a source of direction-specific information. Brain Res 27;82(2):302-8.

Simpson JI, Hulscher HC, Sabel-Goedknegt E, Ruigrok TJ (2005). Between in and out: linking morphology and physiology of cerebellar cortical interneurons. Prog Brain Res 148: 329-340.

Tahon K, Volny-Luraghi A, De Schutter E (2005). Temporal characteristics of tactile stimuli influence the response profile of cerebellar Golgi cells. Neurosci Lett 390: 156-161.

Thach WT, Goodkin HP, Keating JG (1992). The cerebellum and the adaptive coordination of movement. Annu Rev Neurosci 15: 403-442.

Vos BP, Volny-Luraghi A, De Schutter E (1999). Cerebellar Golgi cells in the rat: receptive fields and timing of responses to facial stimulation. Eur J Neurosci 11: 2621-2634.

Watanabe D, Inokawa H, Hashimoto K, Suzuki N, Kano M, Shigemoto R, Hirano T, Toyama K, Kaneko S, Yokoi M, Moriyoshi K, Suzuki M, Kobayashi K, Nagatsu T, Kreitman RJ, Pastan I, Nakanishi S (1998). Ablation of cerebellar Golgi cells disrupts synaptic integration involving GABA inhibition and NMDA receptor activation in motor coordination. Cell 95:17-27.

Winkelman B, Frens M (2006). Motor coding in floccular climbing fibers. J Neurophysiol 95(4):2342-51.

Zee DS, Yamazaki A, Butler PH, Gücer G (1981). Effects of ablation of flocculus and paraflocculus of eye movements in primate. J Neurophysiol 46(4): 878-99.

Chapter II

Preliminary studies and development

Abstract

The overarching problem addressed in this dissertation is the neural processing performed by interneurons in the cerebellar cortex. However, in order to complete the project it was necessary to perform a large amount of preliminary work, including software coding, behavior characterization, and technique development. This chapter presents the results of some of the preliminary work that is most pertinent to the following chapters. It is divided into four independent sections. I will first present a brief description of the software that I wrote to train squirrel monkeys in the oculomotor tasks used throughout my thesis work and to control the tasks during neuronal data acquisition. This is now the software that is used for all experiments on trained monkeys carried out in the Blazquez lab. I will then present the results of a behavioral characterization we performed to compare squirrel monkey oculomotor behavior with the oculomotor behavior of the monkey species more commonly used in oculomotor research, the rhesus macaque. These results are in preparation for publication. Third, I will present the results of an attempt to use juxtacellular labeling to morphologically identify cerebellar interneurons recorded in awake behaving squirrel monkeys. This project produced some positive steps in that direction but was ultimately abandoned due to insufficient yield. However, subsequently published work from other labs rendered juxtacellular labeling unnecessary to complete the experimental goals of the thesis. Last, I will present the results of a study on the use of multibarrel carbon fiber electrodes to record and

pharmacologically manipulate neurons in deep structures of awake behaving animals. These results have been published in the Journal of Neuroscience Methods.

Software environment for oculomotor task control using Spike2 and Power 1401

Introduction

This thesis was the first project in our lab to use trained monkeys, and as such required the development of custom programs to run the tasks and analyze the data. I wrote these programs from scratch in the Spike2 (tasks) and Matlab (analysis) environments. Here, I present details on the most significant of these programs, the Spike2 task control program. The software shares features other programs used in behaving monkey research but was written to work with the equipment used in the Blazquez lab. Briefly, the program generates all of the digital and analog signals required to control a mirror galvo system for moving a laser target that is projected in front of the monkey and two servomotors for rotating the monkey and an optokinetic drum. It operates by monitoring the monkey's eye position relative to the laser target and rewarding the monkey for looking at the target as it moves around the screen according to the particular task being performed. The criterion for accepting that the monkey is correctly following the target is that the monkey's eye position remains within an invisible "window," specified in degrees, that surrounds the target.

The task control program is in a mature stage of development and is extremely stable. All of the code required to implement it is available upon request. To be fully functional, the program requires Spike2 Version 6 or higher, but much of the functionality can be used with Spike2 Version 5.06 or higher.

Architecture of program

The task control program was written for the Spike2 recording system, a data acquisition solution sold by Cambridge Electronic Design (CED) that offers excellent data acquisition performance for electrophysiological experiments. Acquisition is handled by a dedicated device (1401) that connects to a PC running the Microsoft Windows operating system and running a software package called Spike2. The base system provides 8 channels of waveform input via analog to digital converters, 8 TTL inputs for event-based data (timestamps), 4 channels of waveform output via digital to analog converters, and 8 TTL outputs. CED offers access to the instruction set of the 1401 using a programming interface with a low level language resembling assembly language (referred to as the "sequencer"). Additionally, the Spike2 software running on Windows has a higher level scripting language (referred to as the "script") that can be used to customize data display, analysis, and communication with the 1401.

The task control program was designed to make use of the distributed processing capabilities offered by the CED 1401 and Spike2 system. The bulk of the intensive processing takes place on the CPU of the 1401, which is much more robust than MS Windows and is optimized for high performance during data acquisition. The 1401 has limited multithreading capabilities so the task control program running on the sequencer mostly consists of a main loop that handles the timing of the sequence of events in the task, and several side loops that control the individual tasks, monitor the monkey's performance (i.e., checking that the monkey is looking at the target), and perform auxiliary functions. Once initialized these loops run on the 1401 completely independently from the Spike2 script running on the PC, which allows the task to

continue to run without interruption even if the PC crashes. This provides a much needed failsafe when performing tasks that require interaction with servo-controlled motors, such as for a vestibular table.

The script running on the PC primarily serves as a user interface (UI) for the sequencer, allowing the investigator to set task parameters, calibrate the monkey's eye position, and manipulate how the data are displayed during sampling. In addition, the script performs some basic online detection routines to, e.g. display the monkey's eye position in 2-dimensional space, detect the occurrence of saccades, and detect spikes in the extracellular waveform using a manually set amplitude window.

Oculomotor tasks controlled by the program

The program was designed to be flexible, so new tasks can be added with relative ease. Each task consists of a side loop in the sequencer that is conditionally called by the main loop if the user selects that task. Depending on the task, the program outputs analog signals via up to 4 DACs to control the position of the laser, optokinetic drum, and/or primate chair. Any mirror galvo laser system with control voltages within +/-5 Volts is supported. The program is written to work with Kollmorgen servomotors for drum and chair movement, but could be relatively easily modified to provide analog control of any servomotor. In addition to the analog signals, the program also outputs three digital (TTL) signals for switching the laser, optokinetic drum light, and reward solenoid on and off. The current version of the program implements nine different tasks, with most having many variations available. The following tasks are supported.

1. **Fixation** of laser at up to 9 different locations (center, right, up-right, up, up-left, left, down-left, down, down-right).

2. **Saccades** starting at the center and going to peripheral locations in 8 different directions (right, up-right, up, up-left, left, down-left, down, down-right). The task can also be configured for saccades starting at peripheral locations and going to the center or for "out-and-back" saccades, where the monkey makes a saccade to a peripheral location and then back to the center. In addition, any arbitrary horizontal or vertical offset can be added to the saccade start point, allowing the user the ability to program saccades to or from any location within the range of the laser.

3. **Sequential saccades** starting at any arbitrary location and moving along a straight horizontal or vertical line, in steps specified by the user, to a final location. The user has the option of rewarding the monkey on each step or only at the completion of an entire sequence.

4. **Ramp or step-ramp pursuit** in 8 directions. The task can be configured for centrifugal, centripetal, or "full-length" (from one side to the other) pursuit from any arbitrary start point.

5. **Sinusoidal pursuit** at any displacement and frequency. Both horizontal and vertical pursuit can be performed at any positional offset.

6. **Sinusoidal VOR** with or without target at any displacement and frequency supported by the servomotor.

7. **Sinusoidal VOR suppression** at any displacement and frequency supported by the servomotor.

8. **Sinusoidal optokinetic stimulation** (OKS) and **fixation during whole field stimulation** (F-WFS) at any displacement and frequency supported by the servomotor.

9. A **predictive target interception** task, wherein the monkey must make a saccade to location predicted by the motion of a pursuit target and optionally pursue the target after acquiring it.

Fixation and hold times of any duration can be specified by the user, with the option of randomizing the times. The sinusoidal tasks are generally run continuously, though a single trial option is available, and the monkey is rewarded for keeping its eye on the target for a period of time specified by the user. All other tasks are run on a trial-by-trial basis, with the option of pseudo-randomizing the target direction on each trial or having the monkey perform blocks of identical trials.

Layout of UI

The user interface consists of a toolbar and three windows (Fig 2.1). The main window occupies 70% of the screen and displays a time view of the different data channels being acquired. A second window displays an XY plot of the horizontal and vertical positions of the target, target window, and monkey's eye. This display updates every 20 ms and displays the last 10 samples from the eye position data, giving a 200 ms "snake" of the eye trajectory, like the tail on a comet. The user can toggle between this "short snake" and a custom "long snake" length, which can be helpful for monitoring the history of eye positions during the spontaneous (i.e., outside the context of a task) eye movements that

were used extensively in the analyses of Chapters 3 and 4. This allows the user to ensure that the fixation points for spontaneous eye movements cover the entire oculomotor range of the monkey. The third window displays a log containing both the overall and task-specific performance of the monkey.

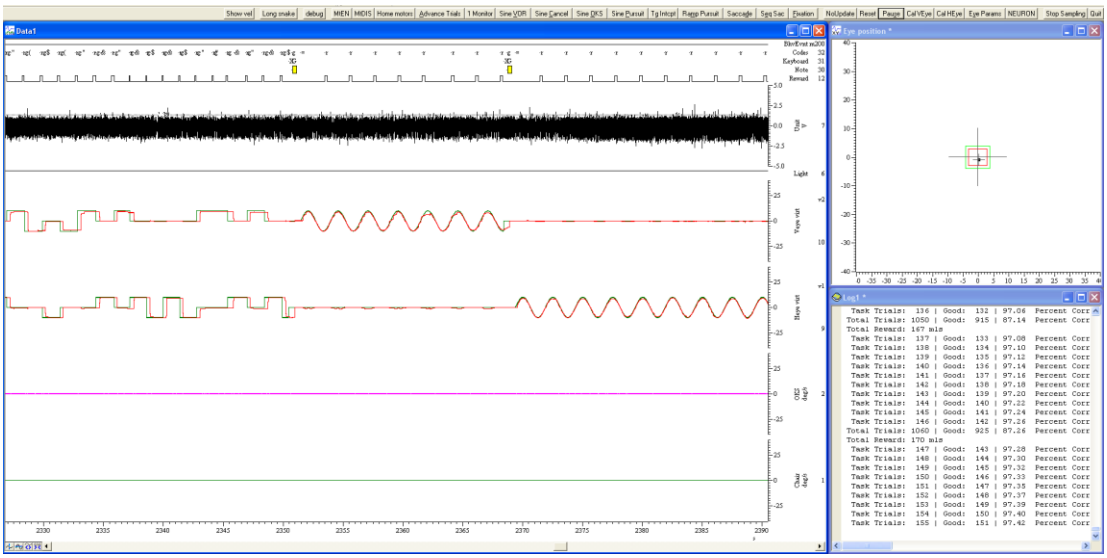

Figure 2.1. Screenshot depicting layout of task control program. The user interface consists of a toolbar at the top and 3 windows for displaying a time view of the data (left), the XY position of the eye (top-right), and a log of the monkey's performance (bottom-right).

The user interacts with the program by clicking buttons on a toolbar above the windows. Keyboard shortcuts are extensively used and most buttons can be "clicked" by pressing the key corresponding to the underlined letter in the button name. There are buttons to start and pause the currently running task, calibrate the eye, toggle acquisition of the raw extracellular neuronal signal (to save disk space if no neuron is isolated), set general parameters, and select individual tasks to run. Clicking some buttons, such as the "Eye Params" or individual task buttons (e.g. "Saccade"), brings up a dialog box with fields to update parameters. Figure 2.2 shows a screenshot of the general parameters that can be changed by clicking the "Eye Params" button. Most of the parameters pertain to the

calibration of the eye signal, such as scale, offset, and crosstalk. These values are automatically set during the calibration routine but can be modified as needed from this dialog. In addition, each animal has a configuration file that stores calibration values from day to day and is loaded when the user selects the animal's name from the dropdown list in this dialog. Miscellaneous parameters for the reward system and eye display ("snake length") are also set from this dialog.

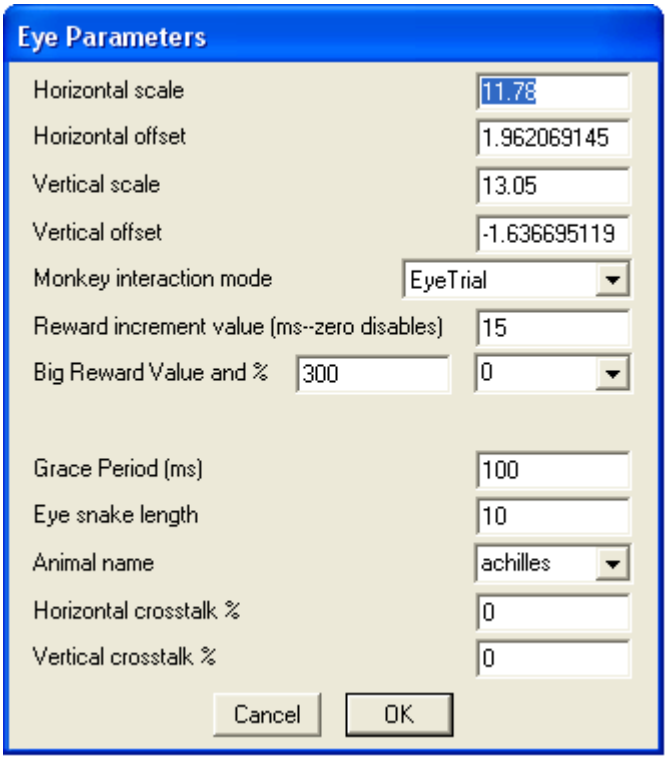

Figure 2.2. Screenshot of general parameters dialog box described in the text. The dialog box is comprised of several editable fields and dropdown listboxes for modifying parameters.

Figure 2.3 shows a screenshot of the dialog box for the saccade task, which gives an indication of the layout for all task dialogs. Tasks are started by clicking the button corresponding to the task the user wishes to run, modifying task parameters as desired, and clicking the "RUN" button. If the user only wishes to modify the task parameters and

save them for later execution, the “Save” button can be pressed. If the user presses “Cancel” all changes are forgotten and the task is not executed. Each task has its own configuration values for general task parameters such as intertrial interval (ITI), fixation and hold times, and reward size, which are saved in separate variables than the general task parameters for other tasks. This allows the user to, e.g., specify different reward sizes for saccades than for ramp pursuit without needing to modify the values each time a different task type is run. To give an idea of the range of task parameters, Figures 2.4 and 2.5 show screenshots of the dialog boxes for the sequential saccade and sinusoidal pursuit tasks.

In addition to the task control interface, all functionality provided by Spike2 is available while the task control program is running.

Additional features

Throughout the development of the program a number of improvements were made to the reward system in order to facilitate training. The first is an option to automatically increment the reward size on each successful trial, up to a maximum of 10 consecutive good trials. After 10 successful trials the reward size resets to its base level. This addition was instrumental in increasing the perseverance of the squirrel monkeys. Another addition was inspired by the success of jackpot lotteries. The user specifies two reward sizes, one large one small, and a value indicating the number of trials out of 100 in which the large reward will be delivered. This encourages the monkey to keep working for small rewards in anticipation of the large reward and can extend the number of trials that a monkey performs before becoming satiated. Lastly, as part of the system for monitoring

overall monkey performance, the program has the ability to monitor the cumulative volume of reward dispensed in an experimental session, allowing the investigator to adjust the reward size as needed to maximize the number of trials performed.

Another improvement that was made throughout the program development was the addition of a second "task window" that can be set to a different size than the initial "fixation window." This allows the user to specify a strict requirement for the monkey to fixate the initial target position while giving some leniency in how closely the eye tracks the target during the performance of the task, e.g. so the monkey is still rewarded despite natural variability in the precision of the movement, and neurological problems such as hypometric or hypermetric eye movements can be studied while still rewarding the animal's effort to perform the task.

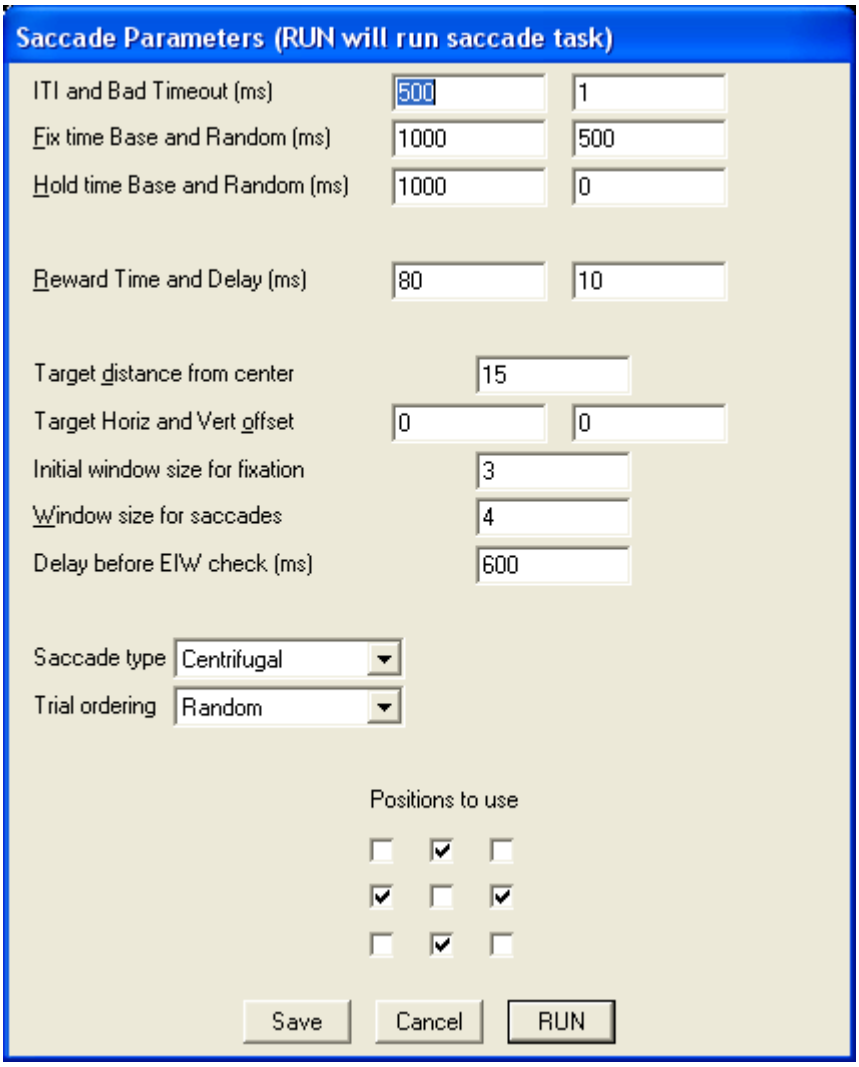

Figure 2.3. Screenshot of parameters dialog box for saccade task. General task parameters such as intertrial interval (ITI), window sizes, and reward size (time that solenoid is open in ms) can be configured independently for each task, and specific task parameters such as target jump (target distance from center), offsets, and saccade type (centrifugal, centripetal, out-and-back) are set from this dialog. The task is executed by clicking the RUN button or pressing enter.

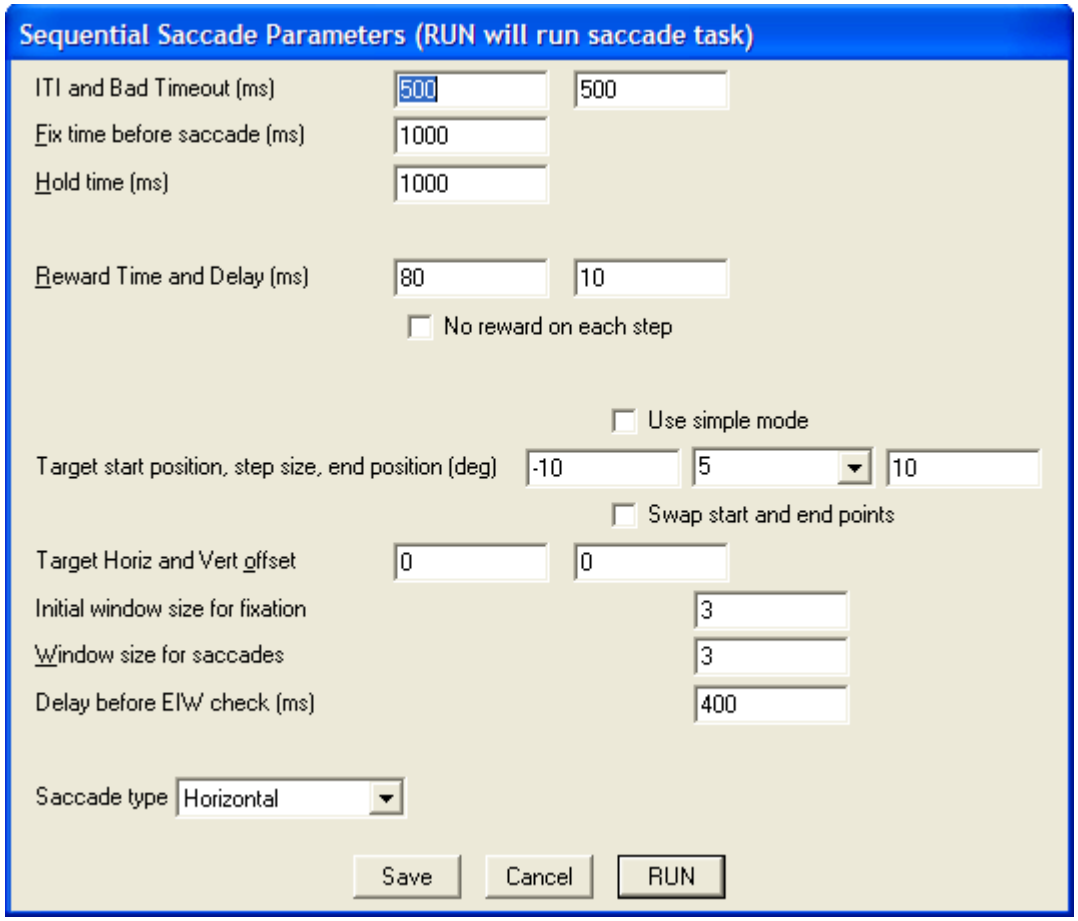

Figure 2.4. Screenshot of parameters dialog box for sequential saccade task. The user sets a start and end position, and a step size, and the target jumps from the start point to the end point in the steps specified, requiring the monkey to hold its eye at each new location for the "hold time." In "simple mode," the target jumps directly from the start point to the end point.

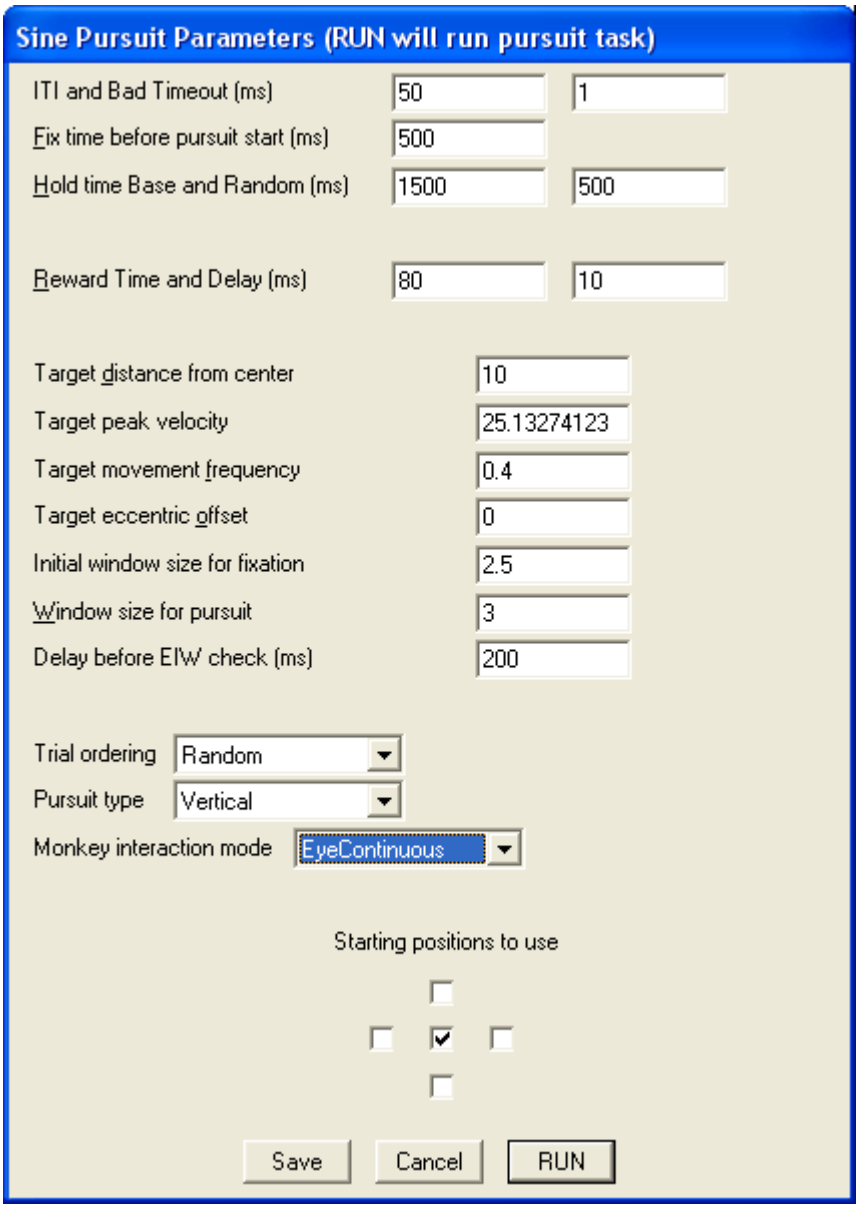

Figure 2.5. Screenshot of parameters dialog box for sinusoidal pursuit task. The same format is used for all sinusoidal tasks. Some of the key differences between the sinusoidal parameters and the trial-based parameters are the use of a callback function to calculate target peak velocity when the user changes either the target displacement ("distance from center") or frequency, and the option of using the "EyeContinuous" monkey interaction mode, where the laser continues moving whether or not the monkey is looking at it and the monkey is rewarded each time it follows the laser for the specified "hold time."

Behavioral repertoire of the squirrel monkey compared with the rhesus macaque

Abstract

The oculomotor system is the motor system of choice to many neuroscientists studying motor control and learning because of its simplicity, easy control of inputs (e.g. visual stimulation), and precise control and measurement of motor outputs (eye position). This is especially true in primates, which are easily trained to perform oculomotor tasks. Here we provide the first detailed characterization of the oculomotor performance of squirrel monkeys, primates used extensively in oculomotor physiology, during saccade and smooth pursuit tasks, and compare it to that of the rhesus macaque. We found that both primates have similar oculomotor behavior but the rhesus shows a larger oculomotor range, better performance for horizontal saccades above 10 degrees, and better horizontal smooth pursuit gain to target velocities above 20 deg/s. These results are important for interspecies comparisons and necessary when selecting the best stimuli to study motor control and motor learning in the oculomotor systems of these primates.

Introduction

For more than half a century neuroscientists have used saccade and pursuit eye movements as models to study a wide range of brain functions such as motor control, attention, and learning (Straube et al., 1997; Shinoda et al., 2008). Saccades are fast eye movements driven by a positional retinal error, and are conceptually similar to other ballistic movements like reaching. Smooth pursuit is a slow eye movement driven by retinal motion error, and is conceptually similar to slow movements like drawing. Saccade and pursuit physiology research have predominantly chosen squirrel monkeys and macaques (e.g. rhesus monkeys) as primate animal models. Each animal model presents its own advantages and disadvantages. For example, macaques are easy to train and are better to use when the experiment demands precise control of the motor output, but these animals are costly, making it unrealistic to use them for histology studies that require a large sample of animals. Squirrel monkeys are harder to train than macaques and have been traditionally used when precise control of eye movements is not necessary. An advantage of squirrel monkeys is that they have been the primate of choice for anatomical studies, and as a result, there is an abundance of squirrel monkey anatomical data available.

Unlike rhesus macaques, the behavior of squirrel monkeys trained in oculomotor tasks has not been characterized in detail. This lack of information could present a problem when data obtained from trained squirrel monkeys is generalized to other primate species. In this study we fill the gap by examining the oculomotor behavior of trained squirrel monkeys during the performance of saccade and pursuit tasks and by comparing the oculomotor performance to that of the rhesus macaque. Our findings suggest that, while

the squirrel monkey is capable of performing the same basic set of tasks as the rhesus, the squirrel monkey performs less consistently and within a narrower range of movement kinematics. This fact has the practical implication of constraining the number of repeatable trials that the monkeys can complete while a neuron is held in isolation, which has necessitated that we adopt a new analytical approach that does not rely on the averaging of identical trials. It has also limited the variety of tasks that the monkey can perform for each isolated neuron, which prevented us from acquiring data from all tasks for each neuron under study. However, we developed solutions to overcome these constraints. The behavior will be presented in this chapter and subsequent chapters will detail the methods we used to overcome limitations in the behavior.

Methods

Animal preparation and surgical methods

We include data from three 4-8 year old squirrel monkeys (083, 087, and 099) and one 5 year old rhesus macaque (Ach). All animals underwent at least one surgical operation where we implanted an eye coil to measure eye movements and a head post for head fixation. Briefly, animals were anesthetized using gas anesthesia (isofluorane 1-2%), and a stainless steel (squirrel monkeys) or titanium (rhesus macaque) head post was implanted using standard techniques (Stoet and Snyder, 2004; Blazquez et al., 2007). In the same surgical procedure we implanted a 3-4 turns coil (insulated stainless steel wire) in the left or right eye. After a minimum recovery period of 3-4 weeks animals were used for behavioral studies. All surgical methods and experimental protocols were approved by the Washington University Committee on Animal Care, and performed in accordance with the National Institute of Health guidelines.

Experimental setup

Animals were head fixed and comfortably seated in a primate chair during the experiments, and their eye movements were monitored using a search coil system. Our visual stimulus consisted of a green (squirrel monkeys) or red (rhesus monkeys) laser projected on a white screen placed in front of the animal (45 cm and front projected in squirrel monkeys and 50 cm and back projected in the rhesus monkey). An infrared camera was mounted above the projecting screen for continuous monitoring of the animal. The tasks were controlled by a PC computer and a Power 1401 (Cambridge

Electronic Design, UK) through a custom made program written in Spike 2 (Cambridge Electronic Design, UK) [see previous section for description].

Behavioral training and tasks

We used a standard water restriction protocol to provide the animals with motivation to perform the behavioral tasks. Animals were trained to perform fixation, saccade and pursuit tasks using a window size of 2 to 3 degrees radius. During the saccade task the initial fixation point was in the center of the screen and the target jumped to a new location in one of the four cardinal directions (up, down, left, right). In the pursuit task, the fixation point was at a position five degrees eccentric from center in one of the four cardinal directions and the target moved to the opposite side of the screen, passing through the center. We used the step ramp pursuit variation of the pursuit task (Rashbass, 1961), where the target was initially displaced in the opposite direction of the subsequent pursuit movement to a position such that at the time of the initiation of the eye movement the target was near the fixation point (center of the screen). The step ramp pursuit task was chosen to reduce contamination of saccades in the pursuit data. During saccade and pursuit tasks we allowed a grace period of 400 and 200 milliseconds respectively for the eye to reach the target. Saccade and pursuit trials were randomly presented in the four cardinal directions, and consisted of a random fixation time (500-800 ms) followed by displacement of the target and a final fixation (400-500 ms). The squirrel monkey setup had a maximum range for target eccentricities of 10 deg horizontal and 12 degrees vertical, while in the macaque setup the range of target movement extended to 22.5 degrees horizontally and 30 degrees vertically. In addition to eye movements recorded during task performance we also recorded the oculomotor behavior during spontaneous

eye movements in the absence of any visual stimulation, called here the "free viewing condition."

Analysis methods

Data were acquired using a Power 1401 and Spike 2 software, and imported into Matlab (Mathworks, Natick, MA, USA) for offline analysis. Eye position and laser position were acquired as analog signals at about 500 Hz, and task events (e.g. reward, laser ON, Laser OFF, etc) were acquired as digital events. Eye position was filtered using a Savitzky-Golay filter (four points window and second degree polynomial). First and second derivatives were calculated to obtain eye velocity and acceleration traces. We calibrated the eye using 8 degree saccades, assuming that perfect fixation occurs 400 ms after the first saccade to the target; if the initial saccade under- or overshot the target this gave sufficient time to generate a corrective saccade to the target. Saccade detection was automated and then manually inspected. Eye velocities rising above and falling below 50 deg/s were detected as saccade onset and offset respectively. Pursuit latencies were calculated by detecting the first point at which the eye velocity increased half a standard deviation above the mean of the noise and remained above half a standard deviation of the noise for at least 100 ms. In addition, all trials were manually inspected prior to inclusion. Saccade gain was expressed as the ratio between absolute target displacement and absolute change in eye position, and pursuit gain as the ratio between target velocity and mean eye velocity in a 20 ms window chosen at different times from pursuit onset. All statistical analyses, and curve fittings were performed over at least 50 data points, usually corresponding to several experimental days.

Results

The majority of the data presented here were obtained in the squirrel monkey. Data obtained in the macaque is shown only for comparison unless stated otherwise; macaque oculomotor behavior has been extensively described in other studies. We will not present upward pursuit data from our macaque because this animal had a clear vertical asymmetry for pursuit consisting of a reduced ability to pursue upward moving targets. This type of asymmetry is naturally present in some animals (Grasse and Lisberger, 1992).

Overall performance

Although squirrel monkeys frequently generate 100% correct trials in a block as macaques do, they get tired soon and tend to nap for several minutes several times during the experimental session (about 2 hours). We quantified the perseverance of the animals in performing oculomotor tasks as the percentage of correct trials during the entire session and the time interval between two consecutive correct trials. The rationale behind measuring perseverance in this way is based on our experience training these animals: fully trained animals committed to perform the tasks show good performance over the entire session and are eager to fixate as soon as the fixation point appears. Thus, not only do they have a higher percentage of good trials overall, but the average interval between two consecutive good trials is shorter, depending mostly on the intertrial interval. Squirrel monkeys performed at 63.0 ± 13.6 % correct during an entire session with an average of 512 ± 235 correct trials per session, and a good trial to good trial interval of 2.8 ± 1.2

seconds. On the other hand, our rhesus macaque performed at 82.2 ± 10.1 %, correct during an entire session with an average of 1238 ± 247 correct trials per session, with a good trial to good trial interval of 1.6 ± 0.2 seconds. Clearly macaques show not only more good trials per session but also more perseverance than squirrel monkeys in performing these tasks. It is also worth noting that our rhesus was eager to perform more trials if given extra training time, but our squirrel monkeys generally were not.

Range of spontaneous saccade eye movements

We measured the natural range of eye movements as the range in degrees that contain 90% of all fixations during the free viewing condition (two tail distribution) during a minimum of 30 minutes of spontaneous eye movements accumulated from several recording sessions. Figure 2.6A shows representative traces of horizontal spontaneous eye movement from a squirrel monkey (083; solid line) and a macaque (Ach; dashed line). We measured the eye movement range in two conditions, while the animals faced the experimental room and while facing the projecting screen. In the first situation animals had a diversity of objects of interest in the visual field including the experimenter, PC monitor, and instruments, located at a distance between 1.5 to 2.0 meters. The horizontal and vertical eye movement range of squirrel monkeys while facing the experimental room was 26 degrees (-15.8 to 10.4) and 26.3 degrees (-12.2 to 14.14) respectively (Fig 2.6B). In the same conditions, our macaque had a range of eye movements of 49.8 degrees (-26.6 to 23.2) horizontally and 53.7 degrees (-27.4 to 26.3) vertically. The eye movement range is substantially smaller for squirrel monkeys when the animals faced the white projecting screen; 15.5 degrees horizontally and 25.7 degrees

vertically. The macaque, however, showed a similar range of eye movements in both conditions, covering 55.5 degrees horizontally and 59.2 degrees vertically during spontaneous eye movements facing the projecting screen. Thus, the eye movement range of squirrel monkeys is two or three times smaller than that of the macaque. There is also a clear difference in the shape of the distribution of spontaneous fixations between our macaque and our squirrel monkey data. All animals preferred fixations around the center of gaze, but while squirrel monkeys distributions slowly fell towards zero for eccentric locations, our rhesus had an almost flat distribution for eccentric locations when facing the screen (Fig 2.6B).

Saccades

Latency: To prevent contamination of express saccades or other forms of prediction, we removed from our data those trials with saccade latencies below 100 ms and those preceded by trials with an identical target displacement direction. Figure 2.6C shows representative raw data from a squirrel monkey (099), and Figure 2.6D a cumulative histogram of saccade latencies for all monkeys. The average saccade latency for squirrel monkeys was between 180 and 243 ms (193 ± 41 for monkey 083, 181± 45 for monkey 087 and 243 ± 64 for monkey 099) with modes of 200, 143 and 205 for monkey 083, 087 and 099 respectively. For comparison, our macaque (Ach) showed an average latency of 219 ± 42 ms and a mode at 194 ms.

Saccade accuracy: We measured saccade accuracy as the difference between the eye position at the end of the initial saccade to a target and the target position, and we measured saccade gain as the change in eye position divided by the change in laser position. Figure 1E and F show saccade amplitude for horizontal and vertical target

displacements. Left and right saccade gains were grouped together because they showed no statistical difference ($p > 0.17$; for 8-10 deg saccades). Up and down saccades also showed no statistical difference and were grouped as well ($p>0.43$ for 8-10 deg saccades). Squirrel monkeys showed average horizontal saccade gains above 0.9 for target displacements less than 8 degrees (Figure 2.6E and F), with gains dropping 15.1 ± 7 % for 9-10 degrees saccades. Vertical saccade gains however were near unity for all target displacements used in the squirrel monkey experiments (gain of 0.96 ± 0.15 for saccades between 10-12 degrees). Macaques are known to have saccade gains near 1 for saccades up to 20 degrees (Robinson et al., 1993). In support, our macaque showed average saccade gains of 0.97 ± 0.04, 0.96 ± 0.06 and 0.95 ± 0.07 for target displacement of 10, 15 and 20 degrees (dotted lines in E and F).

Saccade Main Sequence: The characteristic relationship between saccade parameters that defines the main sequence in humans and macaques was also true for squirrel monkeys. We used data from visually guided saccades to construct the main sequence shown in Figure 2.6G and H. All saccades shared the same main sequence independently of the saccade direction (the population data containing the residuals was not significantly different when fitting separately each single direction or all directions; ANOVA $p>0.45$). In general, our squirrel monkeys generated faster and shorter saccades than our macaque. Thus 4-5 degrees and 8-9 degrees saccades have peak velocities of 378 ± 77 and 515 ± 70 deg/s respectively and durations of 23.3 ± 5 and 28.4 ± 4 ms in squirrel monkeys, which are significantly faster than that of our macaque (ANOVA single factor $p<<0.01$ and $p<<0.01$ for 4-5 and 8-9 degrees saccades respectively): 260 ± 50 and 422 ± 49 deg/s peak velocity with 28 ± 4 and 34.2 ± 5 and ms duration for 4-5 and 8-9 degrees saccade

respectively. This discrepancy is likely animal specific not species specific. The literature shows a highly variable saccade main sequence in macaques, with peak velocities resembling that of our squirrel monkeys (Robinson et al., 1993) and that of our rhesus macaque (Straube et al., 1997).

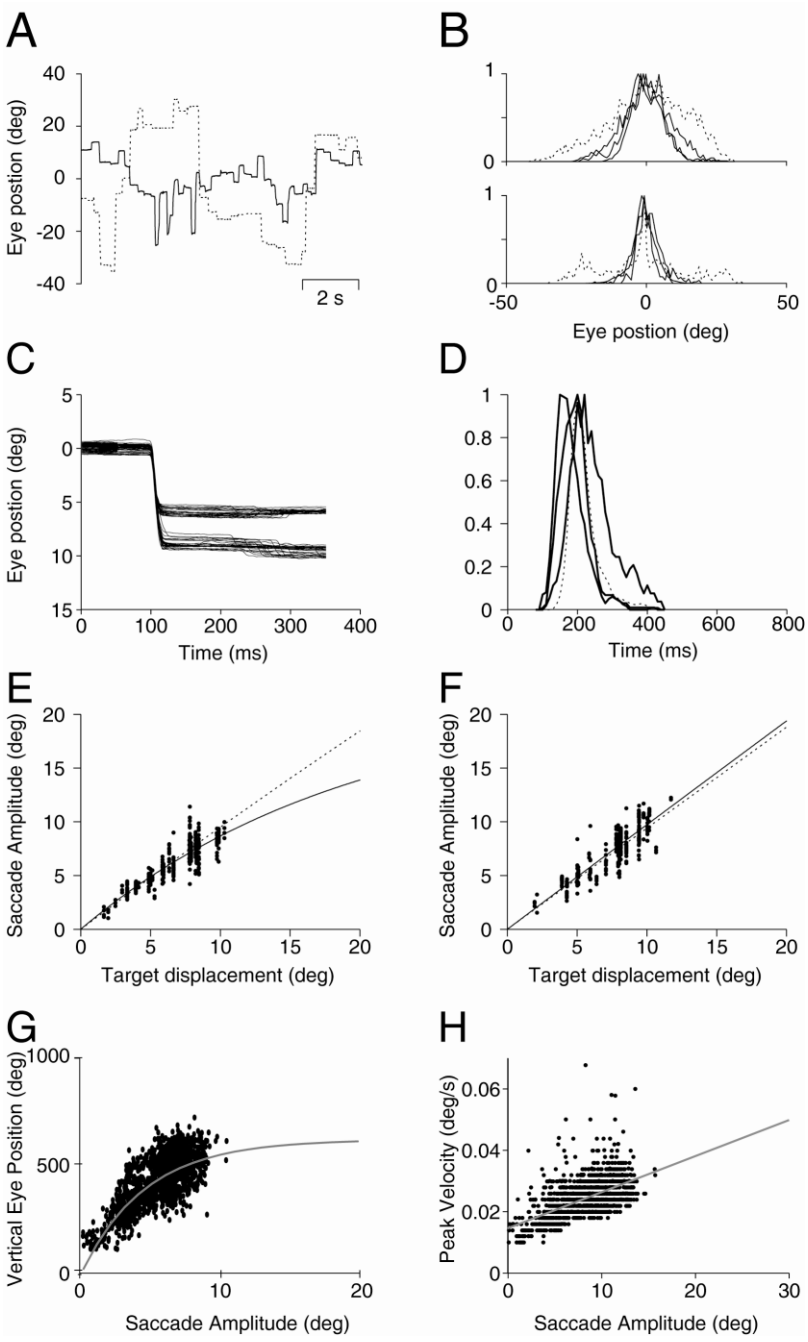

Figure 2.6. Eye movements in the free viewing condition (A and B) and during visually guided saccade task (C-H). A, exemplar raw data during the free viewing condition from squirrel monkey 083 (solid lines) and rhesus macaque (dashed lines). B, histograms showing the frequency of eye positions used for fixation in the free viewing condition normalized with respect to the most frequent eye position. On the top we show data obtained while the animals faced the recording room, and on the bottom while the animals faced the projecting screen. Solid lines show the data obtained in each of our squirrel monkeys, and the dashed lines the data obtained in the rhesus macaque. C, raw data of horizontal saccade eye movements of squirrel monkey 099 for target displacements of 6 and 10 degrees aligned with the initiation of saccades. Notice that while in response to 6 degrees target displacement the eye could either overshoot or undershoot, target displacements of 10 degrees always resulted in hypometric saccades. D, histogram showing the distributions of saccade latencies for the three squirrel monkeys used in this study (solid lines) and the rhesus macaque (dashed lines). E and F show the relationship between the target displacement and corresponding saccade amplitude. Each dot represents a single saccade, the solid line the fitting of the data, and the dashed line the fitting corresponding to similar data obtained from the rhesus macaque. G and H show data obtained in squirrel monkeys and plot the relationship between saccade amplitude and peak velocity (G), or saccade duration (H) representative of the saccade main sequence. The data plotted in this figure were obtained while the animals performed the saccade task. Gray lines show the fittings of the data.

Smooth Pursuit task

Latency: The response latency is an important variable when studying smooth pursuit behavior because it indicates the time period required for visual motion information to be processed and influence the behavior. This time period is called the open loop period of the pursuit system. Figure 2.7A shows representative data for horizontal pursuit eye movements from one of our squirrel monkeys (087). Squirrel monkeys have mean pursuit latencies and modes between 120 and 175ms (121 ± 18, 150 ± 31, and 173 ± 37 for monkeys 083, 099, and 087, with modes of 126, 138, and 175). Macaques have been reported to have latencies as short as 100 ms, but most frequently around 120-150 ms. In line with this, our macaque had a mean and mode pursuit latency of 143 ± 22 ms and 134 ms respectively (Figure 2.7B), which is between the range of latencies we encountered in the squirrel monkey. Pursuit latency in squirrel monkeys and the macaque depended on the direction and velocity of the target (2 factor ANOVA $p<<0.01$, and $p<<0.01$) with generally smaller latencies for lower velocities and horizontal movements. However, latency medians were within 12 percentile of each other, so the target direction and velocity were unpredictable on a trial by trial basis based only on pursuit latency.

Pursuit gain: The gain of pursuit was measured as the velocity of the eye divided by the velocity of the target. Figure 2.7C-D shows pursuit gains measured at different intervals from the initiation of pursuit, using target velocities up to 30 deg/s. We segmented the pursuit behavior into three time periods, corresponding to the early (40 ms) and late (80 ms) phases of the open loop and the closed loop phase (240 ms). There were no significant differences between our three squirrel monkeys in pursuit gain measured at 40, 80 and 240 ms from pursuit onset and for target velocities of 20 deg/s (ANOVA, p

values distributed between 0.1 and 0.77) so data from all squirrel monkeys were combined. The maximum eye velocity achieved during the first 40 ms of horizontal pursuit was 16.9 ± 2.5 deg/s, even with target velocities of 30 deg/s. Higher velocities were reached in the late period of the open loop, such that the pursuit system could compensate well for target velocities up to 20 deg/s, reaching maximum velocities of about 21.2 ± 3.3 deg/s for 30 deg/s target motion. However, the closed loop horizontal pursuit phase provided only small increases in performance, with maximum eye velocities of 20.0 ± 2.3 deg/s for 30 deg/s target motion. Eye velocities were higher during the closed loop phase for vertical compared to horizontal pursuit, with no clear saturation at the highest velocities used in this study (30 deg/s, only monkey 087 was used for vertical pursuit at 30 deg/s). Our rhesus had lower eye acceleration during the open loop period than the squirrel monkeys so it was unable to compensate for target velocities above 10 deg/s during the early phase and 15 deg/s during the late phase of the open loop period. However, our rhesus was better able to match higher target velocities during the closed loop period, generating pursuit velocities of 31.9 ± 5.9 deg/ at 30 deg/s target velocities, in agreement with data shown by other investigators (Stone and Lisberger, 1990).

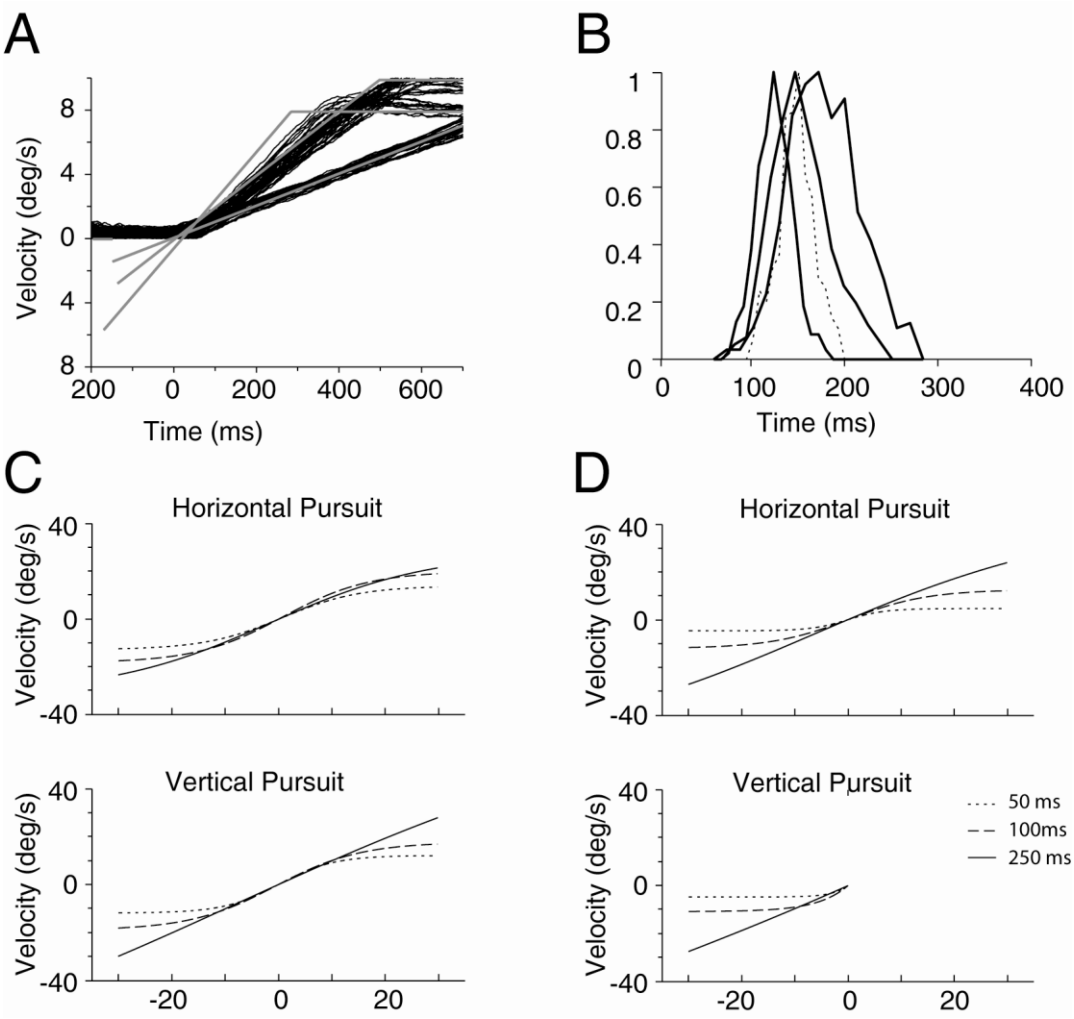

Figure 2.7. Pursuit eye movements. A, horizontal pursuit eye movement raw data of squirrel monkey 087 for target velocities of 10, 20 and 30 deg/s. B, histogram showing the distributions of pursuit latencies for the three squirrel monkeys used in this study (solid lines) and the rhesus macaque (dashed lines). C-D, curves showing maximum eye velocities achieved at different target velocities during three phases of pursuit averaged across all squirrel monkeys (C) and Ach (D): early open loop (40 ms), late open loop (80 ms), and closed loop (240 ms).

Discussion

Our results show that the oculomotor behavior of rhesus macaques and squirrel monkeys is very similar during spontaneous eye movements and during the execution of saccade and pursuit tasks, however there are a few important differences: 1) squirrel monkeys have a narrower oculomotor range than macaques; 2) squirrel monkey saccadic eye movements become inaccurate for horizontal target displacements above 8 degrees, while rhesus macaques maintain accurate saccadic eye movements up to at least 20 degree eccentricities. 3) Similarly, horizontal pursuit gains in the squirrel monkey during the closed loop period fall below unity for target velocites above 20 deg/s, while vertical pursuit gain in the closed loop period are near unity for the range of target velocities used in this study (up to 30 degrees/s). Rhesus macaques however, have no problem matching target velocities of 30 deg/s during the close loop period for both horizontal and vertical laser movements. Our results justify the comparison of behavioral and neuronal data obtained from both animal models, but caution that these comparisons have to be done within the limitations of each species.

The finding that macaques have a larger oculomotor range than squirrel monkeys suggests that head movements for image stabilization are engaged more frequently in squirrel monkeys than in rhesus macaques (Freedman and Sparks, 1997). This might be the result of adaptive differences to optimize the oculomotor systems of the two species for their different physical properties; squirrel monkeys are small animals (between 0.6 to 1 kilogram) and head movements have to overcome smaller inertial forces than macaques (usually above 6 kilograms). It is likely that the larger range of near unity saccade and

pursuit gains of the rhesus macaque is the direct consequence of a more prominent role of eye movements for gaze control. We have no explanation for the better performance of the vertical compared to the horizontal saccade and pursuit system in the squirrel monkey other than it could be related to the fact that these small animals are mostly arboreal and their main predators are birds of prey, such as eagles.

The behavioral differences noted above are not surprising because there are important differences in the oculomotor systems of squirrel and rhesus monkeys at the neuronal level, differences that could ultimately result in different behavioral responses during oculomotor tasks. For instance, following the argument of a different role of head movements for gaze stabilization in squirrel monkey than in rhesus macaques, there appears to be a difference in the wiring of neck proprioceptors between the two species that suggests different strategies for gaze stabilization. Specifically, neck proprioceptor and vestibular information is combined such that many neurons in the vestibular nuclei of the squirrel monkey cannot tell whether the head is moving with respect to a stationary body or the body moving with respect to a stationary head. In the rhesus macaque however, vestibular nuclei neurons do not respond during movements of the body while the head is stationary (Gdowski et al., 2000; Sadeghi et al., 2009). Furthermore, we suggest that the smaller compensatory range of eye velocities during horizontal pursuit in the squirrel monkey is not due to a limitation of the motor or premotor system, because squirrel monkeys can generate eye movements above 100 deg/s during optokinetic stimulation (Blazquez et al., 2007), but a limitation in the pathways responsible for generating smooth pursuit responses. For example, limitations in the neuronal population

decoding of middle temporal area (MT) neurons could make visual motion predictions unreliable for large target velocities.

Our results reveal similarities and differences in the oculomotor behavior of squirrel monkeys and macaques that may be critical when comparing neuronal and behavioral data from both species. Both animal species can perform oculomotor tasks, and both share similar oculomotor behavior; however comparison should be done carefully within the linear limits of the oculomotor behavior of each species. For example, our data argue that neuronal responses to horizontal saccades above 8 degrees eccentricity or fixations above 14 degrees eccentricities might undergo saturation effects in squirrel monkeys but not in rhesus.

References

Blazquez PM, Davis-Lopez de Carrizosa MA, Heiney SA, Highstein SM (2007) Neuronal substrates of motor learning in the velocity storage generated during optokinetic stimulation in the squirrel monkey. Journal of neurophysiology 97:1114-26.

Freedman EG, Sparks DL (1997) Eye-head coordination during head-unrestrained gaze shifts in rhesus monkeys. Journal of neurophysiology 77:2328-48.

Gdowski GT, Boyle R, McCrea RA (2000) Sensory processing in the vestibular nuclei during active head movements. Archives italiennes de biologie 138:15-28.

Grasse KL, Lisberger SG (1992) Analysis of a naturally occurring asymmetry in vertical smooth pursuit eye movements in a monkey. Journal of neurophysiology 67:164-79.

Rashbass C (1961) The relationship between saccadic and smooth tracking eye movements. The Journal of physiology 159:326-38.

Robinson FR, Straube A, Fuchs AF (1993) Role of the caudal fastigial nucleus in saccade generation. II. Effects of muscimol inactivation. Journal of neurophysiology 70:1741-58.

Sadeghi SG, Mitchell DE, Cullen KE (2009) Different neural strategies for multimodal integration: comparison of two macaque monkey species. Experimental brain research. Experimentelle Hirnforschung. Expérimentation cérébrale 195:45-57.

Shinoda Y, Sugiuchi Y, Izawa Y, Takahashi M (2008) Neural circuits for triggering saccades in the brainstem. Progress in brain research 171:79-85.

Stoet G, Snyder LH (2004) Single neurons in posterior parietal cortex of monkeys encode cognitive set. Neuron 42:1003-12.

Stone LS, Lisberger SG (1990) Visual responses of Purkinje cells in the cerebellar flocculus during smooth-pursuit eye movements in monkeys. I. Simple spikes. Journal of neurophysiology 63:1241-61.

Straube A, Fuchs AF, Usher S, Robinson FR (1997) Characteristics of saccadic gain adaptation in rhesus macaques. Journal of neurophysiology 77:874-95.

Juxtacellular injection of neural tracers in the awake behaving squirrel monkey

Abstract

A system was developed for recording neurons in deep structures of the squirrel monkey central nervous system and electroporating charged dyes into the recorded neurons for subsequent histological examination. The system is based on the juxtacellular recording and injection technique developed by Pinault (1996). It consists of a custom-built glass-tungsten hybrid electrode that has the same length and thickness as a conventional tungsten electrode, but has a glass tip that can be filled with any desired solution, and a guide tube assembly that allows clogged electrodes to be easily removed and replaced without removing the guide tube from the brain. A proof-of-concept was accomplished, showing that juxtacellular recording and entrainment to current pulses can be performed in deep structures of the alert monkey, including the floccular lobe of the cerebellum. However, no neurons were able to be recovered upon histological examination, suggesting that the entrainment period achieved was not sufficient to electroporate enough dye into the neurons.

Introduction

The cerebellar cortex offers an unparalleled opportunity to evaluate local processing by neural circuits, given its stereotyped synaptic organization, well-established inputs and outputs, and prominent role in sensorimotor processing. Biologists and computational modelers have long appreciated these properties and over the last several decades have constructed elaborate models to describe the signal processing performed by the unique circuitry of the cerebellar cortex. These models have been bolstered by in vitro experiments using stimulation and pharmacological manipulations to tease apart the influence of various circuit components. Unfortunately, empirical evidence in awake, behaving animals, which is necessary to support or refute these models, has consistently lagged behind the modeling efforts. This lack of empirical data has been in large part due to the difficulty inherent in identifying and characterizing the responses of cerebellar cortical interneurons.

The aim of this component of the project was to develop a recording system, including electrode, off-the-shelf amplifier, and software, that would allow juxtacellular injections in deep brain structures of the alert behaving squirrel monkey and to use this system to label and identify cerebellar cortical interneurons.

Materials and Methods

Subjects and Surgeries

Two adult squirrel monkeys were used for these experiments (066, 404). Both monkeys had been a subject in at least one other study conducted in the lab and was used after those studies were terminated, before the monkey was ready to be euthanized. For the prior experiments, the monkeys had undergone standard surgical procedures under isoflurane anesthesia to be implanted with a head bolt for restraint and a scleral search coil to monitor eye movements (Fuchs and Robinson, 1966). After at least two weeks of recovery, they underwent a second surgery to implant a chronic recording chamber positioned to allow access to the floccular complex, including the flocculus and ventral paraflocculus. Surgical methods and experimental protocols were approved by the Washington University Committee on Animal Care, and were performed in accordance with the National Institute of Health guidelines.

Neuronal recording and juxtacellular labeling

Neuronal data were recorded with custom-built glass-tungsten hybrid electrodes (10-15 MOhm) filled with 5% biotin or biotinylated dextran amine (BDA) in 0.5 M NaCl connected to a bridge amplifier (AxoClamp 2B, Axon Instruments). Extracellular recordings were filtered with 100-8000 Hz passband, amplified and digitized at 40 KHz using a Power 1401 and the Spike2 acquisition program (Cambridge Electronic Design, UK), and stored for offline analysis.

Behavioral data including eye position, head position, and their mathematical derivatives (velocity) were continuously digitized at 500 Hz using the same Power 1401 as the neuronal data, saved to disk, and displayed on a computer monitor.

Neurons were recorded throughout the region of cerebellar cortex accessible with our flocculus chambers. Once single unit isolation of a neuron was achieved, the electrode was slowly advanced while current pulses (1 nA, 200 ms duration, 50% duty cycle) were applied. The current amplitude was gradually increased as the electrode advanced toward the cell, until a juxtacellular position was achieved and the cell entered entrainment with the pulses (Pinault, 1996; Duque et al, 2000; Simpson et al, 2005). Upon this, the current amplitude was reduced to the minimum necessary to maintain entrainment, and the spikes of the neuron were monitored to ensure the health of the neuron. If the spike shape became distorted or the neuron began firing uncontrollably, the current was reduced until the cell recovered.

Histology

After the last recording session, animals were anesthetized with a lethal dose of sodium pentobarbital (50 mg/kg) and perfused transcardially with 0.1 M phosphate buffered saline [PBS] (ph 7.4) followed by 3-4% paraformaldehyde in PB. Brain tissue was extracted and placed in a 0.1 M PBS containing 30% sucrose (for cryoprotection) overnight.

The cerebellum was blocked and coronal sections cut at 60 um thickness using a freezing microtome. The sections were rinsed in cold PBS. Sections were then pretreated with 1%

sodium borohydride in PBS for 20 minutes, rinsed 3-5 times in PBS, incubated for 10 minutes in 1% hydrogen peroxide in PBS, and rinsed again. Labeled neurons were developed using an Avidin-Biotin Peroxidase complex (ABC) kit (Vector Laboratories Inc) and 3,3'-diaminobenzidine tetrahydrochloride (DAB) intensified with nickel.

Labeled neurons were visualized with light microscopy. Landmarks, such as the eighth nerve and electrolytic lesions, were used as references for finding the neural responses that corresponded to the labeled neurons.

Results

I have designed and implemented a novel glass-tungsten hybrid electrode and a guide tube system that allows precise positioning of a solution-filled glass-tipped electrode in the cerebellar cortex, including the floccular complex, of awake squirrel monkeys. Positioning a glass electrode in the flocculus is made difficult by the facts that 1) the required recording depth is tens of millimeters below the surface of the neocortex, which precludes use of standard pulled glass microelectrodes; and 2) there is a portion of dura mater covering the cerebellum (the tentorium), in addition to the dura covering the neocortex, that the electrode must pass through without breaking. My solution to this problem was to construct a series of concentric hyperdermic tubes, wherein the inner tube (23 gauge) can be coupled to a standard tungsten electrode and a microdrive and driven through the tentorium. Passage through the tentorium is indicated by a sudden increase in background activity recorded with the tungsten electrode and often the presence of Purkinje cell complex spikes. After allowing sufficient time for the tissue to stabilize, the tungsten electrode is removed through the back of the guide tube system and the inner guide tube locked in place. Custom-built glass-tungsten hybrid electrodes filled with salt solution (Fig 2.8) are then back-loaded into the inner guide tube using a custom-built adaptor which ensures that the electrode is aligned with the center of the guide tube to prevent the fragile tip from breaking. These steps result in easy passage of the electrode into the cerebellum.

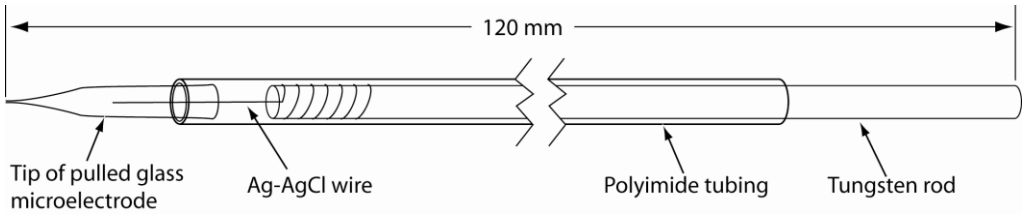

Figure 2.8. Schematic diagram indicating construction of glass-tungsten hybrid electrode. A rigid shank is created by wrapping silver wire around one end of a tungsten rod and insulated by surrounding the whole thing, except the last few millimeters of each end, with polyimide tubing. A glass microelectrode is pulled with a PMP-107 puller and filled with salt solution. The initial 5 mm of glass is broken along the taper and inserted into the polyimide, such that the silver wire contacts the solution as pictured. A small amount of cyanoacrylate (super glue) is applied to hold the tip in place and provide additional insulation.

Using this approach, I have been able to routinely record single unit responses in the cerebellar cortex. The system is reliable enough that on average once per track the glass-tungsten hybrid electrode can be positioned close enough to the neurons to drive their firing rate with small current injections through a bridge amplifier. Figure 2.9A and B show this process for one such neuron recorded in the left cerebellar hemisphere of an awake squirrel monkey. The spontaneous activity of the neuron was relatively stable at about 40 spikes/sec. Once the electrode was in a stable position relative to the neuron, as evidenced by the lack of change in the amplitude of the downward spike deflections, I began injecting progressively larger current pulses of 200 msec, 50% duty cycle. At approximately 5 nA peak-to-peak the neuron reached its "breakpoint current," at which the firing rate of the neuron could be entrained to the current pulses. During this period, pores are believed to form in the cell's membrane, allowing the electrode solution to enter the cell (Rae and Levis, 2002). Juxtacellular positioning was attained and entrainment attempted with more than 30 neurons in the cerebellar cortex of two monkeys. Of these attempts, 7 resulted in entrainment of the neuron to the current pulses that could be maintained for more than 1 minute. The remaining neurons were either injured before entrainment could be achieved or the juxtacellular position was lost. No neurons could be

entrained for longer than 5 minutes because either the juxtacellular position was lost or the neuron firing pattern became unstable and current injection was terminated to prevent injury. Upon histological examination, none of the entrained neurons could be recovered.

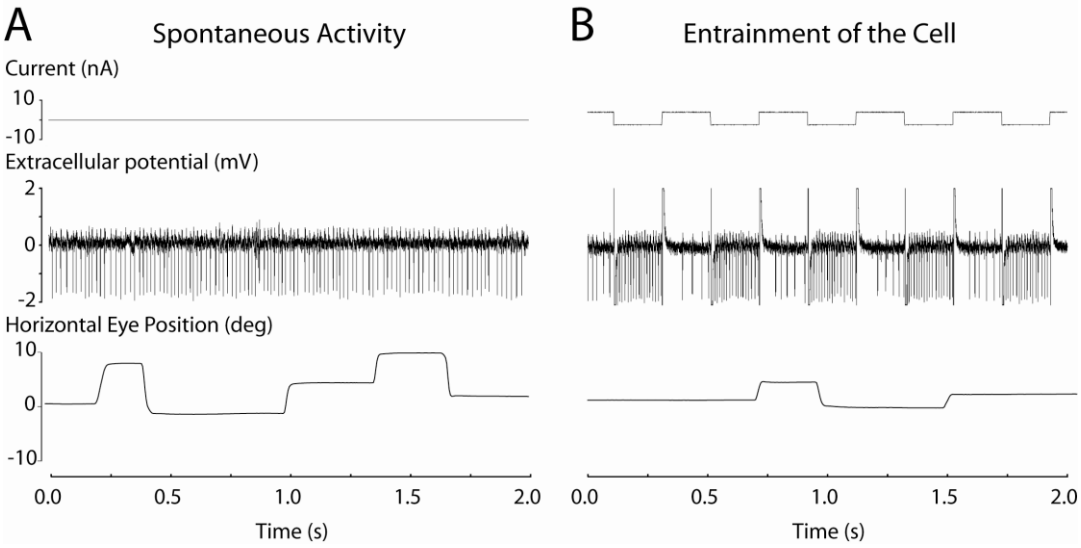

Figure 2.9. Cerebellar interneurons in the awake monkey can be entrained with current pulses. A, Spontaneous activity of neuron recorded in cerebellar hemisphere of awake monkey with glass-tungsten hybrid electrode containing 0.5 M NaCl. Top to bottom: injected current (in this case zero), extracellular potential, and horizontal eye position. B, Same neuron during juxtacellular entrainment with 5 nA peak-to-peak current. Same conventions as A.

Discussion

These results represent the first time to our knowledge that juxtacellular entrainment has been accomplished in a deep structure in the alert behaving monkey. The primary impediment to successful juxtacellular entrainment was the difficulty of maintaining a juxtacellular position of the electrode, which is much closer than the single unit isolation that is typically achieved in alert animals, without injuring the cell or losing isolation. When juxtacellular entrainment could be achieved, the duration was apparently too short to electroporate a sufficient quantity of dye into the neuron to successfully label it. For reference, Pinault (1996) reported successfully labeling of cell somata with as little as 3 minutes of entrainment, but noted that 15 minutes of entrainment was required for successful labeling of the full axonal and dendritic arborizations. Because the rate of success for entrainment was low and no neurons were labeled in the two animals used, this project was abandoned. However, papers published by Holtzman and colleagues (2006) and Barmack and Yakhnitsa (2008) made the criteria for identifying Golgi cells in anesthetized rats and mice more clear, and a paper published by Prsa and colleagues (2009) established a precedent for identifying Golgi cells in the monkey cerebellum. Therefore, it was not necessary to juxtacellularly label Golgi cells in order to complete the thesis project. The electrode design and technique developed could be adapted for any experiment requiring electroporation of charged particles into single neurons in deep structures, provided sufficient stability of the tissue can be maintained.

References

Barmack NH, Yakhnitsa V (2008). Functions of interneurons in mouse cerebellum. J Neurosci 28: 1140-1152.

Duque A et al. (2000). EEG correlation of the discharge properties of identified neurons in the basal forebrain. J Neurophysiol, 84(3): p. 1627-35.

Fuchs AF Robinson DA (1966). A method for measuring horizontal and vertical eye movement chronically in the monkey. J Appl Physiol. 21(3): p. 1068-70.

Holtzman T, Rajapaksa T, Mostofi A, Edgley SA (2006). Different responses of rat cerebellar Purkinje cells and Golgi cells evoked by widespread convergent sensory inputs. J Physiol 574: 491-507.

Pinault, D (1996). A novel single-cell staining procedure performed in vivo under electrophysiological control: morpho-functional features of juxtacellularly labeled thalamic cells and other central neurons with biocytin or Neurobiotin. J Neurosci Methods. 65(2): p. 113-36.

Prsa M, Dash S, Catz N, Dicke PW, Thier P (2009). Characteristics of responses of Golgi cells and mossy fibers to eye saccades and saccadic adaptation recorded from the posterior vermis of the cerebellum. J Neurosci 29: 250-262.

Rae JL and Levis RA (2002). Single-cell electroporation. Pflugers Arch. 443(4): p. 664-70.

Simpson JI et al. (2005). Between in and out: linking morphology and physiology of cerebellar cortical interneurons. Prog Brain Res. 148: p. 329-40.

Manufacture and use of carbon fiber multibarrel electrodes for recording and iontophoresis in awake behaving squirrel monkeys

Abstract

Microiontophoresis of neuroactive substances during single unit recording in awake behaving animals can significantly advance our understanding of neural circuit function. Here we present a detailed description of a method for constructing carbon fiber multibarrel electrodes suitable for delivering drugs while simultaneously recording single unit activity from deep structures, including brainstem nuclei and the cerebellum, in the awake behaving primate. We provide data that should aid in minimizing barrel resistance and the time required to fill long, thin multibarrel electrodes with solutions. We also show successful single unit recording from a variety of areas in the awake squirrel monkey central nervous system, including the vestibular nuclei, interstitial nucleus of Cajal, and the cerebellum. Our descriptions and data should be useful for investigators wishing to perform single unit recordings during microiontophoresis of neuroactive substances, particularly in deep structures of animals with chronically implanted recording chambers.

Introduction

Simultaneous single unit recording and microionotophoresis of neuroactive substances in alert behaving animals can significantly advance our understanding of how neural circuits utilize neurochemicals to control the firing behavior of their constituent neurons, and thus produce behavior. Despite the wide use of this technique in anesthetized preparations (Millar and Williams, 1989; Williams and Millar, 1990; Cudeiro et al., 1997), few labs that work with alert behaving animals employ simultaneous single unit recording and microiontophoresis in their investigations (Alloway and Burton, 1991; Herrero et al., 2008). One reason for the underutilization of such a powerful technique may be the perceived difficulty of producing multibarrelled glass electrodes that are suitable for recording and iontophoretically delivering drugs in chronically-implanted animals on a daily basis.

The potential of microiontophoresis has been recognized for decades by investigators working with anesthetized animals (Millar and Williams, 1989; Williams and Millar, 1990; Rivadulla et al., 2003), and the majority of methods papers to date deal with optimizing the technique for these preparations (Armstrong-James and Millar, 1979; Armstrong-James et al., 1980; Anderson and Cushman, 1981; Millar and Williams, 1988; Fu and Lorden, 1996; Kuras and Gutmaniene, 2000). The technique has been around for over fifty years (Curtis and Eccles, 1958), but Armstrong-James and Millar (1979) made a drastic improvement in the quality and reliability of the single unit recordings that can be achieved by introducing the use of a carbon fiber as the recording electrode. This design has been further improved over the years by introducing new methods of etching the carbon fiber tip (Armstrong-James et al., 1980; Kuras and Gutmaniene, 2000) and

speeding up the manufacturing process (Anderson and Cushman, 1981; Fu and Lorden, 1996; Millar and Pelling, 2001). However, few papers have dealt with the unique challenges faced by investigators who wish to apply the technique to record from chronically-implanted awake behaving animals (Alloway and Burton, 1991), namely penetration of the dura and scar tissue, sterilization of the electrodes, and access to deep structures.

We have spent several years perfecting the manufacture and use of carbon fiber multibarrel electrodes in alert behaving squirrel monkeys and offer here a detailed description of a complete system for daily recording and microiontophoresis in deep structures, including brainstem and cerebellar sites. These electrodes can be produced in under fifteen minutes and provide excellent signal-to-noise characteristics. We describe their manufacture, providing several suggestions to simplify the process; present results from a parametric study of the optimal characteristics for a variety of electrode configurations; and show their suitability for recording and simultaneous iontophoretic drug delivery in several deep structures of the alert behaving primate.

Material and methods

General Supplies

Multibarrel electrodes are constructed from preassembled borosilicate multi-capillary glass tubing and carbon fibers. Preassembled three barrel glass was purchased from World Precision Instrument (Sarasota, FL, USA), four barrel glass from A-M Systems (Carlsborg, WA, USA), and seven barrel glass from FHC (Bowdoin, ME, USA). Bundles of carbon fibers consisting of individual 5 or 7 micron fibers were obtained from TORAY carbon fiber USA. Stainless steel and polyimide tubing were purchased from Small Parts Inc., and were used to make guide tubes and to help separate individual carbon fibers, respectively.

Animal preparation and recording setup

Three squirrel monkeys (monkey 062, monkey 066, and monkey 408) 4-10 years of age were used for these experiments. We used standard surgical procedures performed under Isoflurane anesthesia and aseptic conditions in a fully equipped surgical suite (Blazquez et al., 2003; Blazquez et al., 2007). In a first surgical procedure we implanted a stainless steel post for head fixation and an eye coil to monitor the eye position. In a second surgery we implanted a chamber for neuronal recordings. Surgeries were separated by a minimum period of three weeks to allow for animal recovery. Surgical methods and experimental protocols were approved by the Washington University Committee on Animal Care, and were performed in accordance with the National Institute of Health guidelines.

Animals were comfortably seated in a primate chair during experiments. Our recording setup consists of a custom-made AC coupled differential amplifier, a hydraulic microdrive, a Neurophore BH-2 iontophoretic pump system (Medical Systems Corp), and a search coil eye movement detector system (Neuro Data Instrument Corporation). A Power 1401 (Cambridge Electronic Design) connected to a PC computer and running Spike2 software (Cambridge Electronic Design) was employed for data acquisition (neuronal and behavioral) and stimulus presentation. In addition we use several servo-controlled motors in our experiments, the details of which are not important for this manuscript.

Manufacture of the carbon fiber multibarrel electrode

Others have already reported that the use of a carbon fiber as the recording electrode considerably improves the recording quality compared with a saline-filled barrel alone (Armstrong-James and Millar, 1979; Fox et al., 1980). The carbon fiber can be placed either inside one of the barrels or in the center space between barrels. Below we describe methods we have developed to simplify the manufacture of multibarrel electrodes containing a carbon fiber recording filament.

Separation of individual carbon fiber filaments. A commercial bundle of carbon fibers contains upwards of ten thousand individual carbon fiber filaments, which can be as small as 5-7 microns each. The small size and fragility of each filament make the process of separating carbon fiber bundles into individual filaments tedious. Others have suggested the use of specially modified forceps to remove individual filaments from the bundle (Armstrong-James and Millar, 1979; Fu and Lorden, 1996), however we find it

easier to separate fibers by placing the bundle of carbon fibers on a sheet of glossy photographic inkjet paper (e.g. Kodak), on which we extract individual filaments with the help of a 28 gauge polyimide tube under a dissection microscope (x 6 magnification); polyimide tubes are flexible and do not break the individual filaments upon contact. The carbon fibers stick lightly to the glossy paper, which prevents them from being blown away from air drafts. Once separated, single carbon fibers can be left on the glossy paper where they remain until needed.

Inserting the carbon fiber into a glass barrel. The difficulty of inserting a 5-7 micron carbon fiber filament into one of the glass barrels can be one of the biggest impediments to the successful manufacture of multibarrel electrodes. We have improved current published methods to make this step less time consuming and onerous. The first method we present is similar to one employed by Fu and Loren (1996) in which a narrow tungsten wire (100 micron, Small Parts Inc) a couple of centimeters or more longer than the borosilicate glass is inserted in one of the glass barrels. Under the dissection microscope, a single carbon fiber is then glued to one end of the wire using cyanoacrylate glue. After the glue dries, the wire is slid through the glass barrel such that it carries the carbon fiber through the full extent of the glass barrel to the other end. The second method can be performed much more rapidly than the first, requiring only a length of polyimide tube (28 gauge) a couple of centimeters longer than the borosilicate glass. We insert 1 to 2 mm of the carbon fiber into one of the glass barrels either by hand or by lifting the fiber with the polyimide tube and sliding the glass barrel over the fiber. Under the dissecting microscope, the polyimide tube is then introduced into the same glass barrel and pushed through until it exits the other end. The friction and electrostatic forces

between the carbon fiber and the polyimide tube ensure that the carbon fiber is carried to the other end of the glass barrel with the polyimide tube. This method requires some practice but it is cleaner (no glue) and faster, and is our method of choice. Once it is loaded into the glass barrel, we cut the carbon fiber several centimeters from the end of the glass so that only a few centimeters protrude on either end. Finally, we place a mark on the barrel containing the carbon fiber to keep track of its location as the fiber is difficult to see with the naked eye.

Pulling the multibarrel electrode. We use a horizontal multi-pipette puller (PMP-107L, Micro Data Instrument, S. Plainfield, NJ, USA) because this puller allows for the construction of long, thin tips, but any multistage glass puller that can accommodate multibarrel glass should work as well. While the glass is being pulled and separated into two segments it is critical that the carbon fiber remain static with respect to the glass segment that will ultimatly form the multibarrel electrodes, otherwise the glass will not form a tight seal around the carbon fiber at its tip. The best approach we have found to achieve this with high success is simply to stabilize the carbon fiber protuding from the glass by holding it between our thumb and forefinger during the pulling stages. Alternatively, one may place a small drop of cyanoacrylic glue at the end of the barrel containing the carbon fiber, taking care to not completely obstruct the barrel. Once the glass electrode is pulled, the carbon fiber should be attached to the half of the glass that forms the electrode. Finally the carbon fiber is cut with small scissors at both ends leaving only about 5 mm of extra carbon fiber protuding from the tip of the multibarrel electrode, and no extra carbon fiber protuding from the back of the multibarrel electrode. The carbon fiber will be a uniform diameter along its entire length because it does not

taper when heated and pulled. Once pulled these electrodes can be stored for up to one week in a dry container. We do not recommend storing electrodes beyond this one week period, as we have found that longer storage times (we have tried up to one month) lessen the chances of successfully filling the barrels with solution.

The manufacturing process up to this point takes about 10 minutes. The remaining part of the manufacturing process is performed just before the experiment.

Filling the electrodes with drugs. Each barrel is back-filled using a 34 gauge microfil syringe (MF34G, World Precision Instruments). Because our electrodes are unusually long and thin compared with multibarrel electrodes used in vitro and in more superficial structures in vivo they need long times to fill (see Figure 2.11D). Electrodes must be inspected under the microscope to ensure adequate filling, as electrodes with air bubbles are inadequate for delivering drugs using DC current and must be discarded. In our experience, the chance of encountering bubbles in the electrodes increases with longer tips size. We also found that the type of solution matters. Bubbles are rare in solutions containing substances that easily dissolve (e.g. GABA, gabazine in 165 mM NaCl), while they are frequently found in barrels with solutions containing substances that are hard to dissolve (e.g. bicuculline in 165 mM NaCl). Filters with small pore sizes (ISO-Disc Filters 0.2 μm, Supelco) are necessary when using the latter type of solution.

Before etching the tip of the carbon fiber, all the barrels are filled with the solutions of choice. This is important because etching the carbon fiber tip can contaminate the neighboring glass tips with carbon residue, which could prevent them from filling.

Tip forming. Electrodes in which the carbon fiber has been carefully trimmed at the tip can be used to record multiunit activity and large or sparsely packed neurons in which small tip sizes are not necessary, but we prefer to etch the carbon fiber tip to reduce its surface area (Fig 2.10A). To etch the tip of the carbon fibers we use a setup similar to that employed by other investigators, consisting of a standard AC transformer (9 V, 60Hz) that passes current between the tip of the carbon fiber and a salt solution (Fu and Lorden, 1996). One of the leads of the AC source is connected to a thin metal wire, such as copper or tungsten, which has been bent to form a small hook at its end. A small drop of salt water (e.g. 165 mM NaCl) is placed in this hook. The second lead of the AC source is connected to the carbon fiber. Other investigators have used silver paint or other types of conductive glue to attach the carbon fiber to a connector (Fu and Lorden, 1996; Kuras and Gutmaniene, 2000; Millar and Pelling, 2001), which is then attached to the second lead of the transformer. This procedure can be time consuming, thus complicating the fabrication process. Instead we use a saline solution (e.g. NaCl, 165 mM) as the interface between the carbon fiber and the transformer. The barrel containing the carbon fiber is filled with salt solution, and then a silver wire attached to the second lead of the AC source is introduced into the barrel. During recording the same saline solution will serve as the interface between the amplifier headstage and the carbon fiber. Eliminating the use of silver paint simplifies the manufacture of our multibarrel glass electrodes without compromising the quality of the recording (see Figs 2.12, 2.13, 2.14).

The optimal length of carbon fiber protruding from the tip depends on the target of recording; short tips (about 5 microns) are preferable to record activity in areas with densely packed neurons (e.g. Purkinje cell layer in the cerebellar cortex), while long tips

(15-20 microns) are preferable in areas with large and sparse neurons (e.g., big neurons in the deep cerebellar nuclei or reticular formation).

Guide tube system. We use a custom-built guide tube system to protect our electrodes as they are introduced into the brain. These guide tubes are built using stainless steel hypodermic tubes of increasing size from 25 G to 7 G. The smaller gauge (23 or 25G) penetrates the brain while the larger gauge (which is hollow) holds the body of the multibarrel electrode. Additionally, the large gauge easily fits our X-Y positioner system (Trent Wells). We prefer this compound guide tube system over a simpler single diameter guide tube because it stabilizes the multibarrel electrode and protects the glass from accidental breakage due to shearing forces.

Sterilization method. Because our electrodes are used for chronic recordings it is important to prevent infection by sterilizing any element that will come into contact with the brain. We use a two step sterilization process. In a first step electrodes are placed in a UV sterilizer for 1-2 hours. UV sterilization is typically used for surface sterilization but in our case, because we use glass, both glass and solution are sterilized. In the second part of the sterilization process we dip the tip of the multibarrel electrode in 70% alcohol for a few seconds. Our sterilization process doesn't seem to alter the effectiveness of the drugs (bicuculline, gabazine, GABA, glutamate, DL homocysteic acid, and baclofen).

Guide tubes, X-Y positioner, and polyimide tubes are sterilized in a 70% alcohol solution or an autoclave.

Loading multibarrel electrode into guide tube. Multibarrel electrodes are normally used in experiments that do not require the use of guide tube systems, such as anaesthetized

preparations where the dura mater is removed before the experiment, or in slice recordings. However, during chronic recordings guide tubes are necessary to protect the tip of the electrodes from the hard layers of scar tissue and dura mater. For chronic recordings it is preferable to leave the dura mater, and sometimes also the scar tissue above, intact to reduce the chances of infection. Regular metal microelectrodes can be placed inside the guide tube by passing the back of the electrode through the front of the guide tube in order to protect the delicate electrode tip; however this is not possible with multibarrel electrodes. We suggest a simple and highly successful method to insert the multibarrel electrode inside the guide tube without breaking its tip (Fig 2.10B). This method consists of first inserting into the guide tube a 30 gauge polyimide tube with one end cut at an angle (Fig 2.10Bi). The polyimide tube protrudes from both ends of the guide tube. Under a dissection microscope we carefully place the tip of the multibarrel electrode through the angled end of the polyimide tube, and then carefully advance the guide tube towards the multibarrel electrode (Fig 2.10Bii). The polyimide protects the tip of the electrode as it passes through the guide tube (Fig 2.10Biii).

Other suggestions to improve the success of recording. Although the step-by-step process of building glass multibarrel electrodes with carbon fiber described above should be sufficient to successfully build these electrodes, there are tricks that, if implemented correctly, significantly increase the success of recordings.

1. Dip the tip of the multibarrel electrode in sterile distilled water for 5 minutes before putting it inside the brain. This dissolves the salt crystals that form at the tip of the electrode and removes any alcohol residue.

2. One of the biggest problems we have encountered in our recordings is electrical shorting between barrels. To reduce the chance of this occurring, gently break the back end of each barrel with a pair of sharp forceps (after the barrels have been filled with solution). This breaks the glass filament inside the barrels and prevents the formation of an electrical bridge between barrels through the salt solution. We usually do this just before recording, after the electrode has been loaded into the guide tube and microdrive system. In addition, all electrical connections between the recording barrel and amplifier, and the injection barrels and iontophoretic pump should use insulated wire to prevent shorting between barrels.

3. Do not store the fabricated unfilled electrodes for more than a week. Electrodes that have been stored for long period of time (a week or more) tend to form more bubbles, possibly due to the accumulation of dust.

4. Always examine the electrodes under the microscope before introducing them into the brain, as the tip sometimes gets accidentally broken while handling the electrode in the final stages.

5. Before introducing the guide tube into the brain, clear a path for it by first puncturing the scar tissue and dura mater with a sharpened stainless steel tube.

6. Always try to minimize external sources of electromagnetic noise, as these electrodes can be more susceptible to interference than regular metal microelectrodes. For instance, we use an eye coil system to measure eye movements and have found that we need to optimize the current intensity to the field coils to give good spatial resolution without introducing too much recording noise. The field coils are usually the major source of

noise during our recordings. Decreasing the intensity of the field coils can completely eliminate this noise. In our recordings the intensity of the field coils is reduced to about 30% of its maximum. The resulting eye position spatial resolution is 0.09 degrees, above the minimum required for our experiments.

7. Once a barrel becomes blocked or otherwise stops passing current, it is unlikely that the barrel can be recovered and it is best to replace the electrode.

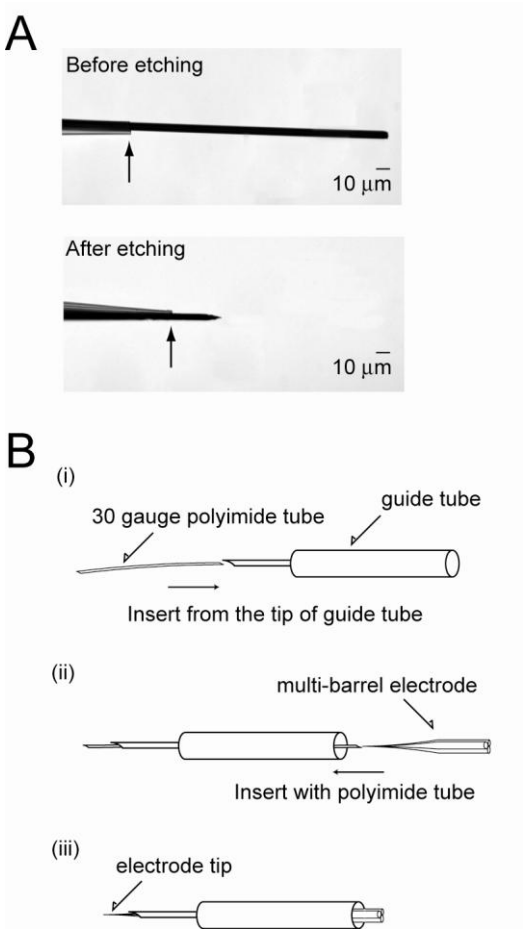

Figure 2.10. Etching carbon fiber (A) and loading multibarrel electrode into guide tube (B). In **A**, photomicrographs of multibarrel electrode tip before (top) and after (bottom) etching the carbon fiber. Arrows indicate edge of glass. In **B**, schematic representation of three step process to load multibarrel electrode into guide tube: (i) Insert polyimide tube into front of guide tube; (ii) Under a dissection microscope, gently insert tip of electrode into polyimide tube; (iii) Push electrode and polyimide forward. The polyimide tube will protect electrode tip as it passes through guide tube.

Results

General characteristics of multi barrel electrodes

We performed a series of measurements on a variety of electrode configurations to determine the "best" multibarrel electrode characteristics for achieving successful recording and iontophoretic injection. The properties we were concerned with were 1) the DC resistance of individual barrels, which gives an indication of both how susceptible the barrel is to clogging during an experiment and how much current can be delivered by the iontophoretic device; and 2) the time required to completely fill the barrels with solution, which determines the convenience and feasibility of preparing the electrodes for an experiment. We varied the concentration of sodium chloride in the filling solution (salinity) and the length of the electrode taper and found that both factors are key determinants affecting the resistance of the barrels and the ability to fill them in a reasonable period of time.

The electrodes used in the following section were all pulled so that they fit inside a 25 Gauge guide tube (25 G extra thin wall, Small Parts) for at least half of their length. The length of the taper was defined as the distance from the shoulder of the electrode where its shank begins to taper until its tip. Visual inspection under a light microscope revealed that the tip diameter of our multi barrel electrodes were 2-3 □m, with no difference among the three, four and seven barrel electrode configurations. The measurements in the following section were repeated on 10 barrels for each condition. All statistical tests for a significant effect of salt concentration or taper length on barrel resistance or fill time were performed using the Spearman Rank Coefficient test because a Bartlett test revealed that

the different groups did not meet the equal variance assumption required by ANOVA and many other statistical tests.

We filled multibarrel electrodes with sodium chloride solutions of several molarities. In those barrels that were free of bubbles after a reasonable waiting period (<4 hours) we measured the resistance with a Neurophore BH-2 (Medical system corporation, Great Neck, NY, USA) after placing the tip of the electrode in a beaker filled with 0.9% sodium chloride irrigation solution (Baxter Healthcare Corp., Deerfield, IL, USA) to approximate the extracellular resistance. Within the range of molarities that we tested, we found that the DC resistance of the barrels decreased as the molarity of the saline solution was increased ($p<0.001$ for all barrel configurations), reaching an asymptote around 150 mM NaCl (Fig 2.11A). This reduction in resistance comes at the cost of a decreased yield, as more of the electrodes that were filled with a high salt concentration had to be rejected due to incomplete filling or broken tips from salt crystallization. Thus saline concentrations above 150 mM offer little advantage in terms of reducing the barrel resistance.

Next, we investigated the dependence of barrel DC resistance on the length of the electrode taper. We constructed electrodes with three, four, and seven barrel configurations, each ranging in taper length from 45 to 65 mm. We filled all electrodes with 100 mM sodium chloride solution and measured their DC resistance using the Neurophore BH-2 and a 0.9% saline external solution. Figure 2.11B presents the measured resistances for the multibarrel electrodes. Within each barrel configuration, the barrel resistance monotonically increased as a function of taper length ($p<0.001$ for all barrel configurations; see Figure 2.11 for individual correlation coefficients and p-

values). In agreement with Figure 2A, the three barrel electrodes had the lowest overall resistance and the four and seven barrel electrodes had fairly comparable resistance, at least for the shorter taper lengths.

We have found that barrels with a resistance above 50 MOhms often become clogged during the course of an experiment, forcing us to replace the electrode. In order to avoid this, we generally strive to use electrodes with barrel resistance below this 50 MOhm threshold. Based on the measurements reported in Figures 2.11A and B, this can be achieved with NaCl concentrations above 50 mM for three barrels and 100 mM for four and seven barrels. This resistance threshold also limits the maximum electrode taper length that can be used. That is, taper lengths of up to 60 mm can be used with the three barrel configuration, while the four and seven barrel configurations are limited to 50 mm tapers.

As stated above, the reduction of barrel resistance created by higher salt concentrations must be weighed against the increased time required to fill the electrodes and the increased likelihood of bubble formation or tip breakage with these solutions. Figure 2.11C shows the time required to fill all barrels of the three, four, and seven barrel electrode configurations using a variety of sodium chloride concentrations ranging over two orders of magnitude (5 to 500 mM NaCl). Within the range of concentrations we used, there was a small but significant dependence of fill time on saline concentration for the three and four barrels ($p<0.01$), but not for the seven barrel configuration ($p>0.05$). Overall, the three barrel electrodes filled the fastest and the seven barrel electrodes filled the slowest.

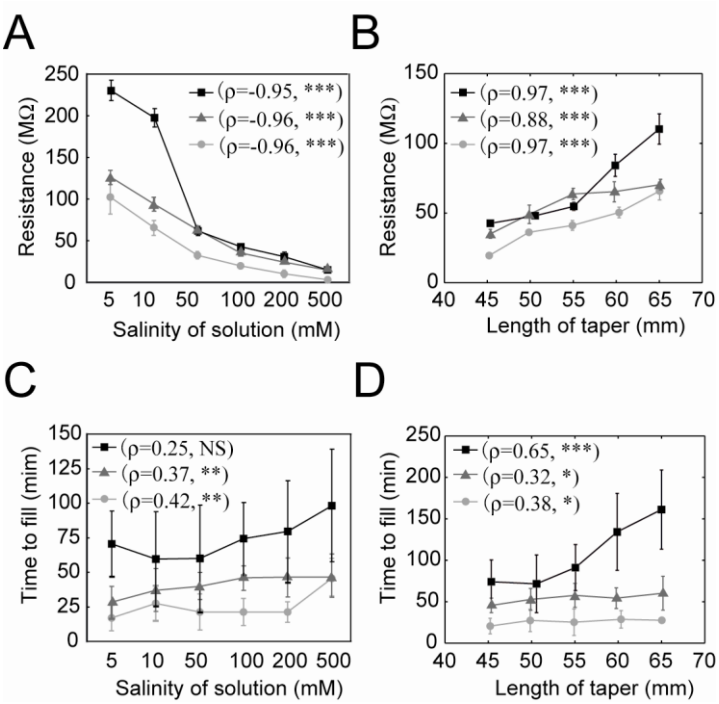

Figure 2.11. Measurements of barrel resistance (A,B) and barrel fill time (C,D) for three (circle), four (triangle), and seven (rectangle) barrel electrodes. A, B: Barrel resistance as a function of sodium chloride concentration (salinity; **A**) or taper length (**B**) for all three electrode configurations. C, D: Fill time as a function of salinity (**A**) or taper length (**B**). In A and C, all electrodes had 45 mm taper length. In B and D, all barrels were filled with 100 mM NaCl. All values are mean +/- 1 SD for 10 barrels. In each panel, ρ and asterisk, respectively, denote Spearman's rank correlation coefficient and level of significance of correlation in the Spearman's rank test: *(p<0.05), **(p<0.01), ***(p<0.001) and NS (no significance).

We next examined whether the time required to fill the barrels is influenced by the electrode taper length. Figure 2.11D summarizes the time required to fill electrodes constructed with different taper lengths using a 100 mM saline solution. Barrel length had a slight but significant effect on the time required to fill the barrels when using the three or four barrel configuration ($p<0.05$), and a larger effect with the seven barrel configuration ($p<0.001$).

Thus, once an electrode configuration is chosen, there are a wide range of salt concentrations and taper lengths that can be used without any major difficulties filling the

barrels. With three and four barrel configurations the limiting factor will likely be the consideration of barrel resistance, whereas fill time only really becomes an issue with the seven barrel configuration. Note, however, that as the number of barrels increases, the number of barrels that must be successfully filled in order to use the electrode also increases. For this reason, we usually choose the three or four barrel over the seven barrel configuration.

Example recordings and iontophoretic injection in different brain areas

To test the suitability of our electrodes for use in a variety of deep brain structures we performed recordings and simultaneous iontophoretic injections from several locations in the central nervous system of the squirrel monkey. For this purpose, we used three or four barrel electrodes up to 50 mm in length because we have found that these are among the easiest to work with for the reasons presented above. The barrel that contains the carbon fiber was filled with saline and used for recording (see Materials and Methods). A second barrel filled with 165 mM sodium chloride solution was used for current compensation. The remaining barrels were filled with solutions containing the drugs of choice (baclofen/DL homocysteic acid/GABA/bicuculline).

Figure 2.12 presents an example recording from a superior vestibular nucleus neuron that responded only during vestibular stimulation (whole body rotation; Fig 2.12A, B). This recording has a good signal-to-noise ratio and the spikes can be clearly separated from the background activity. One barrel of the three barrel electrode contained the GABA-B agonist baclofen, which was retained in the barrel with a -30 nA DC current. When a 40 nA current was injected to deliver the drug in the vicinity of the neuron, the neuron

responded within about 30 seconds by gradually decreasing its firing rate until it was almost completely shutdown, indicating the presence of functional GABA-B receptors within the area reached by the drug (Fig 2.12C) (Herz et al., 1969). The neuron still responded during head rotations, but with reduced amplitude compared with the control (compare Fig 2.12B and D).

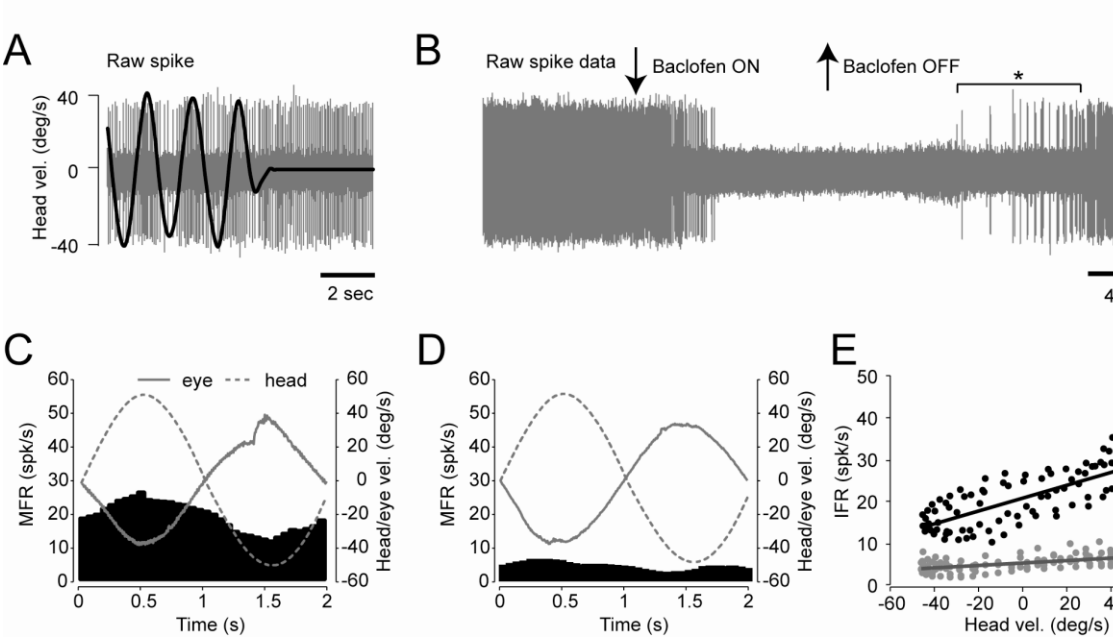

Figure 2.12. Vestibular-only (VO) neuron in superior vestibular nucleus (SVN) recorded before and during injection of the GABA-B agonist baclofen (50 mM, in 165 mM NaCl, pH 3.5) from one barrel of three barrel electrode (one barrel has the carbon fiber). In A, extracellular recording of the VO neuron (gray) with sinusoidal vestibular stimulus overlaid (black) during retention of baclofen in the barrel (-30 nA retention current). The neuron firing rate is modulated in phase with the vestibular stimulation (head velocity; C). In B, extracellular recording for a longer period of time showing time course of neuron firing rate decrease during the iontophoretic injection of baclofen (40 nA injection current). After the baclofen injection was stopped by applying a retention current, but before the neuron firing rate had recovered to its preinjection level, the vestibular stimulation was applied again (section indicated with asterisk; stimulus not shown for clarity), causing modulation of the neuron with a lower DC firing rate. Mean stimulus velocity, eye velocity and firing rate during vestibular stimulation before and during baclofen application are shown in C and D, respectively. In both C and D, black histogram is mean firing rate of neuron, gray dashed line is mean head velocity, and gray solid line is mean eye velocity. Bin size for histograms is 50 milliseconds. E, IFR and head velocity pre (black dots) and post injection (gray dots). Both black and gray solid lines are regression lines. Sensitivity for head velocity and baseline firing rate are 0.15 spk/s/deg/s and 20.7 spk/s before baclofen injection and 0.03 spk/s/deg/s and 5.2 spk/s during baclofen injection.

Figure 2.13 presents a putative flocculus target neuron (FTN) recorded in the Y-Group nucleus. This neuron responded during both eye movements evoked by optokinetic

stimulation (visual following) and vestibular stimulation during vestibular ocular reflex (VOR) suppression. When the excitatory amino acid DL-homocysteic acid was injected, the neuron quickly responded by increasing its mean firing rate (Fig 2.13A). This increase in firing rate did not change the gain of the neuron during optokinetic or vestibular stimulation (Fig 2.13B, C).

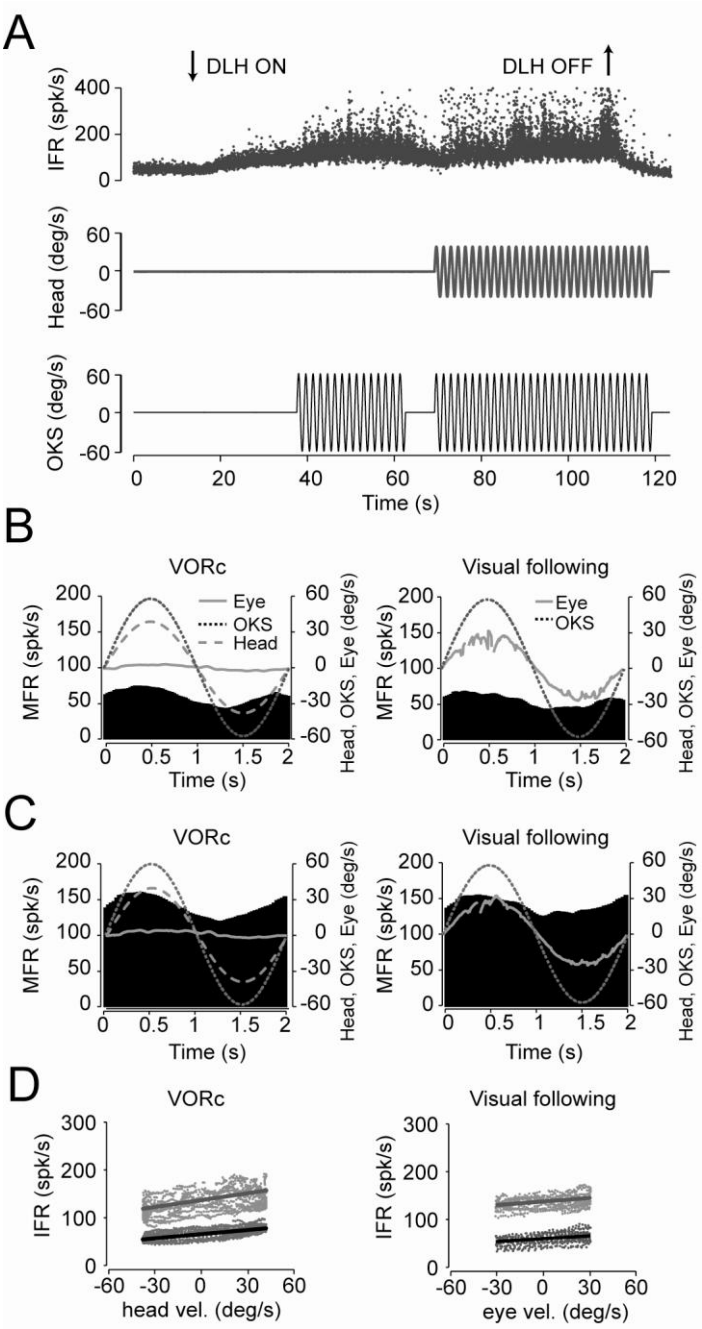

Figure 2.13. Y-Group flocculus target neuron (FTN) recorded before and during injection of the excitatory amino acid DL-homocysteic acid (DLH; 100 mM, in 165 mM NaCl, pH 3.5). In **A**, time course of DLH injection is shown. Top, instantaneous firing rate (IFR) of neuron; middle, vestibular stimulation; bottom, optokinetic stimulation (OKS). First block of stimulation is optokinetic only (visual following); second block is vestibular ocular reflex (VOR) cancellation induced by paired in phase rotation of vestibular table and optokinetic drum. B and C: Mean firing rate, stimulus velocity, and eye velocity before (**B**) and during (**C**) iontophoretic DLH application. Format is same as Fig 3, with the addition of average OKS trace (dotted line). Bin size for histograms is 50 milliseconds. In D, IFR plotted versus head velocity during VOR cancellation (left) or eye velocity during visual following (right). The format is the same as Fig.3. In the VOR cancellation, sensitivity for head velocity and baseline firing rate are 0.28 spk/s/deg/s and 64.4 spk/s before DLH injection and 0.47 spk/s/deg/s and 138.2 spk/s during DLH injection. In the visual following, sensitivity for eye velocity and baseline firing rate are 0.18 spk/s/deg/s and 50.6 spk/s before DLH injection and 0.24 spk/s/deg/s and 135.2 spk/s during DLH injection.

Our multibarrel electrodes are also capable of crossing the layer of dura mater covering the cerebellum (tentorium). Figure 2.14 shows a Purkinje cell recorded in the flocculus with a three barrel electrode in which one barrel contains GABA. The recording quality is similar to that generally achieved for flocculus Purkinje cells with a tungsten electrode. When GABA was injected with a 30 nA current, the neuron immediately responded by substantially reducing its firing rate. The neuron quickly recovered when the GABA injection was stopped by applying a -30 nA retention current, indicating that GABA is readily removed from the synaptic space.

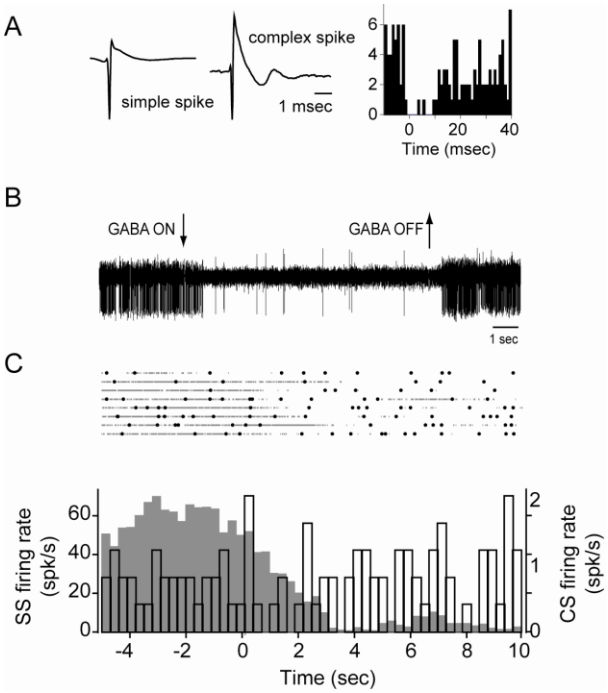

Figure 2.14. Recording of cerebellar Purkinje cell before, during, and after iontophoretic GABA injection (500 mM, in 165 mM NaCl, pH 3.5). In A, an example of simple spike (left), complex spike (middle) and simple spike interval histogram triggered by complex spike. The complex spikes show a characteristic longer "tail" than the simple spikes. In **B**, extracellular recording of simple and complex spikes from Purkinje cell, including time course of GABA injection. When GABA was retained in the barrel, the Purkinje cell had a high spontaneous discharge. Within a couple of hundred milliseconds of applying a 30 nA current to inject GABA, the simple spikes were almost completely shut down, leaving only complex spikes. When the GABA was again retained in the barrel, the neuron quickly recovered and began producing simple spike discharges at the same rate as before injection. In **C**, raster plot of simple spikes (gray lines) and complex spikes (black dots) and peri-stimulus time histogram (PSTH) of them (gray, simple spike; open black, complex spike). Bin size for the histogram is 300 msec. Time zero in the PSTH is the onset of GABA injection.

The real power of multibarrel electrodes is apparent when we load two or more different drugs into the barrels and examine their respective contributions to the neuron firing behavior. Figure 2.15 presents a neuron recorded in the Interstitial Nucleus of Cajal (INC). We used a four barrel electrode, with one barrel containing GABA and another containing the GABA-A antagonist bicuculline. This neuron showed a typical burst-tonic response during spontaneous saccadic eye movements while the drugs were retained during the control period (Fig 2.15A), consistent with the INC's role as part of the velocity to position neural integrator. When bicuculline was injected in isolation (Fig 2.15B), the neuron responded by substantially increasing the tonic eye position component of its firing rate, resulting in a higher baseline firing rate. This increase resulted in a shifting of the firing rate outside the normal range of the neuron. Injection of GABA had the opposite effect, reducing the overall firing rate range of the neuron (Fig 2.15C). Paired injection of bicuculline and GABA brought the neuron firing rate back within its normal range (Fig 2.15D), but the tonic eye position component of the firing rate, represented as the slope of the lines in Figure 2.15E, was higher than during the control period (compare black line in Fig 2.15E with green line). This indicates a specific effect of bicuculline on the neuronal eye position sensitivity that is not due to an increased overall responsiveness.

These example recordings indicate that our multibarrel electrodes are capable of recording from diverse areas deep within the primate brain. More complete characterizations of the neuronal responses to pharmacological manipulation will be presented in subsequent papers.

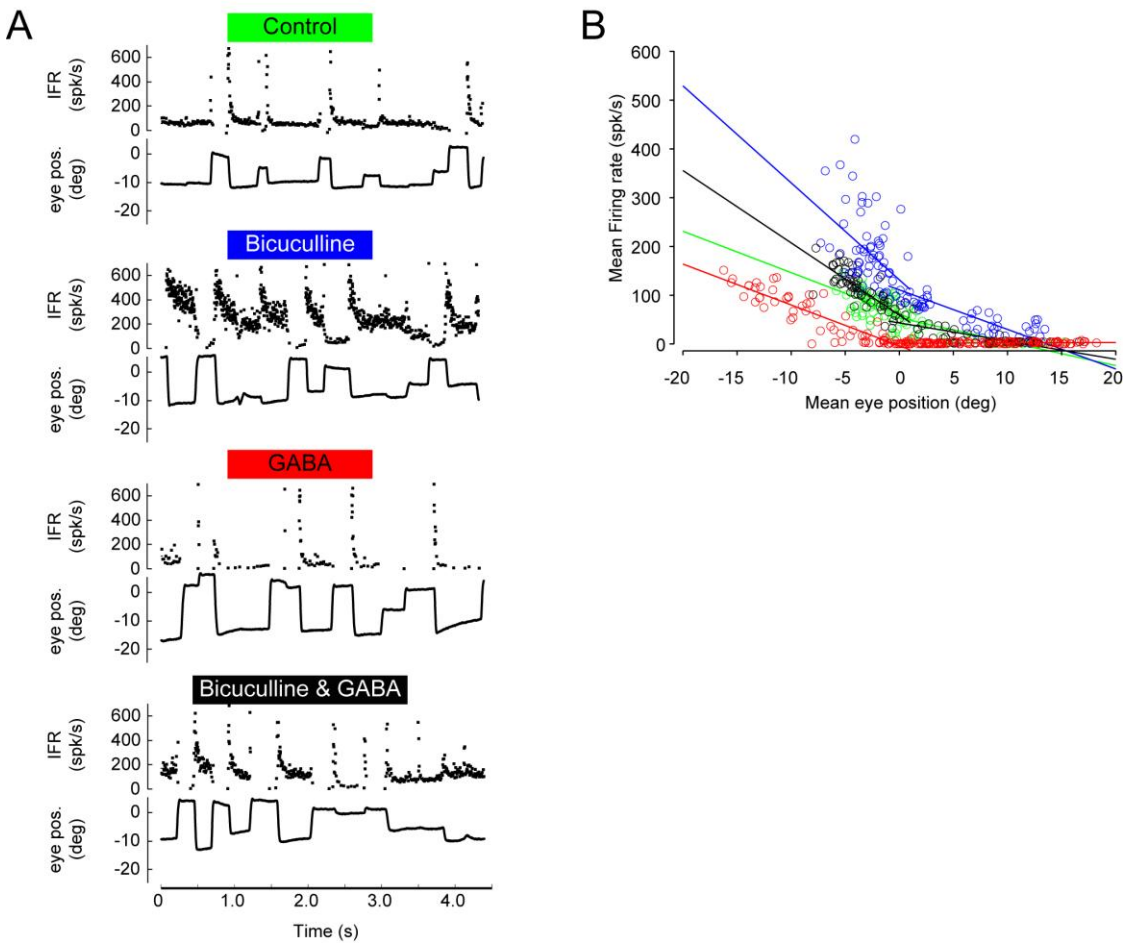

Figure 2.15. Recording of neuron in the Interstitial Nucleus of Cajal (INC) with four barrel electrode containing both GABA (500 mM, in 165 mM NaCl, pH 3.5) and the GABA-A antagonist bicuculline (20 mM, in 165 mM NaCl, pH 3.5). In **A**, example neuron responses during spontaneous eye movements under four conditions: top panel, retention of both drugs; second panel, injection of bicuculline only; third panel, injection of GABA only; bottom panel, injection of both bicuculline and GABA. In each panel, top trace is instantaneous firing rate and bottom trace is vertical eye position. In **B**, mean firing rate during fixation period between saccades (tonic eye position component) as a function of eye position for all four conditions in A. The slope of each line gives the eye position sensitivity of the neuron for each condition. Colors of the points and lines correspond to the headings above each panel in A. Green, control (no injection); Purple, bicuculline; Red, GABA; black, bicuculline and GABA.

Discussion

We have presented a detailed description of a fast and effective procedure for manufacturing multibarrel electrodes that use a carbon fiber for single unit recording. These electrodes can be used for experiments conducted in a variety of deep structures in the alert behaving primate. We have employed this technique with great success for the past three years and have not seen any increase in the number or degree of encephalic infections in our monkeys, indicating that the technique is suitable for recording in chronically implanted animals. The long, thin tapers of these electrodes easily fit inside a 25 gauge guide tube, which ensures limited tissue damage during repeated penetrations. In addition, we performed a parametric study of a variety of multibarrel configurations, including three, four, and seven barrels of different lengths and salt concentrations. This should aid investigators wishing to apply the technique to their own unique experimental needs.

References

1. Curtis, D. R., and Eccles, R. M. (1958). The excitation of Renshaw cells by pharmacological agents applied electrophoretically. *J Physiol* 141, 435-445.

2. Herz, A., Zieglgansberger, W., and Farber, G. (1969). Microelectrophoretic studies concerning the spread of glutamic acid and GABA in brain tissue. *Exp Brain Res* 9, 221-235.

3. Armstrong-James, M., and Millar, J. (1979). Carbon fibre microelectrodes. *J Neurosci Methods* 1, 279-287.

4. Armstrong-James, M., Fox, K., and Millar, J. (1980). A method for etching the tips of carbon fibre microelectrodes. *J Neurosci Methods* 2, 431-432.

5. Fox, K., Armstrong-James, M., and Millar, J. (1980). The electrical characteristics of carbon fibre microelectrodes. *J Neurosci Methods* 3, 37-48.

6. Anderson, C. W., and Cushman, M. R. (1981). A simple and rapid method for making carbon fiber microelectrodes. *J Neurosci Methods* 4, 435-436.

7. Millar, J., and Williams, G. V. (1988). Ultra-low noise silver-plated carbon fibre microelectrodes. *J Neurosci Methods* 25, 59-62.

8. Millar, J., and Williams, G. V. (1989). Effects of iontophoresis of noradrenaline and stimulation of the periaqueductal gray on single-unit activity in the rat superficial dorsal horn. *J Comp Neurol* 287, 119-133.

9. Williams, G. V., and Millar, J. (1990). Differential Actions of Endogenous and Iontophoretic Dopamine in Rat Striatum. *Eur J Neurosci* 2, 658-661.

10. Alloway, K. D., and Burton, H. (1991). Differential effects of GABA and bicuculline on rapidly- and slowly-adapting neurons in primary somatosensory cortex of primates. *Exp Brain Res* 85, 598-610.

11. Fu, J., and Lorden, J. F. (1996). An easily constructed carbon fiber recording and microiontophoresis assembly. *J Neurosci Methods* 68, 247-251.

12. Cudeiro, J., Rivadulla, C., Rodriguez, R., Grieve, K. L., Martinez-Conde, S., and Acuna, C. (1997). Actions of compounds manipulating the nitric oxide system in the cat primary visual cortex. *J Physiol* 504 (Pt 2), 467-478.

13. Kuras, A., and Gutmaniene, N. (2000). Technique for producing a carbon-fibre microelectrode with the fine recording tip. *J Neurosci Methods* 96, 143-146.

14. Millar, J., and Pelling, C. W. (2001). Improved methods for construction of carbon fibre electrodes for extracellular spike recording. *J Neurosci Methods* 110, 1-8.

15. Blazquez, P. M., Hirata, Y., Heiney, S. A., Green, A. M., and Highstein, S. M. (2003). Cerebellar signatures of vestibulo-ocular reflex motor learning. *J Neurosci* 23, 9742-9751.

16. Rivadulla, C., Martinez, L., Grieve, K. L., and Cudeiro, J. (2003). Receptive field structure of burst and tonic firing in feline lateral geniculate nucleus. *J Physiol* 553, 601-610.

17. Blazquez, P. M., Davis-Lopez de Carrizosa, M. A., Heiney, S. A., and Highstein, S. M. (2007). Neuronal substrates of motor learning in the velocity storage generated during optokinetic stimulation in the squirrel monkey. *J Neurophysiol* 97, 1114-1126.

18. Herrero, J. L., Roberts, M. J., Delicato, L. S., Gieselmann, M. A., Dayan, P., and Thiele, A. (2008). Acetylcholine contributes through muscarinic receptors to attentional modulation in V1. *Nature* 454, 1110-1114.

Chapter III

Golgi Cell Characterization in Ventral Paraflocculus

Abstract

Cerebellar processing of incoming information begins at the synapse between mossy fibers and granule cells, a synapse that is strongly controlled through Golgi cell inhibition. Thus Golgi cells are uniquely positioned to control the flow of information into the cerebellar cortex and understanding their responses during behavior is essential to understanding cerebellar function. Here we show for the first time that Golgi cells express a unique oculomotor-related signal that can be used to provide state and time specific filtering of granule cell activity. We used newly established criteria to identify the unique electrophysiological signature of Golgi cells and recorded these neurons in the squirrel monkey ventral paraflocculus during oculomotor behaviors. We found that they carry eye movement, but not vestibular or visual, information and that this eye movement information is only expressed within a specific range of eye positions for each neuron. Because they exclusively code eye movement information reflecting the efference copy pathway and are strategically positioned to modulate mossy fiber to granule cell throughput based on the state of the motor system, Golgi cells are candidate processing elements in the construction of forward models of movement, commonly hypothesized as a major function of the cerebellar cortex in motor control. A paper presenting these results is in review at the Journal of Neuroscience.

Introduction

The cerebellar cortex is among the most well-studied brain structures in terms of its microanatomy and synaptic connections, yet its function is still unknown. Past studies have revealed that the cortical circuit includes several distinct classes of excitatory and inhibitory interneurons whose influence is distributed among three layers: an input (granular) layer, an intermediate processing (molecular) layer, and an output (Purkinje cell) layer (Ramon y Cajal, 1911). The input layer is primarily occupied by granule cells, which receive glutamatergic input via mossy fibers projecting from other brain areas. The granule cells in turn provide the major glutamatergic input to Purkinje cells, which are the output neurons of the cerebellar cortex. Interspersed between this input and output is a rich network of GABAergic interneurons that influence signals at various stages in the circuit. Given all that we know about the circuit, it is astounding that the connection between form and function has not yet been made. One reason for this may be the paucity of data on the responses of the interneurons in alert animals, which has held back efforts to determine the processing that is carried out by the cerebellar cortex during movement. However, definitive identification of one specific class of interneuron in the alert animal has recently become feasible: the Golgi cell (Barmack et al. 2008; Holtzman et al. 2006; Simpson et al. 2005). Golgi cells are the main GABAergic interneurons influencing the input layer. They primarily receive inputs from mossy fibers and granule cell axons (parallel fibers) and strongly inhibit thousands of granule cells via an impressive axonal arborization (Eccles et al., 1964) (Fig 3.1A). Because all signals carried by the mossy fiber inputs must pass through the input stage, it is essential to understand how these signals are shaped by Golgi cell inhibition.

One potentially fruitful way to investigate the role of Golgi cell inhibition may be to consider what signal transformations are required within the cerebellar cortex, given the signals present at the inputs and the outputs of the structure. A hint of the signal transformations performed in the cerebellar cortex is suggested by a contemporary modeling approach to movement control; this approach suggests that the cerebellar cortex performs neural computations necessary for the construction of internal models for motor control (Pasalar et al., 2006; Ebner and Pasalar, 2008). For the oculomotor system, mounting evidence suggests that the cerebellum computes an internal representation of the eye movement (forward model) from an efference copy of the motor command. The output of the forward model is thought to be reflected in the target neurons of ventral paraflocculus (VPFL) Purkinje cells, but not in the eye movement input neurons to the VPFL (Ghasia et al., 2008). If this is true then the signal transformations necessary to compute a forward model of the movement would need to occur within the cerebellar cortex and would most likely involve interneurons such as Golgi cells.

We studied Golgi cells in the VPFL of the alert squirrel monkey during a variety of vestibular and oculomotor behaviors and provide the first evidence of a specific role of Golgi cells in filtering mossy fiber-granule cell throughput temporally and based on the state of the motor system. These results may have implications for the implementation of forward models within the cerebellum.

Materials and Methods

Subjects and surgery. Four adult squirrel monkeys (*Saimiri sciureus*; 3 males, 1 female) were used for these experiments, two of which were trained in oculomotor tasks (083, 087) and two of which were behaviorally naïve (066, 078). Surgery was performed aseptically under 1-2% isoflurane anesthesia to implant a scleral search coil for monitoring eye position and a stainless steel post for head restraint. After the monkeys were initially trained (2 monkeys) or acclimated to head restraint (2 monkeys), a second surgery was performed to implant a stainless steel recording chamber aimed at the cerebellar floccular complex. Additional details of the surgical procedures can be found elsewhere (Blazquez et al., 2003). Ninety percent of the neurons reported here come from the two trained monkeys, with the remaining data from untrained monkeys confirming the general applicability of the results. All procedures conformed to the National Institutes of Health Guide for the Care and Use of Laboratory Animals and were approved by the Washington University Institutional Animal Care and Use Committee.

Neural recording. Single- and multiunit recordings were made in the cerebellar flocculus using 2-5 M□ tungsten electrodes (FHC, Bowdoin, ME). The raw signals were amplified, band-pass filtered between 100 Hz and 8 KHz using an 8-pole filter, and digitized at 40 KHz using a Power 1401 and Spike2 software (CED, Cambridge, UK). Spike times of single units were detected online using a time-amplitude window discriminator (Bak, Mount Airy, MD) and were recorded digitally as time stamps. Spikes were always resorted offline prior to analysis using Spike2 template matching and principal

component analysis routines. Eye position, laser position, and chair and drum positions were sampled at 500 Hz using the same Power 1401.

Recordings were confined to the ventral paraflocculus, which was recognized by its typically strong saccade-related hashing and was verified by histological track reconstruction. Golgi cells were identified based on established criteria, as discussed in the Results section. Briefly, these criteria include localization in the granular layer, large spike waveforms with wide spike widths that often remain isolated for greater than 100 microns of electrode travel, tonic and often extremely regular firing rates, and lack of complex spikes.

Behavioral protocols. Head-restrained monkeys were comfortably seated in a primate chair mounted atop a vestibular table. Oculomotor training consisted of a standard water restriction protocol to motivate the monkey to fixate and pursue a projected laser for liquid reward. Response modality of Golgi cells (i.e., eye movement, vestibular, or visual) was determined by having the monkey fixate or pursue a sinusoidally moving (0.2, 0.4, or 0.5 Hz, +/- 5, 8, or 10 deg) green laser projected on a screen 60 cm in front of the monkey under three conditions: 1) Smooth pursuit, in which the head was held stationary while the laser moved; 2) Vestibulo-ocular reflex suppression (VORS), in which the laser was rotated in phase with the chair and the monkey was required to cancel its VOR); and 3) Fixation during whole-field stimulation (F-WFS), in which the laser and head were held stationary and the monkey was required to maintain fixation on the laser spot during movement of a patterned background.

During the free-viewing condition, monkeys were turned around such that they faced the experimental room instead of the screen, and were encouraged to make eye movements throughout their oculomotor range by the experimenter placing objects of interest at varied horizontal and vertical positions relative to the monkey.

Data analysis. All data were imported to Matlab (Mathworks, Natick, MA) using the SON Library (Malcolm Lidierth, Kings College London) and analyzed in Matlab using custom written routines. Spike times were converted to instantaneous firing rates (IFR) by taking the reciprocal of the interspike intervals. Multi-unit activity was analyzed by rectifying the raw extracellular waveform and smoothing it with a moving average filter (10 ms window) to extract the envelope. The resulting waveform was downsampled to match the sampling rate of the eye.

The median CV_2 was used to quantify the regularity of neurons. It is similar in principle to the coefficient of variation (CV), but it is less susceptible to large variations due to changes in firing rate because it only considers adjacent interspike intervals, and is therefore better suited for analyzing non-stationary firing rates (Holt et al., 1996). CV_2s were calculated from interspike intervals (ISIs) as $CV_2 = 2\,|ISI_{n+1} - ISI_n| \,/\, (ISI_{n+1} + ISI_n)$.

Preferred directions of units were calculated from spontaneous eye movements using a perisaccade time histogram approach with 45 or 90 degrees of resolution, as explained in the Results section. After generating PSTHs we found the directions that produced the

largest peri-saccadic increase and decrease in firing rate and considered these the preferred directions for on and off responses, respectively. We then calculated the mean change in firing rate within a 100 ms window following the first significant change in firing rate for the preferred direction and compared this value with the mean change in firing rate during the same time epoch for each of the three other directions. The first significant change in firing rate was defined as the first time that the firing rate rose above or dropped below two standard deviations of the mean firing rate during a pre-saccade control period and stayed above or below for at least 100 ms. The time difference between saccade initiation (50 deg/s velocity threshold) and this first significant change in firing rate was taken to be the latency of the neuron. We analyzed on and off responses independently.

Golgi cell initial changes in IFR were generally well approximated by a rising or falling exponential. However, because of the limited number of data points (i.e. spikes) occurring during this initial phase an exponential fitting was not always reliable on a saccade-by-saccade basis, so we approximated time constants by measuring the time from the initial change in IFR to the time at which the neuron reached 63% of its maximal or minimal value. Time constants were measured from the IFR data during spontaneous or visually guided saccades. For each neuron, five saccades each were selected in the on or off directions and the time constant of the neuron was taken as the mean of those five measured time constants. When time constants couldn't be measured in the off direction because the IFR went to zero within a single interspike interval, the time constant was assigned a value of zero (e.g., see example neuron in Fig 3.3A).

Because this method of calculating time constants depends on precisely detecting the timing of changes in firing rate on a trial-by-trial basis, time constants could only be measured for the more regular Golgi cells (typically those with median CV_2s below 0.2).

Eye position fields were measured from spontaneous eye movement data using an algorithm that considers the correspondence of changes in firing rate with starting and ending eye positions of saccades. The motivation behind this approach is exemplified in Fig 3.7. When the monkey makes saccades in the on direction of the neuron, the firing rate increases as long as a portion of the eye movement is encompassed by the eye position field of the neuron. That is, saccades made into or out of, as well as within, the eye position field result in changes in firing rate, but saccades made entirely outside of the field produce no change. Considering a series of small sequential saccades in the on direction starting on one extreme of the oculomotor range and ending on the other, the neuron will first start responding when a saccade endpoint crosses into the position field and it will stop responding when a saccade start point crosses out of the position field. Thus, the area between the first saccade endpoint producing a change in firing rate and the last saccade start point producing a change in firing rate defines the position field of a neuron. In practice this was measured using an interactive program that displayed the instantaneous firing rate and eye position traces around each saccade and allowed the experimenter to indicate the change in instantaneous firing rate following a saccade by marking the initial firing rate immediately preceding the saccade and the maximum firing rate during the post saccade fixation period. These measured changes in firing rate were then sorted based on either the starting or ending eye position for the saccade (projected

along the preferred direction vector of the neuron) and averaged in two degree bins to generate two curves, as seen in Fig 3.7C. One curve represents the changes in firing rate for all saccade endpoints and the other represents the changes in firing rate for all saccade start points. The intersection of these two curves defines the eye position field.

Results

To address the role of Golgi cells in cerebellar processing during oculomotor behaviors, we recorded single-unit activity in the granular layer of the ventral paraflocculus (VPFL) in alert behaving squirrel monkeys and used newly established criteria to identify the characteristic activity of Golgi cells *in vivo*. The VPFL granular layer was recognized based on the presence of eye movement-related "hashing" activity, large unitary discharges and presumed mossy fiber discharges, and the absence of complex spikes (Blazquez et al. 2003; Lisberger et al. 1978a; Miles et al. 1980). In the granular layer, we commonly encountered two kinds of single unit activity. The first were units with narrow spikes (~100 us peak to trough time), which usually discharged with a burst/burst-tonic eye movement-related response, a vestibular-related response, or a combination of eye and vestibular-related responses. These units often had short tracking distances, matched the character of the background hashing, and were difficult to maintain in isolation for extended periods of recording. Therefore, these units were presumed to be mossy fibers (Lisberger and Fuchs, 1978b; Miles et al., 1980; Noda, 1986). The second units we often encountered were usually tonically active, had broader spikes (>200 μs peak to trough time) and lower median firing rates, and isolation could often be maintained for more than 10 minutes and sometimes up to an hour. This second type of unit was almost always heard in the background when passing through the granular layer but was not always possible to isolate. These units were determined to be Golgi cells based on the spike profiles and interspike interval distributions of morphologically identified Golgi cells published by others (Vos et al., 1999; Simpson et al., 2005; Holtzman et al., 2006; Prsa et al., 2009), and the absence of complex spike responses characteristic of Purkinje

cells (Thach, 1968). Figure 1B shows the location of an electrolytic lesion made after recording one of these presumed Golgi cells, confirming its position in the granular layer.

We recorded a total of 69 putative Golgi and 40 Purkinje cells in 4 squirrel monkeys (083, 087, 066, and 078). We quantified the spike patterns of the Golgi and Purkinje cells using their median firing rate and median CV_2. Others have shown that the median firing rate is the most useful known criterion for identifying Golgi cells (Holtzman et al., 2006). We found that this was true among our population of neurons as well. In addition, we found that Golgi cells exhibited a high variability in firing rate regularity, which we quantified using the CV_2 metric [(Holt et al., 1996; Shin et al., 2007); see Methods]. Figure 1C shows a scatter plot of median CV_2 values versus median firing rates for all recorded Purkinje and presumed Golgi cells. Although Golgi cells were capable of reaching firing rates as high as 100 Hz, 87% (n=60) of them had median firing rates below 50 spk/s, whereas 93% (n=37) of Purkinje cells had median firing rates above this value. The median CV_2 metric also allows separation of Purkinje and Golgi cells, but with more overlap between distributions than the median firing rate. The majority of Golgi cells (61%, n=42) had CV_2s lower than 0.2, indicating a high regularity absent in the Purkinje cell population. We have included in our plot of Golgi cells the three neurons with median firing rates greater than 80 spk/s because these neurons met our criteria for identification, though they responded differently during our tasks than the rest of the population and we suspect they may be unipolar brush cells. For comparison with Fig 1 of Holtzman and colleagues (2006), Figure 1D shows the median ISI distribution of the neurons displayed in Fig 1C. Despite the difference in species (monkey vs. rat) and

behavioral state (awake vs. anesthetized), our Purkinje and Golgi cell ISI distributions are qualitatively similar to those of Holtzman and colleagues, albeit with ours shifted towards shorter median ISIs. We now describe the characteristic responses of this population of Golgi cells in the context of vestibulo-oculomotor behaviors known to involve the VPFL.

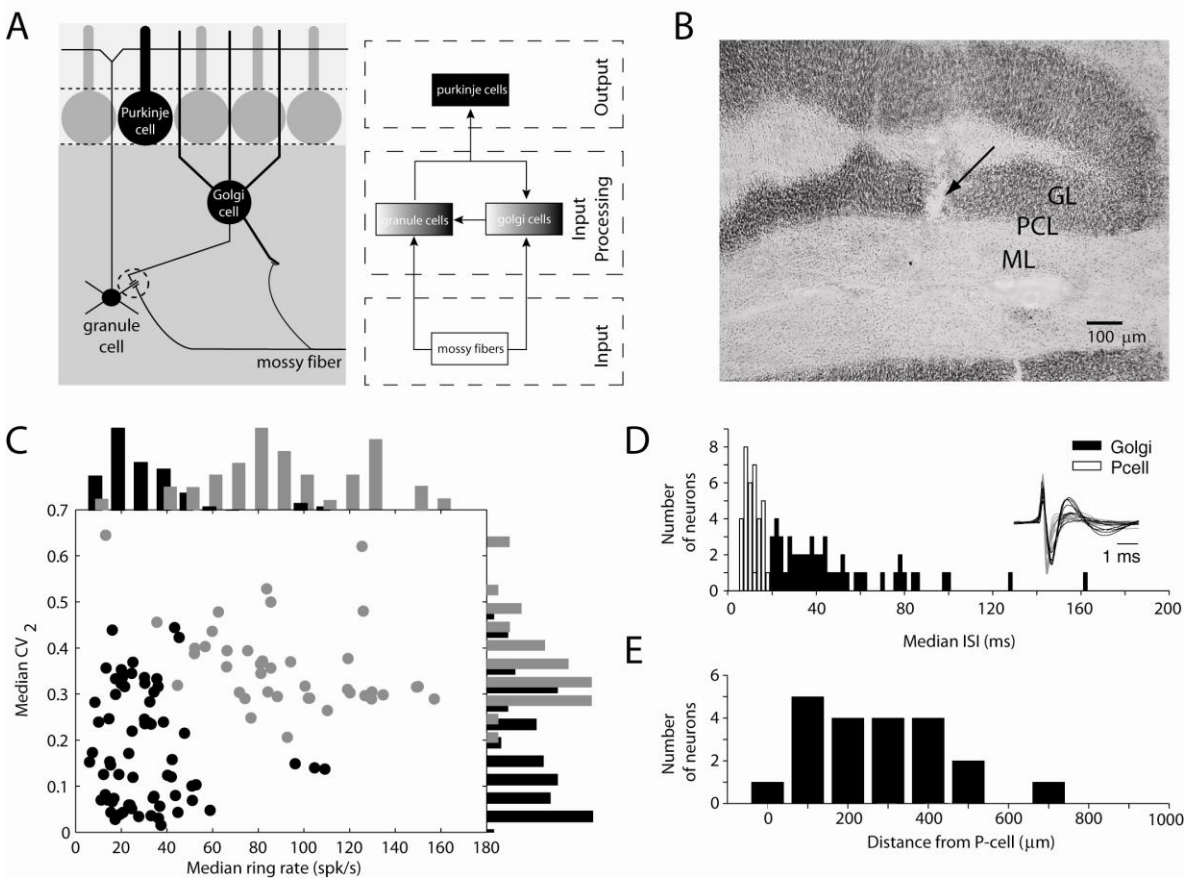

Figure 3.1. Influence of Golgi cells on cerebellar cortex input layer processing and identification of Golgi cells. A, Schematic diagrams illustrating the position of Golgi cells within the cerebellar cortex circuit. Golgi cells receive mossy fiber inputs via their descending dendrites and soma, and parallel fiber inputs via their ascending dendrites. They strongly inhibit granule cells, which are the main glutamatergic input to Purkinje cells. Because granule cells receive inputs from mossy fibers and in turn provide an input to Golgi cells, this circuit configuration gives Golgi cells both feedforward and feedback control over granule cells. B, Location of electrolytic lesion (arrow) placed after recording a putative Golgi cell in the VPFL. The lesion is located in the granular layer (GL), identified as the dark regions in this nissl stain. The Purkinje cell layer (PCL) and molecular layer (ML) are also indicated for reference. Stimulation parameters: 15 uA cathodal current for 15 seconds. The location of the Golgi cell recordings was confirmed in two additional lesions. C, Scatter plot of median CV2 and median firing rate for 69 Golgi cells (black) and 42 Purkinje cells (gray) identified based on the presence of complex spikes. The corresponding normalized density histograms are shown on the upper and right edges of the axes. D, Histograms of median interspike intervals for all of the Golgi and Purkinje cells shown in C and corresponding spike waveforms for a subset of 10 representative neurons from each group. E, Distribution of Golgi cell distances from Purkinje cell layer for 21 neurons for which adequate depth measurements were taken.

Golgi cells in the VPFL exclusively code eye movements during visuo- and vestibulo-oculomotor behaviors

The primate VPFL receives mossy fiber input from diverse sources that convey

vestibular, visuomotor, and eye movement information (Langer et al., 1985). Indeed, single Purkinje cells in the VPFL, the output neuron of the structure, also contain signals reflecting each of these pathways (Lisberger and Fuchs, 1978a; Miles et al., 1980; Noda and Warabi, 1987). Because, like Purkinje cells, the broad ascending dendritic trees of Golgi cells also receive inputs from the parallel fiber system, which is thought to convey converging information from different modalities (eye movement, vestibular, and visual), we hypothesized that single Golgi cells would respond to all major inputs to the flocculus in a similar manner as Purkinje cells. We recorded Golgi cells while the monkeys performed tasks that isolate the signals of each modality, namely pursuit, VOR suppression (VORS), and fixation with whole-field optokinetic stimulation (F-WFS) (see Methods). We recorded a total of 48 Golgi cells during only the pursuit task, 23 Golgi cells during the pursuit and VORS tasks, and 7 Golgi cells during all three tasks. Surprisingly, in contrast to Purkinje cells, Golgi cells responded to eye movements but not to head movements or visual motion. Figure 2 presents the responses of a representative Golgi cell during spontaneous saccades (A), pursuit (B), VORS (C), and F-WFS (D). This Golgi cell had a median CV_2 of 0.09 and median firing rate of 38 spk/s. The neuron modulated to changes in eye position during spontaneous saccades (A) and approximately in phase with changes in eye position during pursuit (B), but was unmodulated during VORS or F-WFS, indicating the lack of a vestibular or visual motion response. Figure 2E-G show the average Golgi cell firing rate over at least 5 cycles plotted against eye position, head velocity, or visual motion (retinal slip) velocity during pursuit, VORS, or F-WFS, respectively. A regression fit to each curve reveals that the changes in eye movement during pursuit contribute the most to the firing rate modulation

(slope=2.3, 0.06, and -0.04, respectively). This dominance of eye movement responses was seen across the population of Golgi cells tested (Fig 2H, mean ratio of pursuit/VORS slopes: 19.5; Fig 2I, mean ratio of pursuit/F-WFS slopes: 7.2). Note the strong clustering of data points along the ordinate axis in Figures 2H and I, indicating a lack of vestibular or visual motion responses by the population of Golgi cells. This exclusive coding of eye movements was also present during behaviors that recruit the different pathways in combination such as head rotation during fixation of an earth-fixed target (Fig 3). Golgi cell modulation during the VOR with target task was identical to the modulation during pursuit in the absence of head movement, which is consistent with an exclusive coding of the eye movement and indicates that Golgi cells in the VPFL respond to eye movements irrespective of whether they are driven by the pursuit or vestibular system.

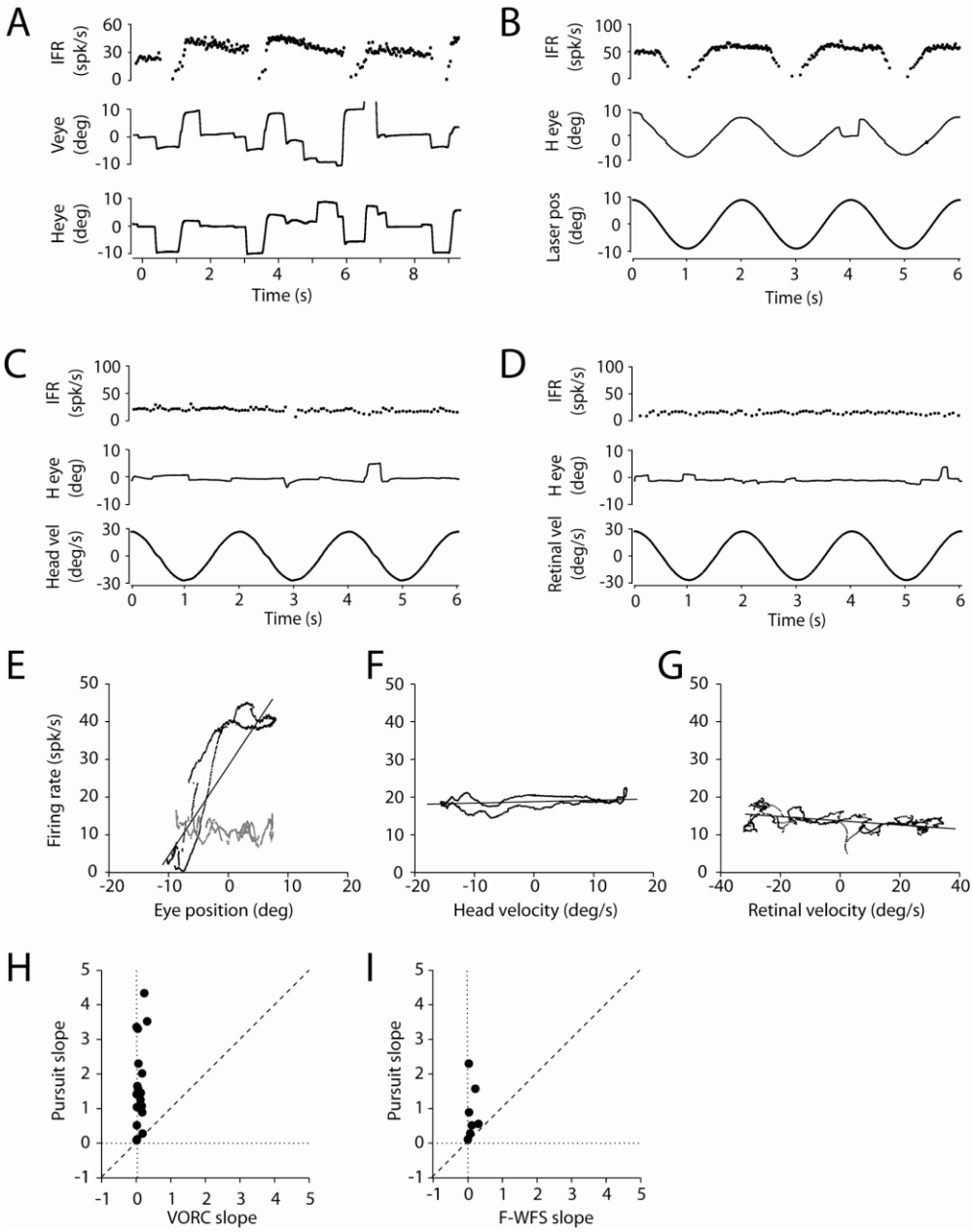

Figure 3.2. Eye movement only coding by Golgi cells. A, Response during spontaneous eye movements for a representative Golgi cell. From top, instantaneous firing rate (IFR), vertical, and horizontal eye position. Response of the same neuron during smooth pursuit (B), VOR suppression (C), and F-WFS (D). E-G, plots of average firing rate versus eye position during pursuit (E), head velocity during VOR suppression (F), and retinal slip velocity during F-WFS with corresponding regression fits (black). E, In black and gray are average firing rate during horizontal and vertical pursuit, respectively. H-I, slope of regression line during pursuit plotted versus slope of regression line during VOR suppression (H) or F-WFS (I) for all neurons recorded during these tasks (H, n=23; I, n=7).

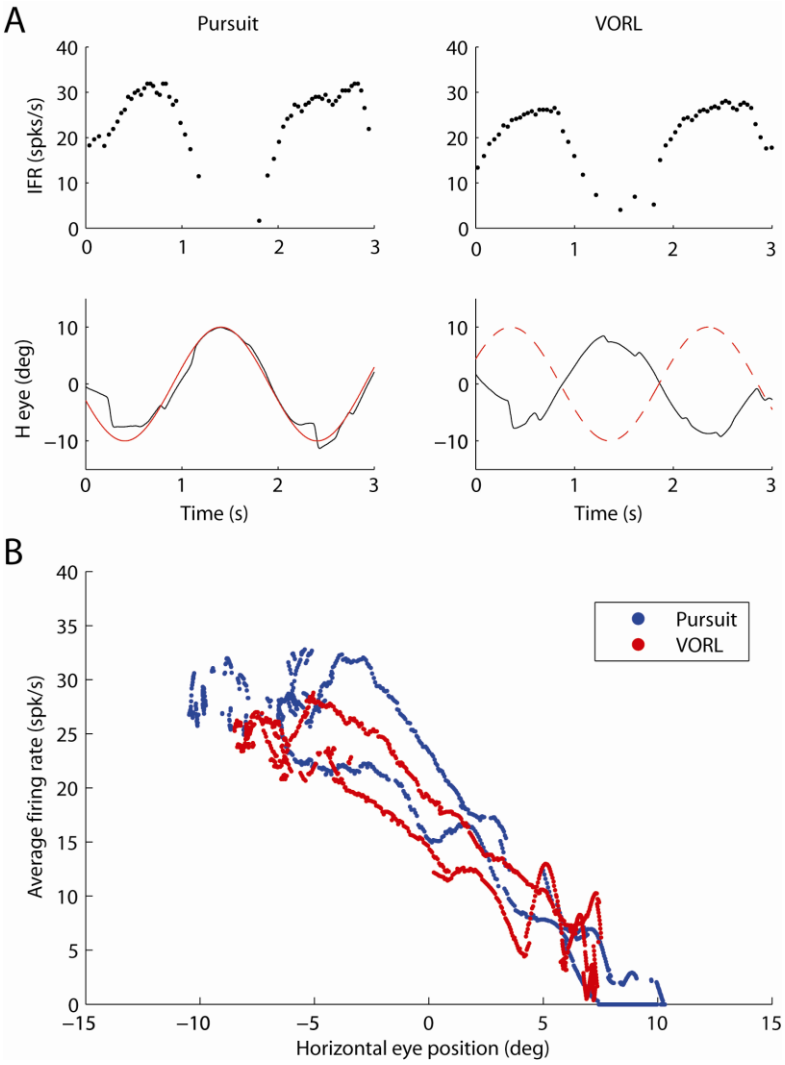

Figure 3.3. Similarity of Golgi cell firing rate modulation during pursuit and VOR with target when net eye movement is similar. A, Instantaneous firing rate (IFR, top) and horizontal eye position (H eye, bottom) for a Golgi cell during pursuit (left) or VOR with a target (VORL, right). Red curves in bottom plots indicate laser (solid) or chair (dashed) position. B, Average firing rate versus horizontal eye position for the same Golgi cell during pursuit (blue) or VORL (red). The firing rates were averaged over at

Similarly to many of the VPFL mossy fibers conveying eye movement signals (Miles et al, 1980), Golgi cells also responded to eye movements during saccades. Therefore, we used spontaneous (free viewing condition; see Methods) and visually-guided saccades to more fully quantify the properties of the eye movement coding by Golgi cells. Figure 4 shows the diversity of Golgi cell responses during spontaneous eye movements for 4 different representative neurons (A-D) and the population as a whole (E-F). The most

common type of response seen in Golgi cells during spontaneous eye movements was a sudden decrease (Fig 4A), and in many cases, a complete pause (Fig 4B) in the firing rate following a saccade in a particular direction, which we refer to as the "off" direction (78% [54/69]). In some cases the pause was preceded by an initial burst, but this was not always present, even for different saccades within the same neuron. Following a pause, the Golgi cell firing rate gradually recovered towards a tonic level. This recovery was usually cut short by a response to the next spontaneous saccade. In some neurons, we were able to measure the time course of the recovery more fully by having the monkey make saccades to laser targets and fixate for more extended periods; the recovery time constants ranged from 110 to 820 ms (mean, 438 +/- 361 ms, n=21).

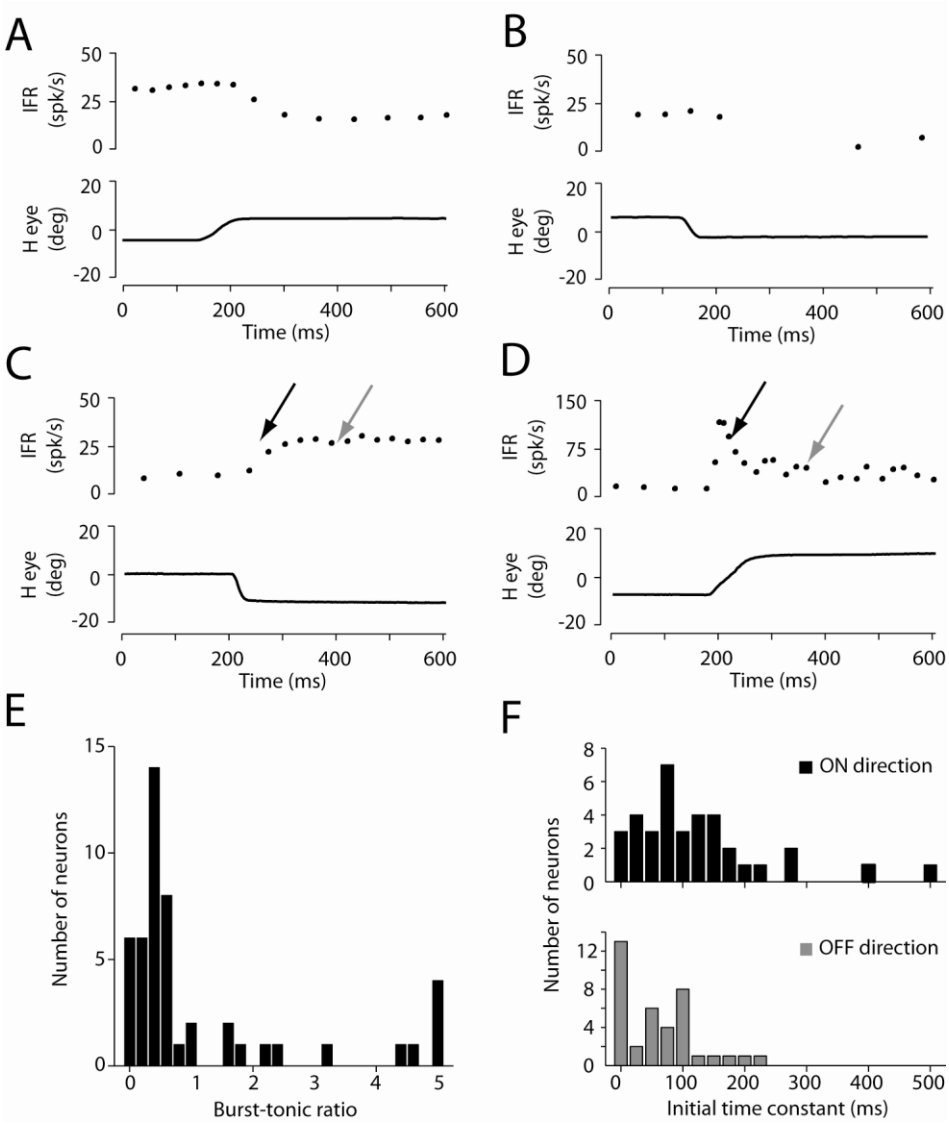

Figure 3.4. Temporal properties of Golgi cell responses. A-D, representative off (A,B) and on (C,D) responses of 4 different Golgi cells during saccades. Top, instantaneous firing rate (IFR); bottom, horizontal eye position (Heye). E, Distribution of burst-tonic ratios for 49 Golgi cells with significant on responses. Arrows in C and D indicate regions used to calculate burst tonic ratios (see text). F, Distributions of on (top) and off (bottom) initial time constants for 34 Golgi cells.

Additionally, 71% (49/69) of Golgi cells showed an increase in firing rate with changes in eye position, which we refer to as an "on" response, that was noticeably distinct from a rebound following an off response (Fig 4C). A subset of Golgi cells displayed rapid

bursts for saccades in the on direction, similar to typical mossy fiber burst-tonic responses (Fig 4D, n=12, 25%), while the majority experienced more gradual increases in firing rate following a saccade in the on direction (n=37, 75%). These gradual increases in firing rate are not seen in VPFL mossy fiber population (Miles et al, 1980; Lisberger and Fuchs, 1978b) and could reflect a low-pass filtering of eye movement signals by the Golgi cells. The "burstiness" of the population of Golgi cells is quantified in Figure 4E as a burst-tonic ratio, calculated as the ratio of the maximum firing rate within the first 50 ms following response onset and the maximum firing rate between 100 and 150 ms from response onset. Ratios above one would indicate that the burst accounts for the dominant change in firing rate of the neuron. Contrary to this, the majority of Golgi cells had burst-tonic ratios below one (median burst-tonic ratio, 0.49), indicating that the population of Golgi cells had gradual excitatory responses compared to burst-tonic mossy fibers. These responses were more gradual than the off direction responses, with time constants often greater than the duration of the saccade (Fig 4F; mean off direction time constant: 61 +/- 62 ms, mean on direction time constant: 124 +/- 107 ms, n=34; $p<0.005$, Mann-Whitney U Test). Similarly to off direction responses, following the initial on response, Golgi cell firing rates decayed down to a tonic rate. The time constants of this decay were often longer than the squirrel monkeys were capable of fixating on a laser target, so we were unable to calculate time constants representative of the population. However, others have found the value of this time constant in the macaque to be around 6.5 seconds on average for a similar population of presumed Golgi cells (Miles et al., 1980).

Contrary to the differences in initial time constants, Golgi cells had similar latencies to the first significant change in firing rate (>2 SDs above or below mean pre-saccadic firing rate) for on and off responses, as measured during spontaneous saccades, and the responses tended to lag the eye movement (on: 36.4 +/- 65.3 ms, off: 29.9 +/- 54.6 ms; mean +/- SD; p=0.88 Mann-Whitney U Test). This suggests that a similarly timed input is responsible for both the on and off responses of the Golgi cells but that the temporal dynamics of the input, or the Golgi cell response to the input, is different for on and off responses.

Because others have reported that Golgi cells in the oculomotor vermis have broad directional tuning for saccades (Prsa et al., 2009) and that Golgi cells in crus I/II have large cutaneous receptive fields (Vos et al., 1999; Holtzman et al., 2006), we sought to determine how broadly tuned Golgi cells in the VPFL are for eye movements. To address this question we analyzed separately the tuning of on and off responses during spontaneous eye movements. To ensure that we had a sufficient number of saccades to produce reliable averages for a large number of cells, we segmented the oculomotor space into four 90 degree zones centered on each of the cardinal directions and assigned each saccade to a zone based on the direction of the saccade vector. We then computed peristimulus time histograms (PSTHs) by binning together Golgi cell spikes, aligned on saccade onset, for all saccades falling within a zone. This gave us four separate PSTHs, each representing the peri-saccadic activity of the Golgi cell for saccade directions falling within +/- 45 degrees of each of the cardinal directions (Fig 5A; see Methods). Figure 5B-C presents the results of this analysis for 49 neurons with significant on responses and

54 neurons with significant off responses. The numbers along the abscissa indicate the cardinal directions with the highest, second highest, third highest, and lowest response for each neuron, and the ordinate axis indicates the response magnitude for that direction, normalized by the response in the preferred cardinal direction. Values of one for every direction would indicate that the neuron has an omnidirectional response, and values of one for only the preferred direction (direction 1) would indicate a narrowly tuned neuron to that cardinal direction. In support of the latter, 65% of neurons (32/49) showed an on response for the second most responsive direction that was less than 50% of the maximal on response (in the preferred direction), and 96% (47/49) showed a less-than-half maximal response for the third most responsive direction. Likewise, 70% of neurons (38/54) showed an off response for the second most responsive direction that was less than 50% of the maximal off response, and 93% (50/54) showed a less-than-half maximal response for the third most responsive direction. Thus our VPFL Golgi cells were more narrowly tuned than the OMV Golgi cells of Prsa and colleagues (2009), as a majority of their Golgi cells would be expected to have greater-than-half maximal responses for at least three zones under our analysis method. The narrow directional tuning of our Golgi cells was further supported by analysis of vertical and horizontal pursuit data obtained from 29 Golgi cells (Fig 6). Seventy-six percent of the neurons (n=22) modulated at least twice as much during pursuit in the preferred plane compared to the orthogonal plane, with a median ratio of 5.5 (slope preferred/slope orthogonal). This result stands in contrast to Golgi cell responses reported in the oculomotor vermis and crus I/II, and may reveal a functional difference between the ventral paraflocculus and other cerebellar areas.

The preferred directions calculated during spontaneous saccades were uniformly distributed among the four zones for both on (n=14/11/15/9; ipsi/contra/up/down) and off responses (n=13/11/13/17; ipsi/contra/up/down). However, not all neurons were tuned for the cardinal directions. The fact that many cells did not respond strongly in the third most responsive direction indicates that many of the cells were tuned for non-cardinal directions. We confirmed this by generating 8 zone PSTHs for 24 cells with a sufficient number of spontaneous saccades and found that 92% of cells had greater-than-half maximal responses for 3 or fewer 45 degree zones, and 58% of the cells had greater-than-half maximal responses for exactly 3 zones. This argues both that Golgi cells are narrowly tuned, and that a sizeable proportion of them have non-cardinal preferred directions. Indeed, when preferred directions were approximated from the 4 zone PSTHs for all Golgi cells by taking the vector average of responses to the first and second maximal directions, 46% of the neurons had preferred on directions and 51% had preferred off directions more than 15 degrees from a cardinal direction. Furthermore, on and off directional preferences tended to be counter-weighted. In 85% (34/40) of the neurons that had both significant on and off responses, the preferred directions for the on and off responses pointed in opposite directions, as seen in the example Golgi cell shown in Fig 5A.

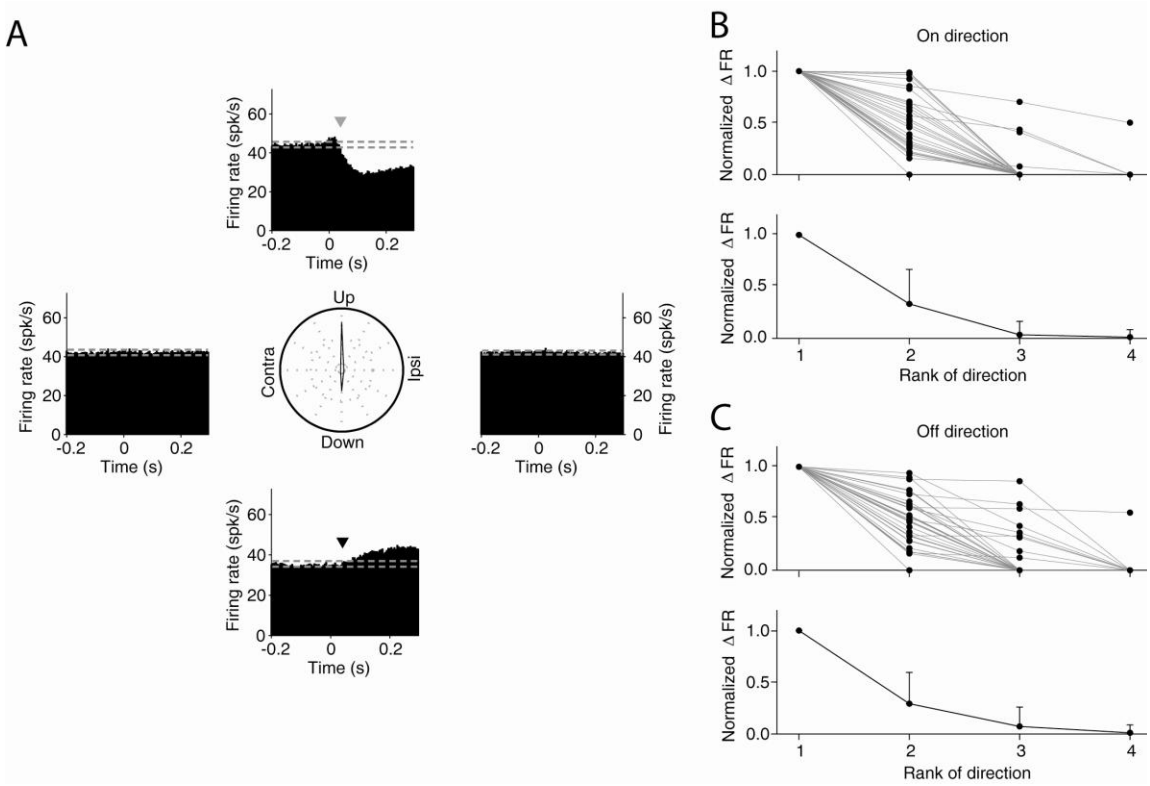

Figure 3.5. Directional tuning of Golgi cells. A, PSTH of a Golgi cell response to spontaneous saccades within +/- 45 degrees of each cardinal direction. Gray dotted lines indicate 2 standard deviations above and below the control firing rate, which was used to calculate the first significant increase or decrease in firing rate, respectively. Center plot indicates absolute depth of modulation for each of the four directions. The distance from the center of the circle to the perimeter equals 20 spks/s. B-C, Number of directions with on (B) or off (C) responses. Each line in the top panel represents a single neuron and the dots indicate the normalized change in firing rate for a particular cardinal direction zone. The directions were ranked by response amplitude such that the numbers along the abscissa indicate the most to least responsive directions, with direction 1 being the preferred direction. For both B and C, the bottom panel shows the mean and standard deviation for all neurons.

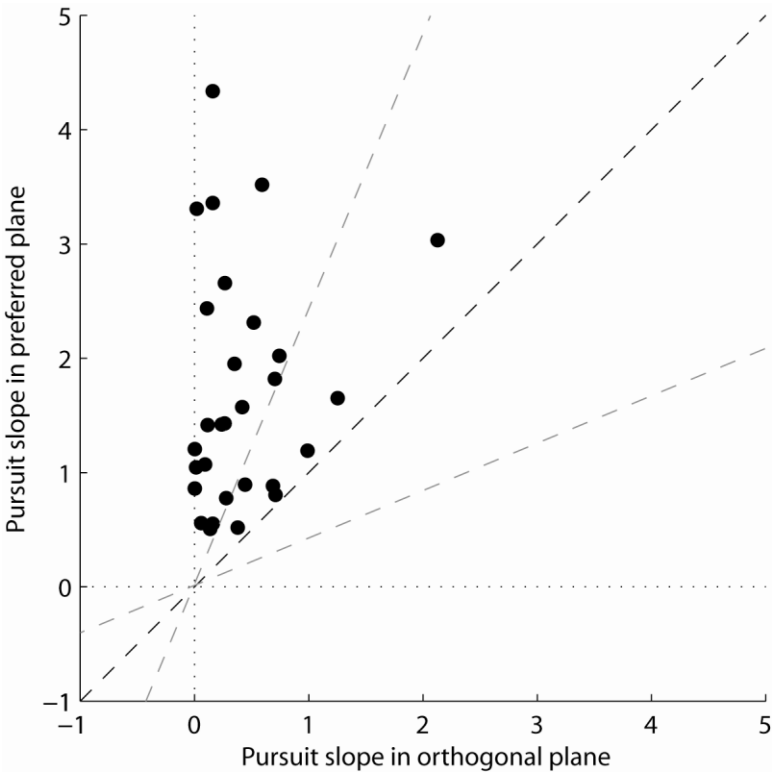

Figure 3.6. Directional specificity of Golgi cell responses during horizontal and vertical sinusoidal pursuit. Slope of average firing rate versus average eye position during pursuit in the plane of maximal activation for the neuron (preferred plane) versus slope during pursuit in the orthogonal plane for 29 Golgi cells. Slopes were calculated as in Fig. 2. Most points fall well above the unity line (black dashed), indicating that the majority of Golgi cells have a single preferred plane of modulation (see Fig 4. and text). Gray dashed lines indicate 2x or 0.5x responses.

Golgi cell responses have "eye position fields"

The Golgi cell shown in Figure 2A-G had an apparent saturation in firing rate during both saccades and pursuit. We determined that this saturation was not due to intrinsic properties of the neuron such as spike refractoriness, but was instead related to an eye position threshold. Figure 7 presents this phenomenon more fully for a representative neuron. When the monkey pursued a sinusoidally moving target centered 5 degrees to the left, the firing rate of the neuron modulated smoothly with changes in eye position (Fig 7A, left panel). However, when the monkey pursued a moving target centered 5 degrees

to the right, the neuron was unmodulated (Fig 7A, right panel). We call the active eye position range of a Golgi cell the "eye position field" of the neuron and we differentiate between eye position fields for on and off responses. Note that there is a difference in baseline firing rate between the two conditions. This is the result of accumulated firing rate increases for eye movements within the eye position field of the neuron due to the long time constant of decay. The eye position field of this same Golgi cell can also be seen during the spontaneous eye movements produced during the free viewing condition (Fig 7B), indicating that the position fields are present during both pursuit and saccades. Note in Figure 7B that a rightward (positive) saccade starting around -7 degrees resulted in a corresponding change in firing rate of the neuron (black arrow), whereas a rightward saccade of a similar amplitude starting around 2 degrees had no effect on the firing rate (gray arrow). By applying an algorithm that looks for changes in firing rate resulting from saccades with many different start and end points covering the entire oculomotor range of the monkey (see Methods), we determined that this Golgi cell had an eye position field between -18 and 2 degrees for increases in firing rate (on direction; Fig 7C, left). That is, for rightward (on direction) saccades this neuron was not responsive to saccades starting and ending at less than -18 degrees or more than 2 degrees, but it was responsive to saccades starting or ending within the range defined by these two boundaries. Likewise, for leftward saccades (off direction; Fig 7C, right), this neuron was not responsive for saccades made outside a range of -14 to 5 degrees. Figure 8A-B show the distribution of on eye position fields for 19 Golgi cells and off eye position fields for 20 Golgi cells for which we had sufficient data to apply our algorithm. We confined our analysis of spontaneous eye movements to only those Golgi cells with median CV_2s less

than 0.2 because the regularity of the spike times allowed us to detect changes in instantaneous firing rate on a saccade-by-saccade basis without relying on averaging. Using this approach, we found that individual Golgi cells have eye position fields distributed throughout the squirrel monkey oculomotor range that we report in Chapter 2, with the population blanketing the entire range and being centered roughly around the center of gaze, but with individual Golgi cell fields only occupying a portion of the total range. The mean eye position field size across the population was 15.7 +/- 7.4 deg in the on direction and 17.9 +/- 8.0 deg in the off direction, with a strong correlation between the size of the on and off fields on a per neuron basis for the 17 neurons in which we were able to calculate both the on and off position fields (Pearson correlation coefficient=0.81, $p<<0.05$; Fig 8C).

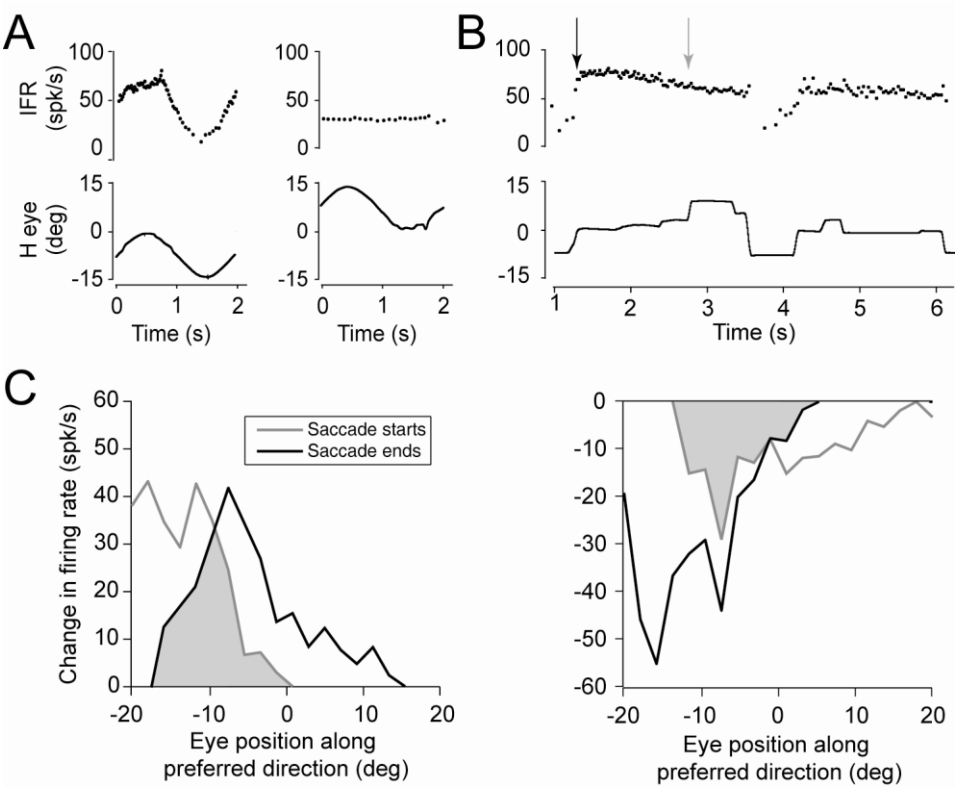

Figure 3.7. Eye position fields of a single Golgi cell. A, Response of Golgi cell during pursuit of a target to the left (left panel) or right (right panel) of the center of gaze. Top, instantaneous firing rate (IFR). Bottom, horizontal eye position. B, Response of same Golgi cell during spontaneous eye movements. Arrows indicate on response (black) or absence of on response (gray) for two saccades of similar amplitude, but with different starting positions. C, calculated on (left) and off (right) eye position fields for the same neuron. For both panels, the gray curve indicates changes in firing rate during saccades versus saccade start points and the black curve indicates changes in firing rate during saccades versus saccade end points. The shaded region is the intersection of these two curves, which defines the eye position field of the neuron (see Methods).

In addition, there was a high degree of overlap between the on and off position fields for a given neuron, such that the eye position at which a Golgi cell first began to respond with a decrease in firing rate in the off direction was usually within a few degrees of the eye position at which a Golgi cell stopped responding in the on direction. Figure 8D shows a plot of the upper response field border for the off direction versus the upper response field border for the on direction for the 17 neurons with sufficient data to measure both the on and off position fields. Most points align along the unity line, indicating a correspondence between these two borders for most neurons. This suggests

that a similarly tuned input to the Golgi cells accounts for both the on and off responses of the neurons. We address the nature of this input in the next chapter.

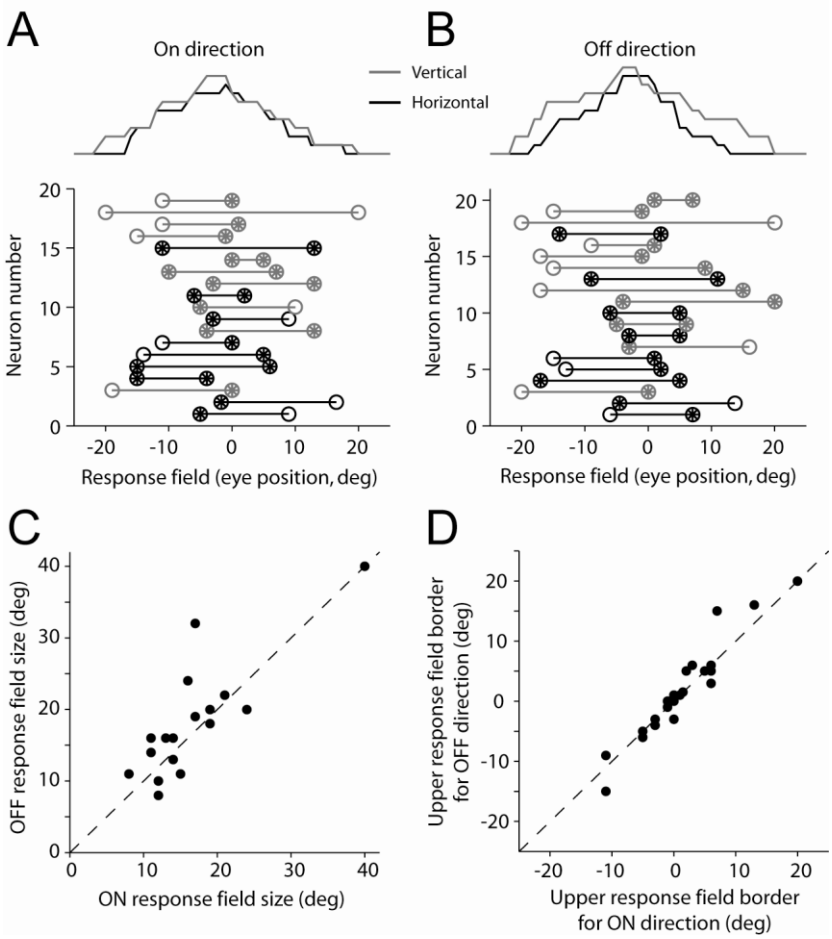

Figure 3.8. Eye position fields for the population of Golgi cells. A-B, extent of eye position response fields for 19 Golgi cells in the on direction (A) and 20 Golgi cells in the off direction (B). Circles indicate borders of position fields. Open circles correspond to estimates of borders that were not clear due to an insufficient number of saccades beyond that position. Gray, vertical eye movement cells; Black, horizontal eye movement cells. Positive numbers are up and ipsilateral. Histograms on top indicate distributions of eye position field extents using 1 degree bins and summing the bins across all neurons. C, Relationship between eye position response field sizes for on and off directions in 17 Golgi cells. Diagonal line indicates equal sizes. D, Relationship between the eye position at which a Golgi cell first starts to respond in the off direction (upper off border) and stops responding in the on direction (upper on border) for the same 17 Golgi cells. Points falling along the diagonal line would indicate that the on and off upper eye position field borders are the same.

Discussion

Golgi cells exert strong inhibitory control over granule cells, placing them in a strategic position to control the information entering the cerebellar cortex (Eccles et al., 1967). We quantified for the first time the response properties of VPFL Golgi cells in the alert monkey, revealing the following three primary characteristics that will help us to better understand the role of Golgi cells in cerebellar cortical processing. First, VPFL Golgi cell firing rates are predominantly driven by ongoing eye movements. Second, VPFL Golgi cell firing rates change on at least two time scales, an initial increase or decrease in firing rate with mean time constants of tens to hundreds of milliseconds and a longer decay or rebound in firing rate with time constants of hundreds of milliseconds to tens of seconds. Third, VPFL Golgi cells have eye position fields covering only a portion of the entire oculomotor range of the monkey. We discuss these properties in more depth below and offer our hypotheses about their functional significance in the cerebellar cortical circuit. First we comment on the identity of the recorded units and offer further evidence that they are Golgi cells.

Identity of recorded units

There are several pieces of evidence arguing that the neurons we report here are Golgi cells. First, these units were the only ones we consistently isolated in the granular layer, and isolation could often be maintained for greater than 10 minutes. Furthermore, we could often hear their unique discharge patterns in the background even when it was not possible to isolate a single unit. This suggests that these units have large cell bodies

consistent with Golgi cells (Eccles et al., 1967). Second, when not driven by ongoing eye movements (e.g., when the eye is outside the eye position field) the spike regularity and interspike interval distributions of our recorded units match those of morphologically identified Golgi cells recorded in anesthetized preparations (Holtzman et al., 2006), as detailed below. Finally, some of the key characteristics we have identified in our recorded units have been previously reported in Golgi cells. Specifically the predominance of off responses, bursts sometimes preceding pauses in firing rate, and rebound excitations at the offset of stimulation have all been seen in Golgi cells by previous investigators (Vos et al., 1999; Tahon et al., 2005; Holtzman et al., 2006).

Knowledge of Golgi cell eye position fields allowed us to address a problem we encountered in comparing our presumed Golgi cells with the morphologically identified units described in other studies (Simpson et al., 2005; Holtzman et al., 2006), namely that our experiments were carried out in the awake behaving monkey, where firing rates are often higher and cannot be considered stationary due to modulation by the ongoing behavior. Therefore, the interspike interval (ISI) criteria established by other investigators may not apply to our data. But because Golgi cells are unmodulated by eye movements that occur outside their eye position fields, we could, in essence, examine spike patterns in the absence of external stimulation. Figure 9A shows the ISI histogram for a presumed Golgi cell during a 30-second period in which the monkey was making spontaneous eye movements within the active range of the neuron. This neuron showed many ISIs below 10 milliseconds, indicating that the neuron reached firing rates as high as 100 Hz during active eye movements, and a median ISI of 15 milliseconds, corresponding to a median

firing rate of 67 spk/s. This neuron would not be classified as a Golgi cell based on the ISI criteria established in anesthetized preparations. However, when an ISI histogram was constructed for the same neuron during a 30-second period in which the monkey made spontaneous eye movements outside the eye position field of the neuron (Fig 9B), the ISI distribution appeared identical to those found in anesthetized preparations (e.g., Holtzman et al, 2006). The ISI distribution in Fig 9B shows few ISIs below 50 milliseconds, indicating a maximum firing rate below 20 Hz, and the median ISI is 60 milliseconds, corresponding to a median firing rate of 17 spk/s. This observation provides a link between the neurons we recorded and the morphologically identified Golgi cells recorded by others.

While we cannot rule out the possibility that our presumed Golgi cells in fact represent more than one type of granular layer interneuron, including Lugaro and unipolar brush cells, the consistency of response properties seen across the entire spectrum of median firing rates and CV_2 values indicate a relatively homogenous population, suggesting a single cell type. The exceptions to this homogeneity are the three units in Fig 1C with median firing rates above 80 spk/s and CV_2s below 0.2. These units were classified as Golgi cells because they meet our criteria for inclusion, namely they were recorded in the granular layer and have spike peak-to-trough widths exceeding 200 □s; however, none of them was modulated during eye movements, nor could isolation be maintained for more than a few minutes. Therefore, we suspect these units may correspond to unipolar brush cells, which have smaller cell bodies than Golgi cells and are preferentially located in the vestibulocerebellum (Nunzi and Mugnaini, 2000). This point will likely be clarified when

unipolar brush cells become better described *in vivo* (Simpson et al., 2005; Barmack and Yakhnitsa, 2008).

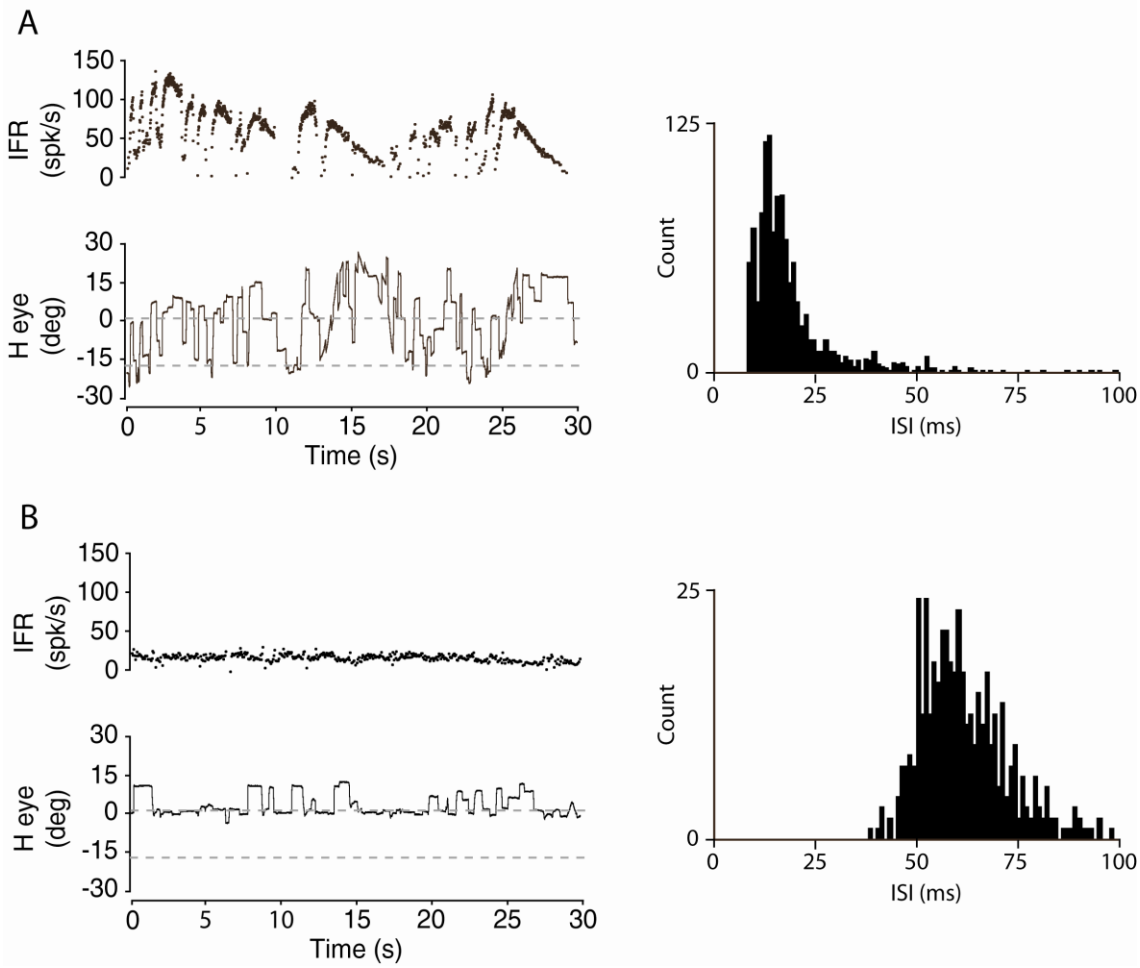

Figure 3.9. Golgi cell interspike interval distributions in the presence and absence of firing rate modulation due to ongoing behavior. A, Golgi cell instantaneous firing rate (IFR, top left) and horizontal eye position (Heye, bottom left), and corresponding interspike interval (ISI) distribution for the same spike data (right), when eye movements occurred within the eye position field of the neuron (indicated by dashed lines). B, IFR, eye position, and ISI data in the same format as A for the same neuron when eye movements occurred outside the eye position field of the neuron.

Eye movement coding by VPFL Golgi cells

The Golgi cells we recorded appeared to be exclusively driven by eye movement-related inputs and were unmodulated by vestibular or visual signals. This specificity of input is surprising not only because the large ascending dendritic fields of the Golgi cells suggest

that they receive a broad convergence of diverse inputs, but also because vestibular, visual, and oculomotor signals are often already combined at the level of many VPFL projecting neurons (Mustari et al., 1988; Nakamagoe et al., 2000). The fact that VPFL Golgi cells respond specifically to the eye movement inputs suggests a highly specific connectivity in the input layer of the cerebellar cortex that to our knowledge has not been previously reported. The eye movement inputs are likely derived from brainstem areas such as the nucleus of the prepositus hypoglossi (NPH) and paramedian tract (PMT), which contain burst-tonic eye movement-related signals thought to convey an efference copy of oculomotor commands (Green et al., 2007). Within the computational framework of cerebellar cortex function in motor control, this exclusive coding of an efference copy signal suggests that Golgi cells, through their regulation of granular layer throughput, may play a critical role in the construction of internal models of the oculomotor system (e.g., forward models).

In contrast to their burst-tonic mossy fiber inputs, VPFL Golgi cells have relatively slow time dynamics (Fig 4E, F), with firing rate rise times in the on direction often outlasting the duration of the saccade. The off direction responses tend to occur more rapidly (on average, twice as fast as on direction responses), with a complete pause in firing often occurring within a single interval of the instantaneous firing rate (e.g., Fig 2A, 4B), but with some neurons having off direction time constants on the order of hundreds of milliseconds. In addition, VPFL Golgi cells have a second, longer time constant for recovery from off responses and decay from on responses. These longer time constants were reported by Miles and colleagues (1980), but the shorter initial ones were not.

Taken together, the varied time constants give these Golgi cells the properties of a bandpass filter on behaviorally relevant time scales. Specifically, the majority of VPFL Golgi cells reject high-frequency inputs such as bursts (Fig 4F) and low-frequency inputs such as tonic eye position signals during steady fixations. Because Golgi cells strongly inhibit granule cells, this passband would be inverted at the level of granule cells, allowing only relatively high- or low-frequency mossy fiber inputs to readily pass the input stage of the cerebellar cortex. This is consistent with previously reported observations that granule cells exhibit short, well-timed bursts in response to stimulation (Chadderton et al., 2004). Such a scheme could provide a mechanism for granule cells to compute the time derivative of mossy fiber inputs, thus giving Purkinje cells their observed phase advanced eye signal relative to the mossy fibers (Lisberger and Fuchs, 1978a). On the other hand, the long time constant could be utilized in computations involving events occurring on longer time scales, such as learning, because the time course of the decay holds a *de facto* short-term memory of past eye positions.

Miles and colleagues (1980) previously noted that firing rates of putative Golgi cells in the flocculus often saturate at a particular eye position, usually near the center of gaze. We extend this finding by showing that the eye position-related saturations are often bounded on two sides, forming an eye position field in which each neuron is active. These eye position fields do not appear to be limited to a particular hemifield, as Miles suggested, but rather can span both hemifields (Fig 8A-B). Furthermore, we show that the eye position at which a given Golgi cell firing rate saturates in the on direction corresponds, within a few degrees, with the eye position at which the same neuron begins

responding in the off direction (Fig 8D). Our simultaneous recordings of mossy fibers and Golgi cells presented in the next chapter suggest a plausible mechanism for generating the eye position fields that will be discussed in that chapter. The fact that the axonal fields of individual Golgi cells appear to be mostly non-overlapping (Eccles et al., 1967), suggests that as little as a single Golgi cell will provide the main inhibitory control over a cluster of granule cells. Consequently, individual granule cells may only "see" one eye position field. Functionally, this arrangement could create "modules" of granule cells defined within a volume of space, with each module governed by at most a few Golgi cells and each reflecting a different state- and time-filtered signal that can be combined by downstream neurons such as Purkinje cells.

It is not clear how much these results can be generalized to other areas of the cerebellum, since we found considerably higher specificity in our population of recorded VPFL Golgi cells than was seen in OMV Golgi cells (Prsa et al., 2009). While one would hope that Golgi cells play a similar role in the processing performed in these two areas, the differences seen between Golgi cells in VPFL and OMV may be a reflection of the different roles presumably played by these two areas in oculomotor control (Ilg and Thier, 2008). More experiments will be necessary to resolve this question.

References

Barmack NH, Yakhnitsa V (2008). Functions of interneurons in mouse cerebellum. J Neurosci 28: 1140-1152.

Blazquez PM, Hirata Y, Heiney SA, Green AM, Highstein SM (2003). Cerebellar signatures of vestibulo-ocular reflex motor learning. J Neurosci 23: 9742-9751.

Chadderton P, Margrie TW, Häusser M (2004). Integration of quanta in cerebellar granule cells during sensory processing. Nature 428: 856-860.

Dieudonne S (1998). Submillisecond kinetics and low efficacy of parallel fibre-Golgi cell synaptic currents in the rat cerebellum. J Physiol 510: 845-866.

Ebner TJ, Pasalar S (2008). Cerebellum predicts the future motor state. Cerebellum 7: 583-588.

Eccles J, Ito M, Szentágothai J (1967). The Cerebellum as a Neuronal Machine (Heidelberg: Springer-Verlag).

Eccles J, Llinas R, Sasaki K (1964). Golgi cell inhibition in the cerebellar cortex. Nature 204: 1265-1266.

Ghasia FF, Meng H, Angelaki DE (2008). Neural Correlates of Forward and Inverse Models for Eye Movements: Evidence from Three-Dimensional Kinematics. J Neurosci 28: 5082-5087.

Green AM, Meng H, Angelaki DE (2007). A reevaluation of the inverse dynamic model for eye movements. J Neurosci 27: 1346-1355.

Holt GR, Softky WR, Koch C, Douglas RJ (1996). Comparison of discharge variability in vitro and in vivo in cat visual cortex neurons. J Neurophysiol 75: 1806-1814.

Holtzman T, Rajapaksa T, Mostofi A, Edgley SA (2006). Different responses of rat cerebellar Purkinje cells and Golgi cells evoked by widespread convergent sensory inputs. J Physiol 574: 491-507.

Ilg UJ, Thier P (2008) The neural basis of smooth pursuit eye movements in the rhesus monkey brain. Brain Cognition 68:229-240.

Langer T, Fuchs AF, Scudder CA, Chubb MC (1985). Afferents to the flocculus of the cerebellum in the rhesus macaque as revealed by retrograde transport of horseradish peroxidase. J Comp Neurol 235: 1-25.

Lisberger SG, Fuchs AF (1978a). Role of primate flocculus during rapid behavioral modification of vestibuloocular reflex. I. Purkinje cell activity during visually guided

horizontal smooth-pursuit eye movements and passive head rotation. J Neurophysiol 41: 733-763.

Lisberger SG, Fuchs AF (1978b). Role of primate flocculus during rapid behavioral modification of vestibuloocular reflex. II. Mossy fiber firing patterns during horizontal head rotation and eye movement. J Neurophysiol 41: 764-777.

Miles FA, Fuller JH, Braitman DJ, Dow BM (1980). Long-term adaptive changes in primate vestibuloocular reflex. III. Electrophysiological observations in flocculus of normal monkeys. J Neurophysiol 43: 1437-1476.

Mustari MJ, Fuchs AF, Wallman J (1988). Response properties of dorsolateral pontine units during smooth pursuit in the rhesus macaque. J Neurophysiol 60: 664-686.

Nakamagoe K, Iwamoto Y, Yoshida K (2000). Evidence for brainstem structures participating in oculomotor integration. Science 288: 857-859.

Noda H (1986). Mossy fibres sending retinal-slip, eye, and head velocity signals to the flocculus of the monkey. J Physiol 379: 39-60.

Noda H, Warabi T (1987). Responses of Purkinje cells and mossy fibres in the flocculus of the monkey during sinusoidal movements of a visual pattern. J Physiol 387: 611-628.

Nunzi MG, Mugnaini E (2000). Unipolar brush cell axons form a large system of intrinsic mossy fibers in the postnatal vestibulocerebellum. J Comp Neurol 422: 55-65.

Pasalar S, Roitman AV, Durfee WK, Ebner TJ (2006). Force field effects on cerebellar Purkinje cell discharge with implications for internal models. Nat Neurosci 9: 1404-1411.

Prsa M, Dash S, Catz N, Dicke PW, Thier P (2009). Characteristics of responses of Golgi cells and mossy fibers to eye saccades and saccadic adaptation recorded from the posterior vermis of the cerebellum. J Neurosci 29: 250-262.

Ramon y Cajal S (1911). Histologie du Systeme Nerveux de L'Home et des Vertebres (Paris: Maloine).

Shin SL, Hoebeek FE, Schonewille M, De Zeeuw CI, Aertsen A, De Schutter E (2007). Regular patterns in cerebellar Purkinje cell simple spike trains. PLoS ONE 2, e485.

Simpson JI, Hulscher HC, Sabel-Goedknegt E, Ruigrok TJ (2005). Between in and out: linking morphology and physiology of cerebellar cortical interneurons. Prog Brain Res 148: 329-340.

Tahon K, Volny-Luraghi A, De Schutter E (2005). Temporal characteristics of tactile stimuli influence the response profile of cerebellar Golgi cells. Neurosci Lett 390: 156-161.

Thach WT (1968). Discharge of Purkinje and cerebellar nuclear neurons during rapidly alternating arm movements in the monkey. J Neurophysiol 31: 785-797.

Vos BP, Volny-Luraghi A, De Schutter E (1999). Cerebellar Golgi cells in the rat: receptive fields and timing of responses to facial stimulation. Eur J Neurosci 11: 2621-2634.

Chapter IV

Mossy fiber and Purkinje cell characterization in the ventral paraflocculus and effects on Purkinje cell responses of blocking GABA-A receptors

Abstract

In an effort to better understand the signal transformations carried out by the cerebellar cortex circuit, we recorded from the input and output elements of the ventral paraflocculus, mossy fibers and Purkinje cells, during vestibulo-oculomotor behaviors. We compared their responses with each other and with the responses of Golgi cells to unveil what role Golgi cells may play in the signal transformations carried out by the ventral paraflocculus. In addition, we studied the role of molecular layer interneurons in cerebellar processing by studying the effect of blocking GABAergic inhibition near Purkinje cells. We found that, when compared to Purkinje cells, mossy fibers, like Golgi cells, are narrowly tuned for eye movements and have a larger burst component in their responses during saccades. Further, we found that mossy fiber eye position activation thresholds and zero saturation points fall within the same range as Golgi cell eye position field borders. Simultaneous recordings of Golgi cells and nearby mossy fibers revealed that Golgi cells have the opposite directional tuning of the mossy fiber(s) that likely drive their responses, and that these responses are more sluggish than their mossy fiber counterparts. Because the mossy fiber inputs appear to convey the activity of burst-tonic neurons in the brainstem, Golgi cell responses reflect a time-filtered negative image of the motor command sent to the extraocular muscles. Lastly, we found that blocking

GABAergic inhibition near Purkinje cells increased the burstiness of Purkinje cells during saccades, suggesting that molecular layer inhibition acts to suppress the burst component present in the population of mossy fibers. We attempt to synthesize these findings to develop working hypotheses about the varied roles of inhibition in cerebellar cortical processing for oculomotor control.

Introduction

Cerebellar physiologists have long focused on the signal transformations and general role of the glutamatergic synapses between parallel fibers and Purkinje cell dendritres (Thach, 1968; Lisberger and Fuchs, 1978a). Over the past decade however, work by several laboratories, mostly in anaesthetized or slice preparations, has exposed the critical role of inhibitory interneurons (Watanabe et al., 1998; Mittman et al., 2005; Santamaria et al., 2007). This recent work suggests that important signal transformations occur at each node of the circuit and that only when all these transformations are considered together, within the contex of the architecture of the circuit, can a coherent picture of cerebellar function emerge. My thesis work was designed on this premise and the previous chapter presented important insights into the response of a key GABAergic interneuron located at the input stage of the cerebellar cortex, the Golgi cell. But to better interpret our findings on the Golgi cell response and the signal transformations carried out at this node of the circuit we decided to examine the response properties of mossy fibers and Purkinje cells, which represent the input and output signals of the cerebellar cortex, in light of our Golgi cell findings.

A number of investigators have examined the responses of mossy fiber and Purkinje cell in the VPFL of the alert primate (Lisberger and Fuchs, 1978a,b; Miles et al., 1980; Noda et al., 1987). They have found that mossy fibers convey visual, vestibular, and eye movement-related signals to the VPFL in relatively independent streams (i.e., different mossy fibers carry different information), and that individual Purkinje cells combine these signals to various extents. Our results on the Golgi cells presented in the previous

chapter build upon this previous work and raise new questions about the differential responses found in the input and output elements of the VPFL. Specifically, we were interested in determining how characteristics such as directional tuning width, burst-tonic ratios, and activation thresholds compare between these elements and what role Golgi cells may play in cerebellar cortical processing.

Although this work mostly focuses on input layer processing, specifically the role of Golgi cells, in the last part of the thesis, and with the goal of offering a more complete picture of the role of internerons in cerebellar processing, we begin to examine the role of molecular layer interneurons in the alert animal by studying the effect of removing GABAergic inhibition near VPFL Purkinje cells using the multibarrel recording and injection technique we developed (Chapter 2).

Materials and Methods

Most of the methods used for these experiments were described in Chapter 3 and the details can be found therein. Here we provide details of methods specific to this chapter.

Additional method for calculating preferred directions

Because we desired a finer spatial resolution for the preferred direction vectors in the paired Golgi cell-mossy fiber analysis than in the independent Golgi cell and mossy fiber recordings, we used a second approach in which we calculated a saccade vector for each saccade greater than 2 degrees in amplitude that resulted in a change in firing rate, scaled each vector by the corresponding change in firing rate, and computed the vector average of all such vectors. The direction of the vector average was taken as the preferred direction of the neuron.

Electrode preparation, unit recording and drug application

We used carbon fiber multibarrel electrodes for neuronal recordings and drug application. Electrodes were custom made in our lab using procedures described in Chapter 2.4. Briefly, a carbon fiber filament (5-7 microns) was inserted into one of the barrels of a three-barrel capillary glass, the glass ensemble was then pulled (PML 107) and the two remaining barrels filled with solution. One of these remaining barrels was used for drug injection and contained 2-(3-carboxypropyl)-3-amino-6-methoxyphenyl-pyridazinium bromide (SR-95531, 10mM, Sigma Aldrich) dissolved in 0.165 M NaCl (pH=3). The third barrel was filled with 0.165 mM NaCl solution (pH=3) for balance compensation.

The values for current retention and injection were: SR95531, -50 to -75nA (retention) and +50 to +75nA (ejection).

The two Purkinje cells presented in Figure 4.11 were recorded with a piggy-back electrode consisting of a standard tungsten electrode glued to a multibarrel glass electrode without the carbon fiber. The multibarrel tips were spaced 50-100 μm back from the tip of the tungsten (examined under a light microscope).

Results

We recorded mossy fibers and Purkinje cells in the ventral paraflocculus (VPFL) while squirrel monkeys performed a variety of vestibulo-oculomotor behaviors. Here, we present a description of these units, focusing on the properties that will facilitate comparison with the VPFL Golgi cells presented in the previous chapter. In addition, we performed minute pharmacological manipulations using a GABA receptor antagonist while recording Purkinje cells in order to unmask the effects of inhibition on Purkinje cell responses. This section is broken into two parts. In the first, we present the mossy fiber properties and compare them with the properties of nearby or simultaneously recorded Golgi cells. In the second, we present the properties of Purkinje cells and compare them with the mossy fibers and Golgi cells. We then present our results on the pharmacological manipulations of Purkinje cells.

Types of mossy fiber responses encountered

Consistent with other studies in the VPFL (Lisberger and Fuchs, 1978; Miles et al., 1980), the mossy fiber responses that made up the largest proportion of recorded units were the burst-tonic (BT) eye movement mossy fibers (n=27/30). These units discharge during saccades with a burst lasting approximately the same duration as the saccade and a tonic component that changes linearly with eye positions within a specific range. These responses predominated the background activity in the granular layer, likely accounting for the well-known "hashing" sound that is used to identify the granular layer in the VPFL. In addition to the BT mossy fibers, we also routinely encountered units with highly regular firing rates that, when isolation could be maintained during testing, usually

discharged during vestibular stimulation. Those of these units (n=3/6) that met the spike width criteria we used for BT mossy fibers were classified as vestibular mossy fibers. The others were putatively labeled as unipolar brush cells. Because of the difficulty maintaining single unit isolation during vestibular stimulation, the vestibular mossy fibers were not extensively tested and will not be discussed in the remainder of this chapter. A third class of mossy fiber response that has been previously documented in the VPFL is the visual mossy fiber. These fibers respond in phase with retinal slip velocity when the monkey is required to fixate a laser spot while a patterned background moves. We did not attempt to identify these visual mossy fibers in our recordings, though we have no reason to think that they were not present in the areas we recorded, as others have found them in the macaque VPFL (Miles et al., 1980; Noda et al., 1986). In the remainder of the chapter we focus exclusively on the BT mossy fibers because they are the candidate inputs to Golgi cells that produce the eye movement only responses of Golgi cells shown in the previous chapter.

Response properties of eye movement mossy fibers

The response properties of BT mossy fibers in the rhesus macaque have been well described by other investigators. Here we include an analysis of our sample of BT mossy fibers recorded in the squirrel monkey, and include some additional analyses of the mossy fibers not previously done, to facilitate comparison with Golgi and Purkinje cells recorded in the same area.

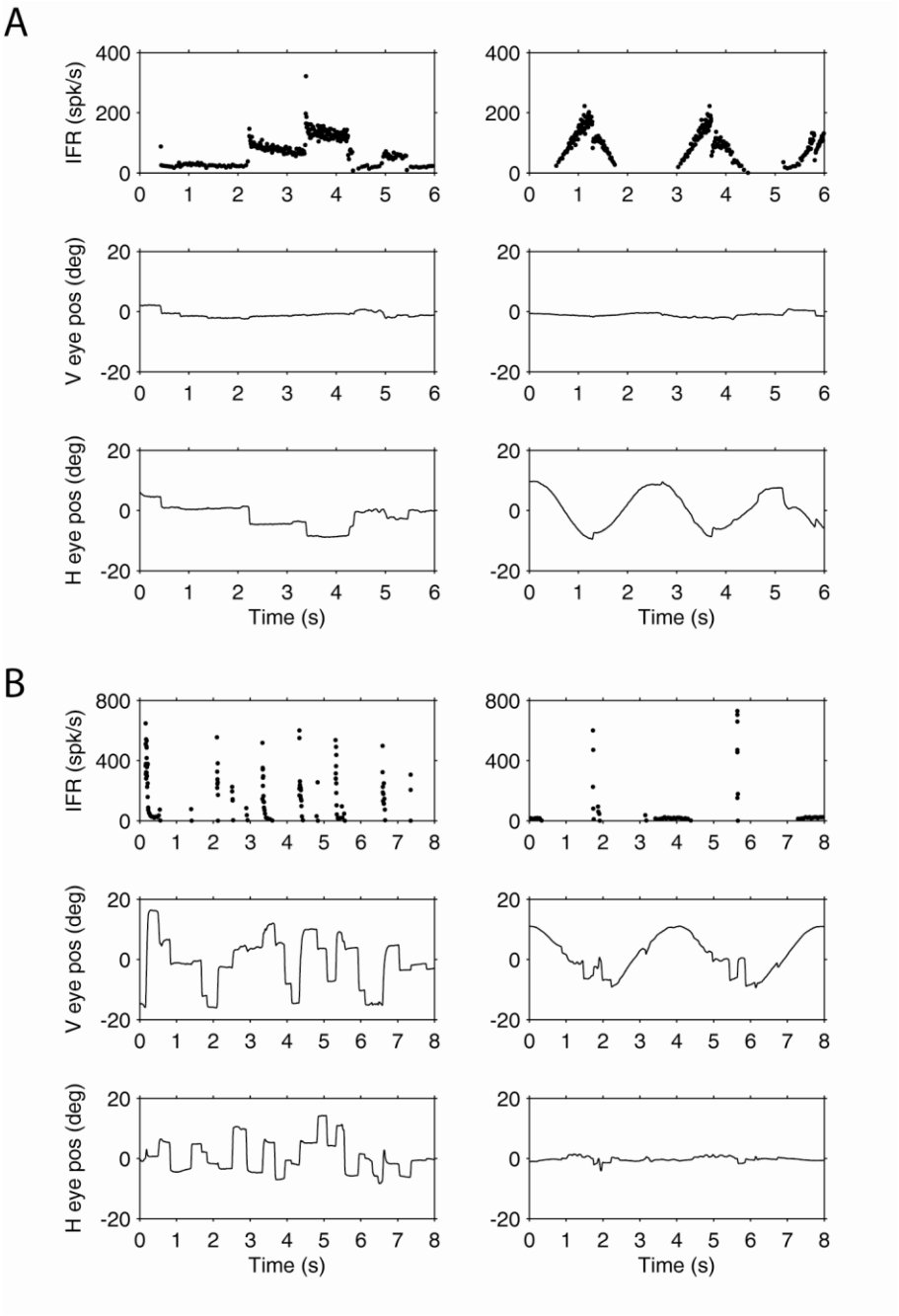

Figure 4.1. Two example mossy fibers (A and B) during spontaneous (left panels) and pursuit (right panels) eye movements. Format is same for A and B: from top to bottom, Instantaneous firing rate (IFR), vertical, and horizontal eye positions.

Figure 4.1 presents examples of the responses of the two most typical BT mossy fiber responses during spontaneous saccades and smooth pursuit. The unit in A had a brief

burst during contraversive saccades followed by a maintained tonic component related to the new eye position. The burst component of this mossy fiber was capable of reaching instantaneous firing rates as high as 400 spks/s and the amplitude of the burst appeared to be related with the amplitude of the saccade, and hence the saccade velocity. Though we did not make an effort to systematically quantify this property, others have previously described it in VPFL mossy fibers (Miles et al., 1980). During pursuit, the peak firing rate led peak contraversive eye position by 16 degrees at 0.4 Hz, indicating that it was modulating mostly in phase with eye position. The example unit in B had strong bursts for saccades, sometimes approaching 800 spks/s, which far exceeded the tonic component related to eye position. The bursts occurred for saccades in multiple directions. During pursuit, this unit led peak eye position by 11 degrees at 0.5 Hz, indicating that this unit was also modulating mostly in phase with eye position. Figure 4.2 shows a different representation of the same two mossy fibers that makes the differences between the two units more clear. In this figure, we represent the perisaccade averages of the two units during spontaneous saccades by dividing the movement space into four 90 degree zones and averaging the activity of the mossy fiber for all saccade vectors falling into a directional zone. This is the same analysis that was applied to the Golgi cells in Fig 3.5. The unit in 4.2A is the same one depicted in 4.1A and the unit in 4.2B is the same one depicted in 4.1B. In Fig 4.2A we see that the mossy fiber from Fig 4.1A had a strong excitatory burst-tonic response for contraversive saccades and was inhibited for ipsiversive saccades, while it had no detectable change in firing rate for upward or downward saccades. On the other hand, Fig 4.2B reveals that the unit from Fig 4.1B bursted for upward, contraversive, and ipsiversive saccades, with the dominant response

being for upward. This indicates that the second mossy fiber was more broadly tuned than the first.

Among the population, the majority of BT mossy fibers behaved like the example in 4.2A, with relatively narrow directional tuning. This is quantified in Figure 4.3, where we plot the change in firing rate corresponding to saccades in each of the four direction zones depicted in Fig 4.2 for all mossy fibers with sufficient data (n=22). Each line in Fig 4.3A and 4.3B represents a single mossy fiber and the dots indicate the normalized change in firing rate for a particular direction zone. The directions were ranked by response amplitude such that the numbers along the abscissa indicate the most to least responsive directions, with direction 1 being the preferred direction. Eighty-two percent (18/22) of mossy fibers had less than half-maximal responses for the second most responsive direction, indicating that the population of mossy fibers as a whole is more narrowly tuned than the population of Golgi cells (Fig 3.5), though a large proportion of Golgi cells has similar a tuning width as the mossy fibers.

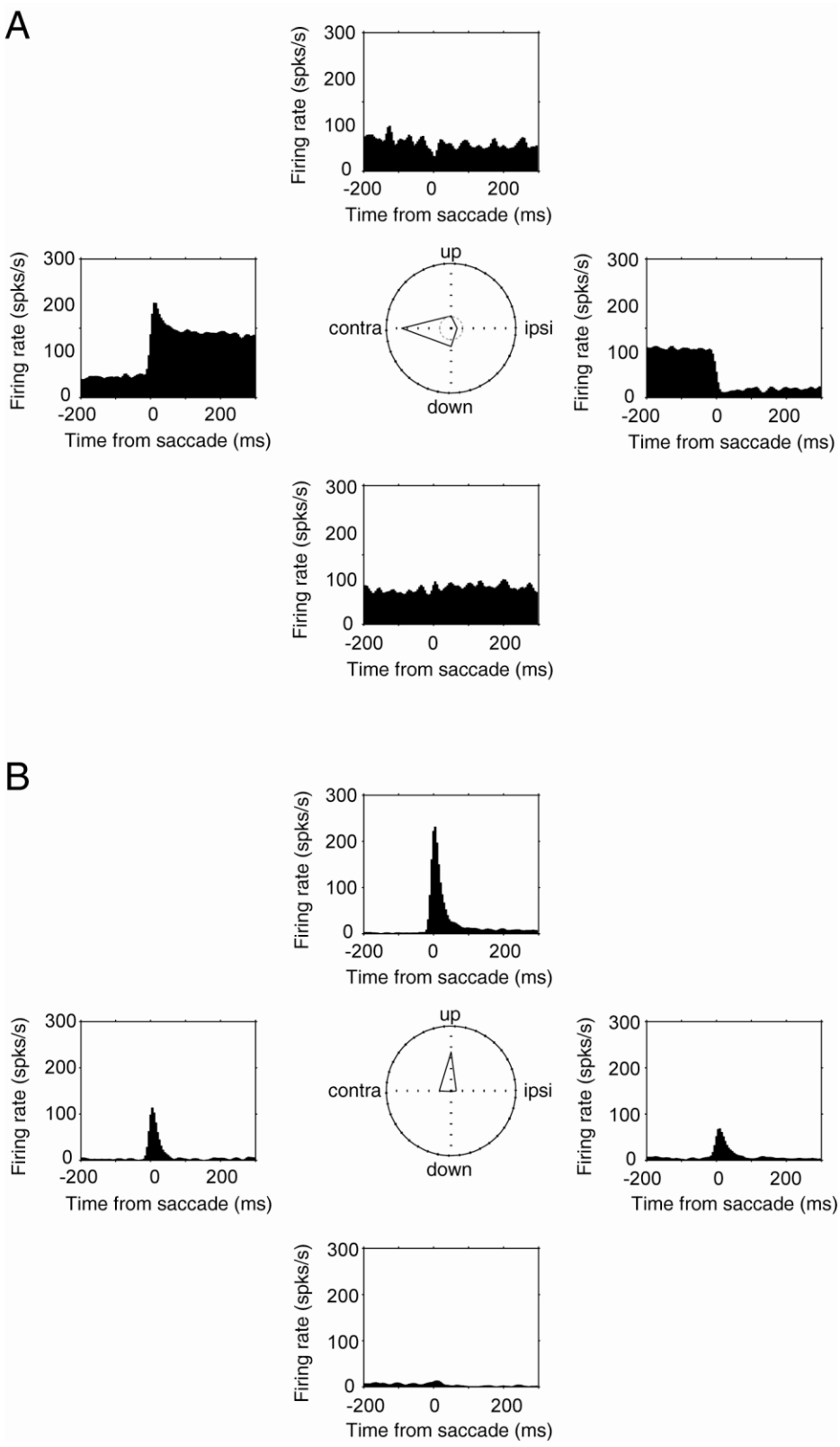

Figure 4.2. Four zone PSTHs generated from spontaneous saccades for same two mossy fibers as Fig 4.1. PSTHs were calculated as described in Methods for Chapter 3. Bin size for histograms is 5 ms and histograms were smoothed with gaussian kernel with 5 ms standard deviation. Center plots in both A and B indicate depths of modulation normalized by pre-saccade firing rate, shown as inner gray circle in A, so that excitatory responses fall outside the circle and inhibitory responses fall inside the circle. Circle is not visible in B because the magnitude of the excitatory response is so high relative to the presaccade firing rate.

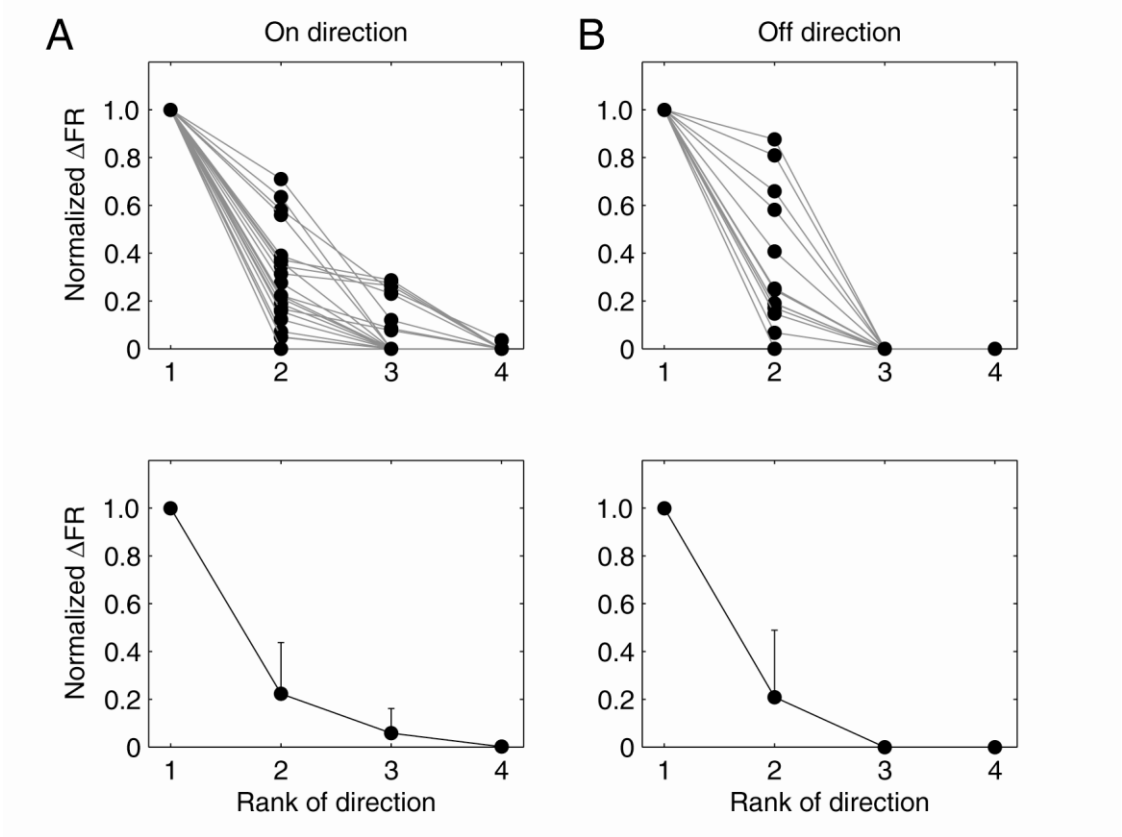

Figure 4.3. Directional tuning widths of mossy fibers for on and off responses based on number of directions with significant on (A) or off (B) responses. Format is same as Fig 3.5. Each line in the top panel represents a single neuron and the dots indicate the normalized change in firing rate for a particular direction zone. The directions were ranked by response amplitude such that the numbers along the abscissa indicate the most to least responsive directions, with direction 1 being the preferred direction. For both A and B, the bottom panel shows the mean and standard deviation for all neurons.

As a population, BT mossy fibers tended to have a larger burst component than Golgi cells. This was quantified using the burst-tonic ratio, as shown in Fig 4. Here we have overlaid the distribution of BT ratios of the mossy fibers with those of the Golgi cells from Fig 3.4 for comparison. The majority of BT mossy fibers had BT ratios exceeding 1 (median=2.2), indicating that the burst is the dominant component of the firing response, whereas the majority of Golgi cells had BT ratios below 1 (median=0.49). Thus VPFL

Golgi cell on responses were more sluggish than those of mossy fibers recorded in the same area.

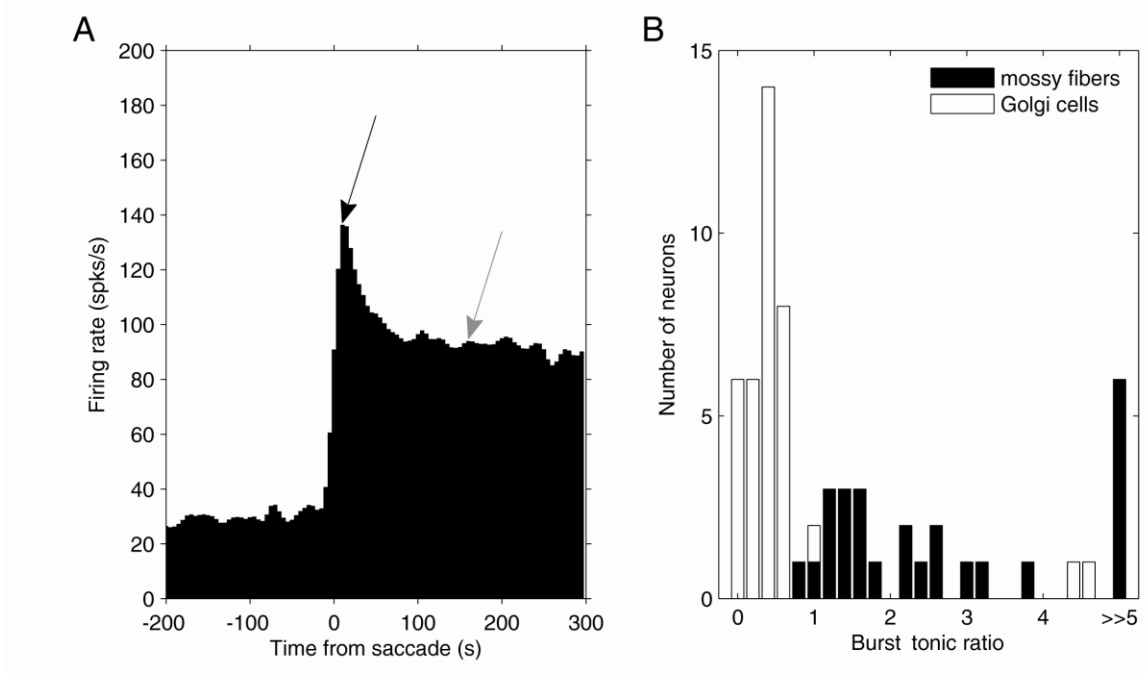

Figure 4.4. Burst-tonic ratios for mossy fibers compared to Golgi cells. A, demonstration of how the burst-tonic (BT) ratio is calculated: maximum firing rate during 50 ms window starting at the first significant change in firing rate (black arrow) divided by maximum firing rate during a 50 ms window starting 100 ms after response onset (gray arrow). B, distributions of BT ratios for mossy fibers (black) and Golgi cells (white; data from Chapter 3). Values above 5 are represented in the last bin, which includes values ranging from 6 to 300.

The burst typically preceded the initiation of saccades. Latencies to the first significant change in firing rate (2 SDs above pre-saccade rate) ranged from 25 ms lead to 10 ms lag (median=7.5 ms lead, n=18). Pauses in the off direction had similar latencies (median=5 ms lead, range=15 ms lead to 20 ms lag, n=11).

BT mossy fiber recruitment thresholds were found throughout the oculomotor range, with the majority falling within +/- 5 degrees of the center of gaze. Within their range of activity, BT mossy fibers tended to have relatively linear rate-position curves, as seen in

example unit in Figure 4.5A-B. For 13 mossy fibers, we had a sufficient number and range of saccades to make linear fits to quantify the eye position recruitment thresholds for saccades in the on direction. Of these units, 10 had recruitment thresholds within +/- 5 degrees of the center of gaze. To aid in the comparison with Golgi cell eye position field borders, we also quantified the eye position at which the firing rate saturates at zero for saccades in the off direction for 12 mossy fibers. Of these, 9 had zero saturation points within +/-5 degrees of the center of gaze. In 11 of the 14 total mossy fibers for which we could measure either an activation threshold or zero saturation, we were able to measure both values for the same unit (Fig 4.5C). In these mossy fibers, there was a strong correlation between the activation threshold and zero saturation point (Pearson correlation coefficient=0.92, $p<<0.001$).

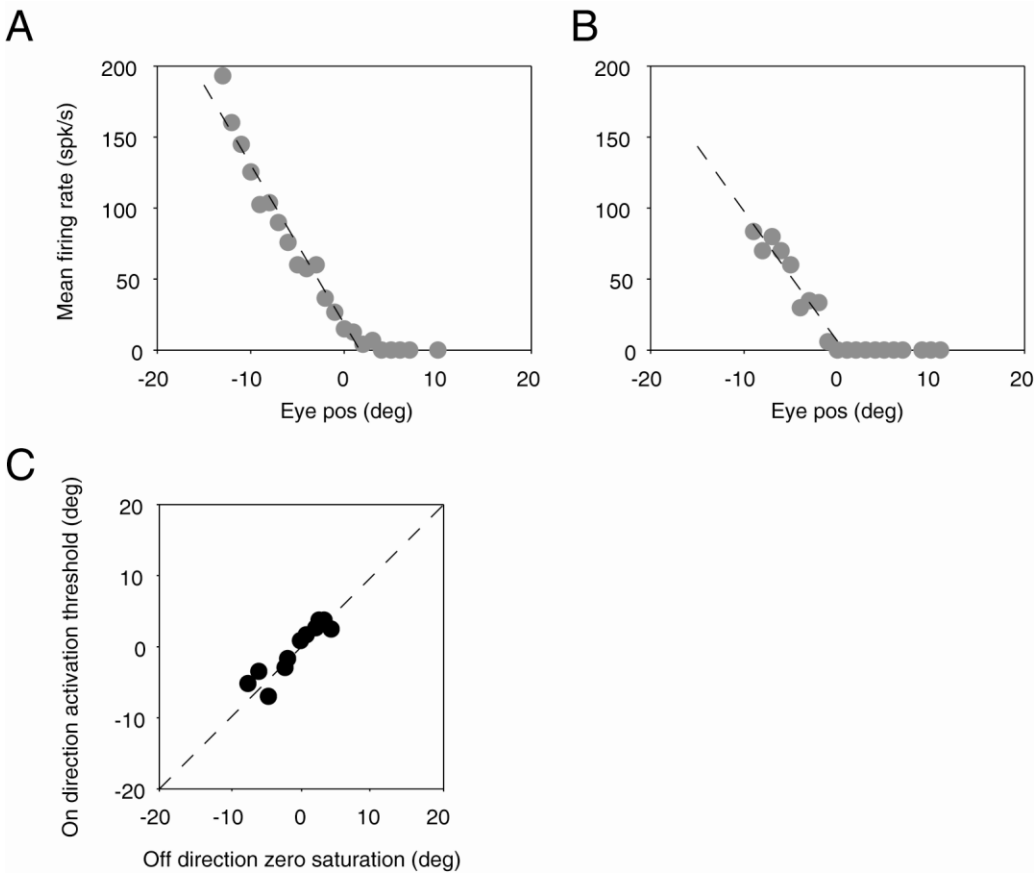

Figure 4.5. Eye position thresholds for mossy fiber activation in the on direction and zero saturation in the off direction. A and B show rate-position curves for an example mossy fiber. A, on direction eye position activation threshold. B, off direction zero saturation. Rate-position curves were calculated from spontaneous eye movements by finding all saccade vectors that occurred within +/- 45 degrees of the preferred or anti-preferred direction and calculating the mean firing rate during the post-saccade fixation period (150 ms window starting 150 ms after the saccade). Only fixation periods lasting at least 300 ms were used for this analysis. For all fixations, the mean firing rate was plotted against the mean eye position during the same period. The firing rates were then averaged in 1 degree bins to produce curves like those shown in A and B. Activation thresholds and zero saturation points were calculated as the x-intercept of a linear function fit to the rate position curves for all mean firing rates greater than 5 spk/s (dotted lines in A and B). C, relationship between activation thresholds and zero saturation points for 11 mossy fibers, showing a strong correlation between these values for individual mossy fibers.

Comparison of mossy fiber response properties with nearby or simultaneously recorded Golgi cells

As depicted in the cerebellar cortex circuit schematic in Figure 1.2, Golgi cells receive glutamatergic input via two separate pathways, a direct mossy fiber input to the Golgi cell soma and descending dendrites and a feedback input via the parallel fibers (Eccles et al., 1967; Chan-Palay and Palay, 1971). The mossy fiber synapses are known to be strong (Kanichay and Silver, 2008) and the parallel fiber synapses relatively weak (Dieudonne, 1998), so we wondered to what extent the mossy fiber input could explain the Golgi cell firing rate responses described in Chapter 3. In nine recording sessions we were able to record simultaneously from a Golgi cell and either an isolated mossy fiber single unit (n=5) or multiunit "hashing" activity made up of one or a few single units that could not be fully isolated (n=4). The single unit activity was thought to represent mossy fiber terminals rather than granule or other cell types because the spike profile and response type matched the characteristics previously described for mossy fibers (Lisberger and Fuchs, 1978; Miles et al., 1980; Noda, 1986) and because the impedance of our electrodes was probably too low to reliably isolate small, densely packed neurons such as granule cells. The multiunit hashing was also thought to reflect the activity of one or a few mossy fiber terminals because the response type and directional tuning of the hashing tended to match that of mossy fiber single units recorded nearby.

The results of these nine simultaneous Golgi cell-mossy fiber recording sessions are presented in Figure 4.6. Figure 4.6A shows the raw extracellular recording trace and the instantaneous firing rates for the sorted mossy fiber and Golgi cell of one such session.

Surprisingly, given the glutamatergic nature of the mossy fiber-Golgi cell synapse, the two units appear to have an antiphasic relationship, whereby an increase in firing rate of one unit is accompanied by a decrease in firing rate of the other unit. This relationship was confirmed by calculating a peristimulus time histogram of Golgi cell spikes aligned with respect to either the mossy fiber burst (4.6B top panel) or pause (4.6B bottom panel). A clear dip in the Golgi cell firing rate is observed following mossy fiber bursts, and a clear rise in the Golgi cell firing rate is observed following mossy fiber pauses. Note that the Golgi cell off responses evolved faster than the on responses (initial time constants), as also seen in the population of Golgi cells (c.f., Fig 3.4F). A potential explanation for this phenomenon becomes clear from examining the simultaneous mossy fiber and Golgi cell responses. That is, the fast Golgi cell off responses coincide with mossy fiber bursts, which are a rapid and strong stimulus, whereas the slower Golgi cell on responses coincide with cessations of mossy fiber tonic activity, a relatively weaker stimulus. This suggests that Golgi cell time constants are a reflection of both the intrinsic membrane properties of the neurons (Forti et al., 2006) and the level of activity of the mossy fibers that innervate them.

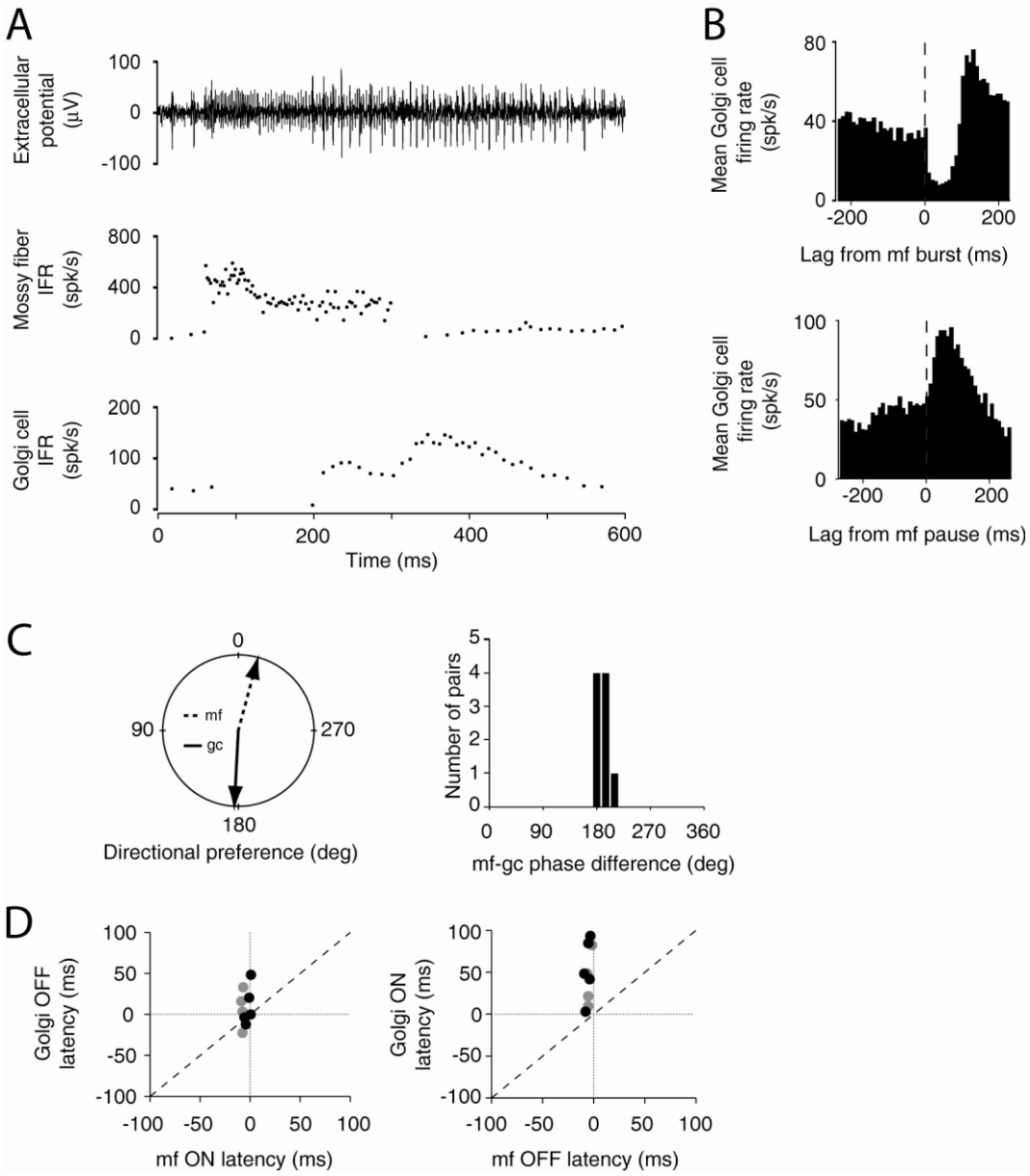

Figure 4.6. Relationship between mossy fiber and Golgi cells simultaneously recorded during spontaneous eye movements. A, Raw trace from extracellular recording of a mossy fiber-Golgi cell pair on the same electrode (top) and corresponding instantaneous firing rate (IFR) for the mossy fiber (middle) and Golgi cell (bottom). An upward saccade occurred around 90 ms and a downward saccade occurred around 300 ms, producing a burst and then a pause in the mossy fiber firing rate. Note that the Golgi cell appears to be negatively coupled to the mossy fiber. B, This negative coupling is explored further in PSTHs of the same Golgi cell triggered on the mossy fiber burst (top) or pause (bottom). C, The negative coupling between the same mossy fiber-Golgi cell pair is also expressed as opposite directional preferences for on responses (left). This is true for the entire population of 9 pairs (right). D, Relationship between Golgi cell off response latencies and mossy fiber on latencies (left), and Golgi cell on response latencies and mossy fiber off latencies for all 9 mossy fiber-Golgi cell pairs. Mossy fiber single units are shown as black dots and multiunit hashing is shown as gray dots. Dots falling above the diagonal line indicate that the mossy fiber responds before the Golgi cell. The cluster of three dots at the top of the right panel in D correspond to Golgi cells with on latencies that fall outside the range displayed in the plot. These latencies are 114, 113, and 157 ms.

The apparent antiphasic relationship was further explored by calculating the preferred direction vectors for both the mossy fiber and Golgi cell, which were found to point in opposite directions for this pair and for the population of paired recordings as a whole (Fig 4.6C). The relative latencies from saccade initiation of mossy fiber bursts and Golgi cell pauses and vice versa suggest that both the mossy fiber increases and decreases in firing rate precede the corresponding changes in Golgi cell firing rate (Fig 4.6D). Finally, for the 9 pairs tested there was a strong correlation between the eye position activation threshold for a mossy fiber and the off direction upper eye position field boundary of the corresponding Golgi cell (Pearson correlation coefficient=0.91, $p<<0.05$).

To get a better picture of how widespread the antiphasic mossy fiber-Golgi cell responses were we analyzed an additional 10 Golgi cells for which mossy fibers had been isolated in the same folium during the same recording session, but were not recorded simultaneously. Of these, 9 Golgi cells had pauses in firing rate for saccades in the on direction of a nearby mossy fiber, suggesting that the mossy fiber may have been contributing to the pause. The remaining Golgi cell had the same on direction as a mossy fiber recorded nearby. It was not clear how the mossy fiber terminals themselves were distributed in terms of preferred directions. On the one hand, multi-unit activity was often narrowly tuned for eye position (n=11/13), suggesting some response homogeneity of mossy fibers in the volume of space picked up by our electrodes; on the other hand, mossy fibers with different directional tunings were routinely recorded within the same folium on a single electrode track (n=7/8), often less than 100 microns apart. It is

interesting to note that on those sessions where multiple mossy fibers were recorded near a Golgi cell, the Golgi cell pause was only explained by the directional preference of one of the mossy fibers (n=3).

These data taken together support the hypothesis that the mossy fiber inputs contribute to the Golgi cell's pause in firing rate and suggest that Golgi cells may only sample a subset of the available mossy fiber activity.

Types of Purkinje cells encountered

Based on response profiles during visuo-vestibular behaviors, previous investigators have determined that there are two predominant types of Purkinje cells in the VPFL (Miles et al., 1980; Belton and McCrea, 2000), eye movement only and eye movement plus head movement (gaze). The latter tend to have responses during both pursuit and VOR cancelation that are in phase with eye or head velocity, while the former tend to have phases between eye position and eye velocity (Belton and McCrea, 2000). The criterion for segregating the two populations of Purkinje cells is that gaze velocity Purkinje cells are defined as those with a "significant modulation during VORS," which can sometimes be a tenuous distinction. Therefore, rather than attempt a categorization between the two types we chose to lump them together and examine their responses as a whole. This approach also allows us to compare eye movement and vestibular responses for the population of Purkinje cells as a whole with the population of Golgi cells presented in the previous chapter.

Response properties of eye movement and gaze velocity Purkinje cells

As presented in Chapter 3, the spike patterns of Purkinje cells are generally more irregular than Golgi cells. Figure 4.7 shows the instantaneous firing rate of a typically defined gaze velocity Purkinje cell during pursuit and horizontal VORS. This neuron had a median firing rate of 110 spks/s and a median CV_2 of 0.27, both of which fall within the range of typical values for Purkinje cells. The neuron modulated approximately in phase with ipsiversive eye velocity during pursuit (Fig. 4.7A; 91.9 degree phase advance from peak eye position) and ipsiversive head velocity during horizontal VORS (Fig 4.7B; 96.7 degree phase advance from peak chair position). Because the phases of most Purkinje cells fell somewhere between position and velocity coding, we chose to represent the responses of the neurons to pursuit and VORS as the amplitudes and phases of least squares sinusoidal fits to the average firing rate over at least five cycles, rather than as sensitivities to position or velocity, as is often done. Neurons were classified as horizontal if they modulated more during horizontal pursuit than during vertical, and as vertical if the converse was true. As a population, our VPFL Purkinje cells were more responsive during pursuit than during VORS (Fig 4.8). The mean ratio of horizontal VORS modulation to pursuit modulation was 0.74 +/- 0.45 (mean +/- SD) for horizontal units (n=12), which is slightly less than the ratio of sensitivities previously reported in the squirrel monkey (Belton and McCrea, 2000; Blazquez et al., 2003) and reflects the fact that we included a portion of Purkinje cells that would not normally be classified as gaze velocity. The mean ratio of horizontal VORS and pursuit modulation for vertical units was 0.43 +/- 0.19 (n=13). Presumably the ratio would have been higher if we were able to stimulate the vertical semicircular canals during VORS. On the other hand, Golgi cells had a mean ratio of horizontal VORS and pursuit modulation of 0.21 +/- 0.18 (n=18),

with the modulation during VORS being explained by the neurons' sensitivities to residual eye movement from imperfect VOR cancelation.

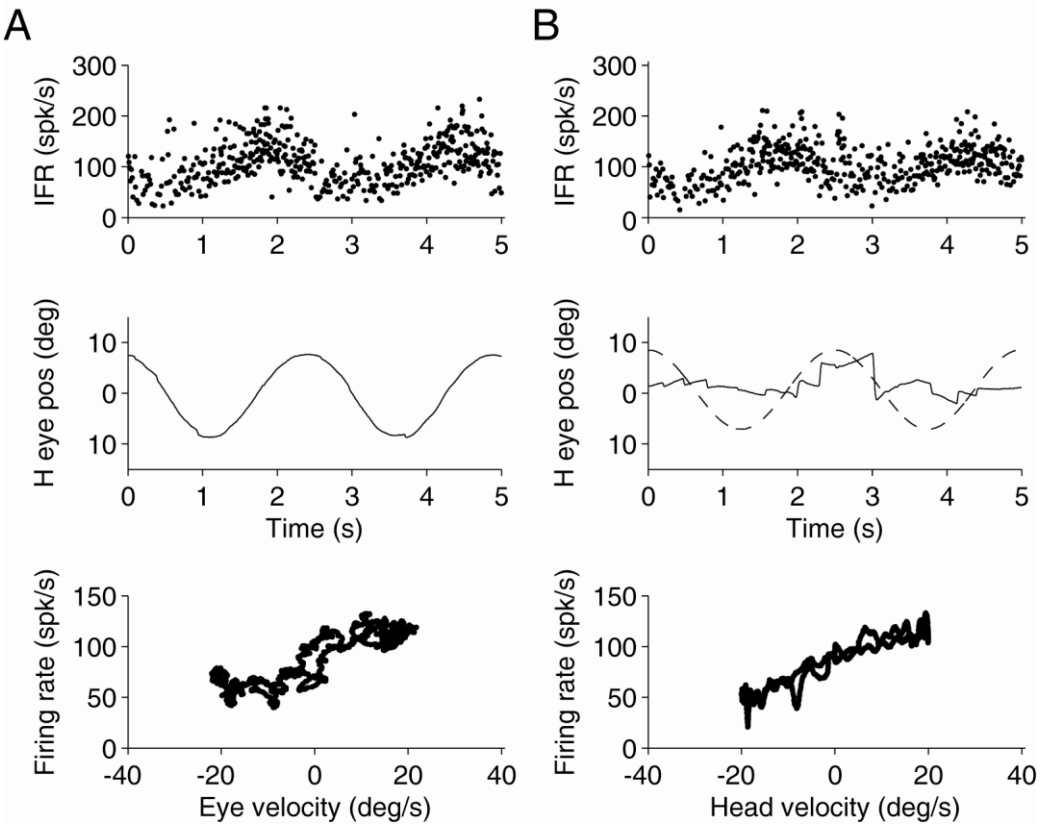

Figure 4.7. Example horizontal "gaze velocity" Purkinje cell during pursuit (A) and VORS (B). A-B: From top to bottom, instantaneous firing rate (IFR), horizontal eye position, cycle averaged firing rate vs eye velocity (A) or head velocity (B). Averages were computed over at least 5 cycles. In middle panel of B, dotted lines indicate head velocity.

Despite the classification as horizontal or vertical units, the majority of Purkinje cells responded during both horizontal and vertical pursuit, as depicted in Figure 4.9. On average, neurons modulated approximately half as much during pursuit in the non-maximal plane (mean ratio non-maximal/maximal=0.52 +/- 0.26, n=36), and 55% of neurons modulated at least half as much during pursuit in the non-maximal plane. This contrasts with Golgi cells, where only 22% (6/27) modulated at least half as much during pursuit in the non-maximal plane. This suggests that Purkinje cells are more broadly

tuned than Golgi cells. However, previous authors have shown that the overall directional tuning of Purkinje cells during pursuit is determined by a linear interaction between eye position and velocity signals that do not necessarily have the same directional preferences (Leung et al., 2002). Consistent with this, when we examined the phases of our Purkinje cell population, we found that the responses were broadly distributed between "position" and "velocity". Moreover, when we examined all Purkinje cells with firing rate modulations exceeding 10 spk/s for both horizontal and vertical pursuit, we found a broad distribution of phase differences between the horizontal and vertical responses.

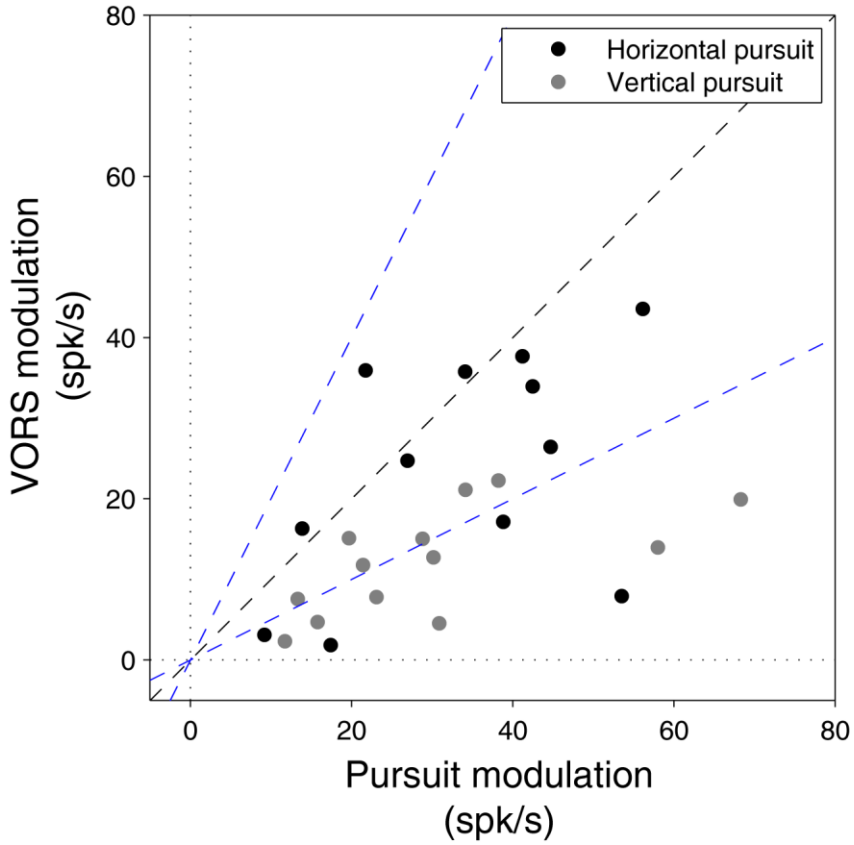

Figure 4.8. Relationship between individual Purkinje cells' modulation during horizontal VORS and pursuit. Pursuit modulation amplitude was plotted for the plane that maximally excited the neuron, horizontal (black) or vertical (gray). Black dotted line indicates unity and blue dotted lines indicate 2x or 0.5x.

However, another possibility is that a greater proportion of Purkinje cells than Golgi cells have non-cardinal preferred directions. We attempted to address this by applying the same analysis of spontaneous saccades to our Purkinje cell population as we did for the Golgi cells and mossy fibers, but we found that the Purkinje cell responses during spontaneous eye movements were too heterogeneous for this approach to work. This was compounded by the fact that a large proportion of Purkinje cells in the VPFL are tuned for velocity during smooth pursuit (Miles et al., 1980; Belton and McCrea, 2000), so it wasn't clear how much of the response would be apparent in spontaneous saccades. Figure 4.10 presents the four zone PSTHs for three example Purkinje cells, showing the three primary types of responses that we observed during spontaneous saccades. The response types during saccades could be roughly classified as burst-tonic/tonic (Fig 4.10A; 17/32), burst only (Fig 4.10B; 4/32), and pause (Fig 4.10C; 11/32). The median burst-tonic ratio of Purkinje cells in the first two categories was 1.4 (range: 1.1-2.4), which is in between the median ratio for Golgi cells and mossy fibers. The third category is especially interesting because it reflects a response type not seen in the eye movement mossy fiber inputs. We explored the origin of these responses using pharmacological manipulation.

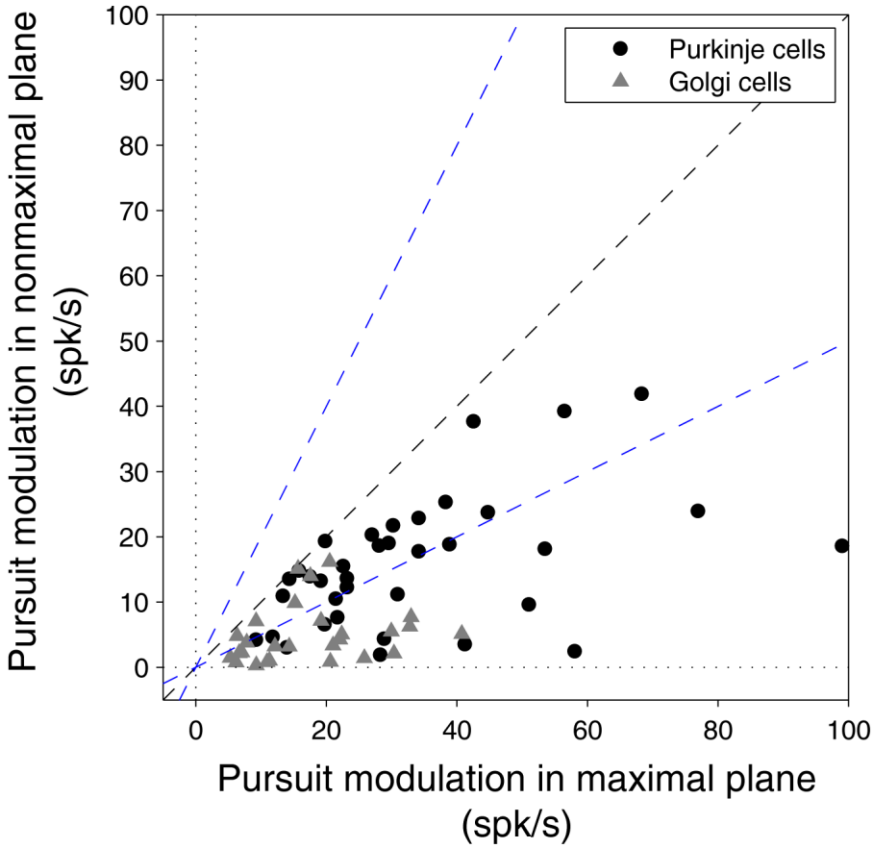

Figure 4.9. Directional specificity of Purkinje and Golgi cell responses during horizontal and vertical sinusoidal pursuit. Modulation amplitude during pursuit in the non-maximal activation plane for the neuron versus modulation amplitude during pursuit in the maximal plane. Blue dashed lines indicate 2x or 0.5x responses.

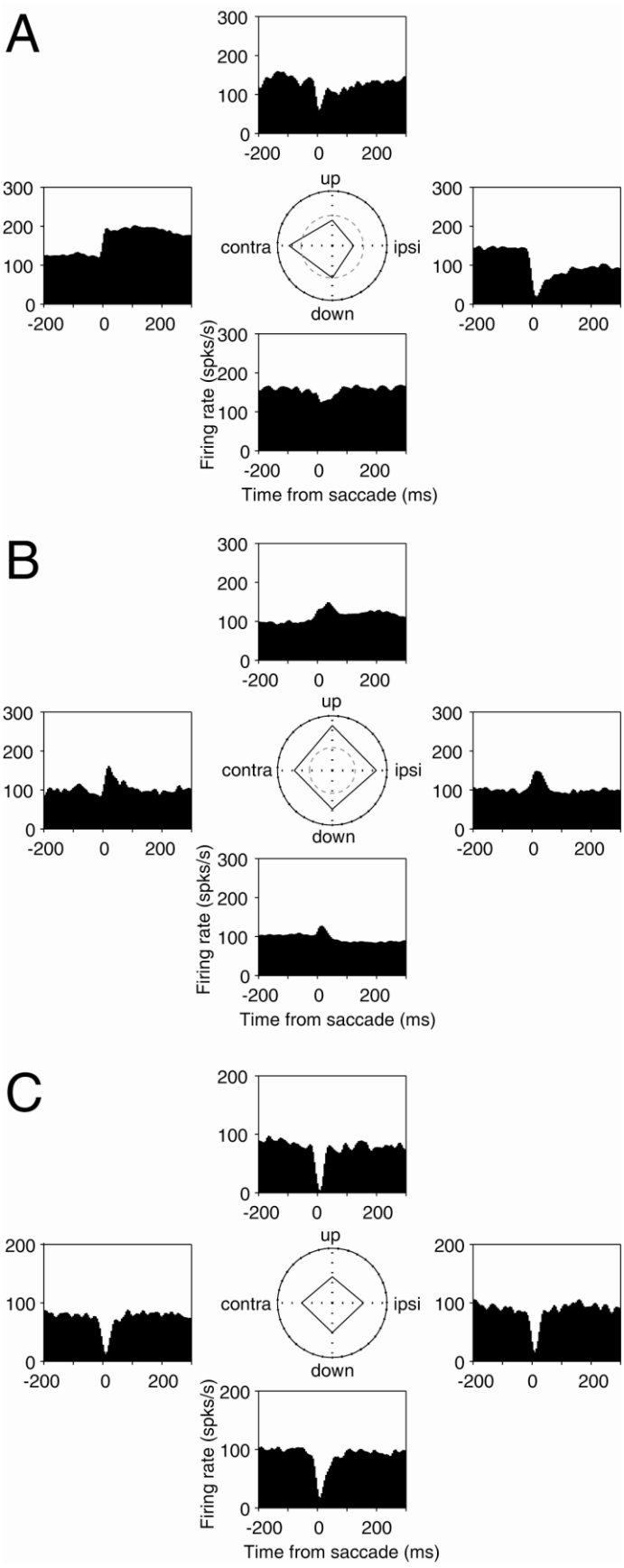

Figure 4.10. Four zone PSTHs for 3 representative Purkinje cells. Format is the same as Fig 4.2.

Effect of blocking GABAergic inhibition near Purkinje cells

We hypothesized that the saccade-related pauses in Purkinje cell firing rate are due to inhibition from molecular layer interneurons. To test this, we employed the multibarrel carbon fiber electrodes detailed in Chapter 2 to iontophoretically inject minute amounts of SR-95531 (gabazine), a potent GABA-A receptor antagonist, while recording Purkinje cell responses during spontaneous saccades. Figure 4.11 presents the four zone PSTHs of two Purkinje cells before (A,C) and during (B,D) gabazine injection. The neuron in Fig 4.11A had a subtle burst-tonic or tonic excitatory response for downward saccades and rapid and sustained pause for upward saccades. It also had small, barely detectable pauses for rightward and leftward saccades. During gabazine injection (Fig 4.11B), this neuron substantially changed its firing pattern, now responding with robust bursts for downward and rightward saccades, moderate bursts for leftward saccades, and a less pronounced pause for upward saccades, despite no difference in the average direction or amplitude of the saccades for those zones. Thus, the effect of gabazine on this neuron was to reduce the amplitude of pauses, sometimes flipping the sign of the response (i.e., for leftward and rightward saccades), and enhance the amplitude of bursts. The increased "burstiness" seen in this neuron was generally seen among the population of Purkinje cells recorded during gabazine injection, producing burst-tonic ratios different than the Purkinje cells without gabazine ($p=0.02$, Mann-Whitney U Test) and more like the population of mossy fibers (median BT ratio=2.3; range: 1.03-3.6; $p=0.15$, Mann-Whitney U Test). However, the effect of gabazine was not simply to increase the burst amplitudes of neurons during saccades. The Purkinje cell in Figure 4.11C initially paused for saccades in all directions. Injection of gabazine (Fig 4.11D) abolished the pause for downward and leftward

saccades, with little if any reduction in the amplitude of the pauses for upward and rightward saccades. Thus, the effect of gabazine on this neuron was to abolish the pauses in a directionally selective manner.

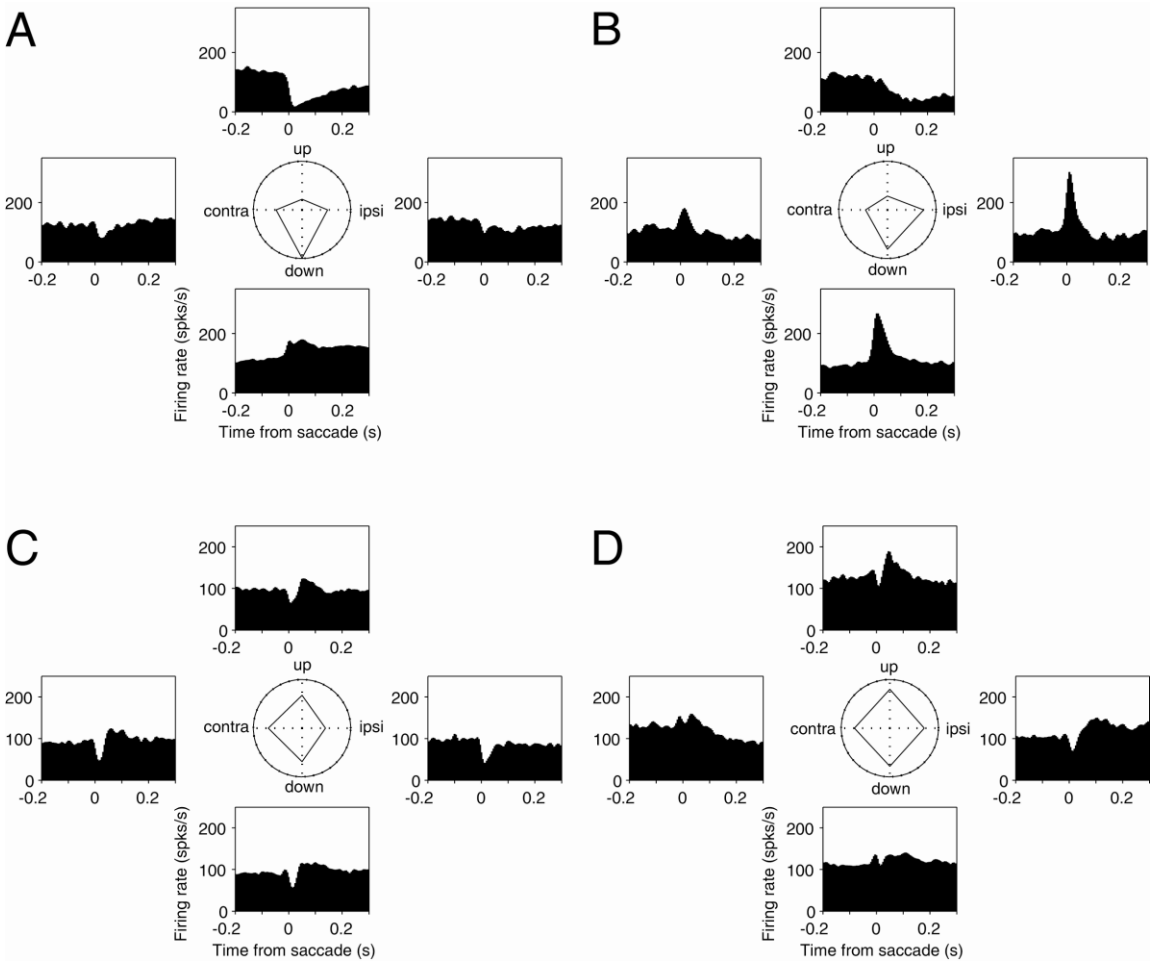

Figure 4.11. Four zone PSTHs for two Purkinje cells before (A,C) and during local gabazine injection (B,D). Format is same as Figs 4.10 and 4.2.

Because not all neurons could be recorded during a control period before injection due to leakage of the drug in some sessions, we sought to compare the responses of the population of Purkinje cells during gabazine with the population of Purkinje cells we

recorded with standard tungsten electrodes. We did this by generating four zone PSTHs during spontaneous saccades for every neuron in the two populations and measuring the depth of modulation during a 50 ms window starting 10 ms before saccade onset (roughly the latency of BT mossy fibers). Depth of modulation was calculated as the difference between the mean firing rate during the 50 ms window and the mean firing rate during a 100 ms control period starting 150 ms before saccade onset. We then quantified the range of responses for the four directions by taking the minimum and maximum depth of modulation. For example, the neuron in Fig 4.11A had a minimum depth of modulation of around -100 spk/s and a maximum of around 50 spk/s before the injection. The results of this analysis are presented in Figure 4.12, where we plot the minimum and maximum depths of modulation for all 32 neurons recorded before or without gabazine injection and 10 neurons recorded during gabazine injection. The two neurons from Figure 11 are indicated by the numbers "1" and "2". The distributions of minimum and maximum depths of modulation were significantly different for the two populations ($p<0.001$ for comparison of minimums and $p<0.0005$ for comparison of maximums; Mann-Whitney U Test). In addition, while the majority of neurons recorded before or without gabazine injection have minimum depths of modulation below zero (25/32, 78%) and a large proportion have maximums below zero (10/32, 31%), only 30% (3/10) of the neurons during gabazine have minimums below zero and none have maximums below zero. This indicates that the effect of gabazine is not only a reduction in the amplitude of pauses and an enhancement in the amplitude of bursts, but also a sign reversal, where pauses become bursts. This suggests that gabazine is acting to eliminate an inhibitory signal that may be acting to suppress saccade-related bursting in Purkinje cells.

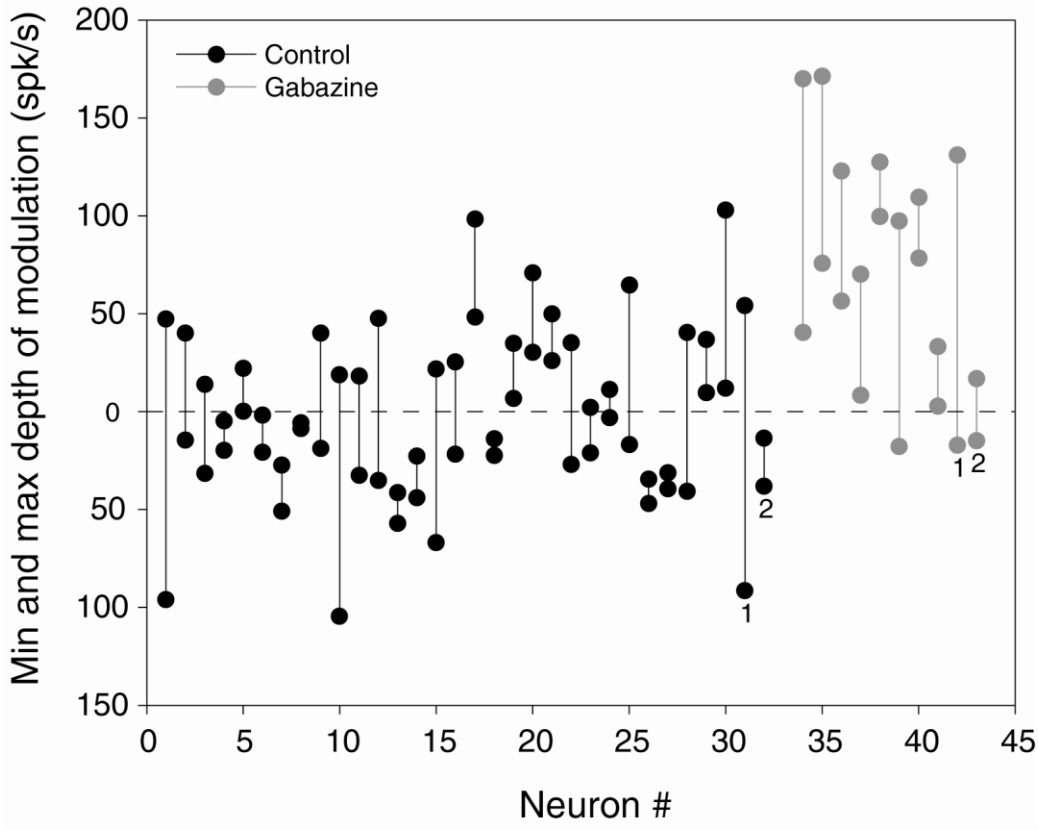

Figure 4.12. Effects of gabazine on saccade-related firing rates of Purkinje cells. For each neuron, the minimum and maximum depths of modulation were taken from four zone PSTHs as described in the text. The minimum and maximum depths of modulation are connected by solid lines. Black dots and lines indicate normal Purkinje cells and gray dots and lines indicate Purkinje cells recorded during gabazine injection. The data points marked with "1" and "2" are for the same two neurons before and during gabazine injection.

Discussion

We recorded mossy fibers and Purkinje cells in the ventral paraflocculus of the squirrel monkey during vestibulo-oculomotor behaviors and have compared the response characteristics of these units with the responses of Golgi cells in an attempt to discern what role the Golgi cells may be playing in VPFL processing. In addition, we performed pharmacological manipulation of GABAergic inhibition near Purkinje cells to examine the role of inhibition in shaping Purkinje cell responses during saccades. We found that mossy fibers have similar tuning widths as Golgi cells, but Purkinje cells are more broadly tuned. Purkinje cell tuning during smooth pursuit is most likely determined by an interplay of differently tuned eye position and velocity signals (Leung et al., 2002). We also found that mossy fibers and Golgi cells as a population have similar eye position thresholds for activation (mossy fibers) and inhibition (Golgi cells), and that a strong correlation between these parameters exists at the level of individual mossy fibers and Golgi cells recorded simultaneously. This suggests that Golgi cell activity may be strongly driven by a small number of specific inputs, raising the possibility that a highly specific connection between mossy fibers and Golgi cells produces contextual filtering of mossy fiber to granule cell throughput via Golgi cell inhibition of a patch of granule cells.

Origin of Golgi cell responses

We found that Golgi cells had highly specific responses, suggesting the possibility that a small number of inputs with similar tuning define a Golgi cell's firing rate modulation. Additionally we found that, consistent with earlier studies, the dominant response of

Golgi cells is a pause in firing rate (Holtzman, et al. 2006). It is difficult to reconcile these observations with classical descriptions of the cerebellar cortical microanatomy, wherein the dominant inputs to Golgi cells are glutamatergic, via mossy and parallel fibers (Eccles et al., 1967; Palay and Chan-Palay, 1974). Moreover, assuming that the units we recorded simultaneously with Golgi cells were indeed mossy fibers, it is puzzling that the pairs were antiphasic. However, there are at least two mechanisms that can be invoked to explain these phenomena (Fig 4.13). First, Golgi cells have been proposed to receive inhibitory input (via GABAergic and glycinergic synapses) from molecular layer interneurons, including basket and stellate cells (D'Angelo and De Zeeuw, 2009). Little is known about the synaptic efficacy of this inhibition, but if the molecular layer interneurons are driven by inputs with a similar tuning as the mossy fiber recorded simultaneously with the Golgi cell, they would presumably produce a Golgi cell pause in response to a mossy fiber burst. This action through a "third player" could explain the antiphasic relationship between the mossy fiber and Golgi cell. But it is difficult to imagine how the tight correlation between the mossy fiber and Golgi cell could be maintained through a third player unless the same mossy fiber provides strong innervation of the molecular interneurons inhibiting the Golgi cell. Another possibility is that mossy fibers act directly on Golgi cells through an inhibitory mechanism mediated by mGluR2 receptor activation of G-protein coupled inward rectifying potassium (GIRK) channels (Watanabe and Nakanishi, 2003). This is a similar mechanism to that of the mGluR6 receptors at the photoreceptor-bipolar cell synapse in the retina (Snellman et al., 2008). Interestingly, some of our Golgi cells occasionally showed a transient (1-2 spikes) burst in firing rate immediately preceding the pause, which could reflect activation of

excitatory ionotropic glutamate receptors such as AMPA prior to the opening of the GIRK channels. Thus the decreases in firing rate may result from a net dominance of mGluR2 receptor mediated inhibition over AMPA and NMDA channel mediated excitation. A small number of mossy fibers could substantially influence the Golgi cell firing pattern, particularly if they act via large *en marron* synapses between mossy fiber rosettes and Golgi cell somata (Chan-Palay and Palay, 1971). But even the mossy fiber inputs to the descending Golgi cell dendrites could be sparse and strong enough to derive this specificity. This was predicted over forty years ago by Eccles and colleagues (1967, pg. 61):

> *By means of its descending dendrites the Golgi cell has also direct synaptic contacts with the mossy fibers. Some at least of these contacts have a considerable area so that this synaptic articulation may be quite powerful. On the other hand the descending dendrites arborize rather sparsely in the granular layer and with less spread than the ascending dendrites. This means that they can be excited only from a much more limited field of active mossy fibers….*

We propose that a given Golgi cell's eye position field is determined by the activation threshold and response range of the mossy fiber or fibers providing its dominant input(s). Since Golgi cells in the VPFL appear to only reflect the activity of the eye movement pathway and the relationship between the mossy fibers and Golgi cells is antiphasic, the Golgi cell activity in essence provides a negative image, with an additional temporal transformation, of the motor command being sent to the extraocular muscles. This may have implications for the construction of forward models for movement control. In this scheme, the parallel fiber inputs may serve to synchronize the spontaneous spike times of on beam Golgi cells (Maex and De Schutter, 1998; Maex et al., 2000) rather than contributing significantly to moment-to-moment modulations in firing rate. Further investigation using pharmacological manipulation will be necessary to better understand

the origin of the antiphasic response between Golgi cells and mossy fibers and the generation Golgi cell eye position fields.

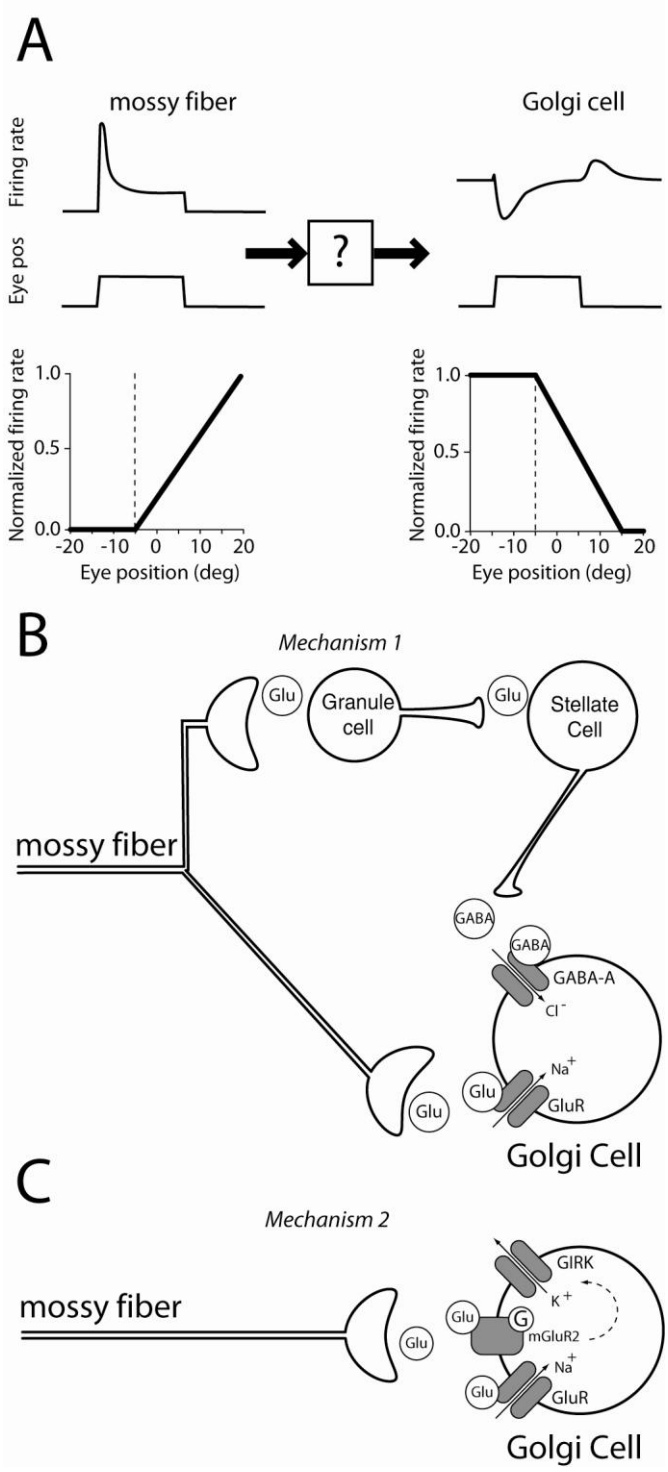

Figure 4.13. Plausible mechanisms to explain Golgi cell responses. A, On left, typical mossy fiber burst-tonic response (top) to a change in eye position resulting from a saccade (middle) and hypothetical firing rate versus eye position curve (bottom). Vertical dashed line indicates mossy fiber eye position activation threshold. On the right, typical Golgi cell response for the same eye movement. Note that Golgi cell off response corresponds to mossy fiber burst and on response corresponds to mossy fiber pause. This antiphasic coupling results in the Golgi cell having an inverted eye position response range compared to the mossy fiber (dashed line). B-C, Two possible mechanisms to explain antiphasic coupling of mossy fiber and Golgi cell responses based on known connections and synaptic properties (see text). B, Mechanism 1: Indirect mossy fiber effect over Golgi cell via inhibitory interneurons receiving similarly tuned mossy fiber-granule cell input as Golgi cell. Glutamate (Glu) released from mossy fiber terminals activates ionotropic glutamate receptors (GluR) on Golgi cell and inhibitory interneuron, such as stellate cell. Stellate cell then releases inhibitory neurotransmitter, such as GABA, to generate a Golgi cell firing rate pause in response to mossy fiber burst. GluR activation on the Golgi cell generates initial burst (c.f. Fig. 4A) preceding the pause. C, Mechanism 2: Direct mossy fiber effect over Golgi cell via mGluR2 activation of G-protein coupled inward rectifying potassium (GIRK) channels. Glutamate released from mossy fiber terminals activates ionotropic and metabotropic glutamate (i.e., mGluR2) receptors on Golgi cell. The balance between inward current through GluR and outward current through GIRK determines net response of Golgi cell.

Role molecular inhibition revealed by gabazine injections

Our injections of gabazine near simultaneously recorded Purkinje cells likely had the largest effect on inhibition of Purkinje cells by molecular layer interneurons such as basket and stellate cells, rather than e.g. Golgi cell inhibition of granule cells, because gabazine injected with the currents we used is not expected to spread further than approximately 100 ums (Herz et al., 1969). Because the effect of gabazine was to reduce the amplitude of pauses and increase the amplitude of bursts, sometimes turning a pause into a burst, we propose that inhibition from molecular layer interneurons normally serves to partially suppress the burst component of BT mossy fibers that the selective Golgi cell filtering allows to pass to granule cells. This may allow the inhibitory network comprised of Golgi cells and molecular layer interneurons to produce Purkinje cell responses that are phase advanced with respect to the mossy fiber inputs without being dominated by bursts, thus producing the variety of phases seen in VPFL Purkinje cells during pursuit.

References

Belton T, McCrea RA (2000). Role of the cerebellar flocculus region in cancellation of the VOR during passive whole body rotation. J Neurophysiol 84(3):1599-613.

Blazquez PM, Hirata Y, Heiney SA, Green AM, Highstein SM (2003). Cerebellar signatures of vestibulo-ocular reflex motor learning. J Neurosci 23: 9742-9751.

Chan-Palay V, Palay SL (1971). The synapse en marron between golgi II neurons and mossy fibers in the rat's cerebellar cortex. Zeitschrift für Anatomie und Entwicklungsgeschichte 133: 274-287.

D'Angelo E, De Zeeuw CI (2009). Timing and plasticity in the cerebellum: focus on the granular layer. Trends Neurosci 32: 30-40.

Dieudonne S (1998). Submillisecond kinetics and low efficacy of parallel fibre-Golgi cell synaptic currents in the rat cerebellum. J Physiol 510: 845-866.

Eccles J, Ito M, Szentágothai J (1967). The Cerebellum as a Neuronal Machine (Heidelberg: Springer-Verlag).

Eccles J, Llinas R, Sasaki K (1964). Golgi cell inhibition in the cerebellar cortex. Nature 204: 1265-1266.

Forti L, Cesana E, Mapelli J, D'Angelo E (2006). Ionic mechanisms of autorhythmic firing in rat cerebellar Golgi cells. J Physiol 574:711-729.

Herz, A., Zieglgansberger, W., and Farber, G. (1969). Microelectrophoretic studies concerning the spread of glutamic acid and GABA in brain tissue. Exp Brain Res 9, 221-235.

Holtzman T, Rajapaksa T, Mostofi A, Edgley SA (2006). Different responses of rat cerebellar Purkinje cells and Golgi cells evoked by widespread convergent sensory inputs. J Physiol 574: 491-507.

Kanichay RT, Silver RA (2008). Synaptic and cellular properties of the feedforward inhibitory circuit within the input layer of the cerebellar cortex. J Neurosci 28: 8955-8967.

Leung HC, Suh M, Kettner RE (2000). Cerebellar flocculus and paraflocculus Purkinje cell activity during circular pursuit in monkey. J Neurophysiol 83:13-30.

Lisberger SG, Fuchs AF (1978a). Role of primate flocculus during rapid behavioral modification of vestibuloocular reflex. I. Purkinje cell activity during visually guided horizontal smooth-pursuit eye movements and passive head rotation. J Neurophysiol 41: 733-763.

Lisberger SG, Fuchs AF (1978b). Role of primate flocculus during rapid behavioral modification of vestibuloocular reflex. II. Mossy fiber firing patterns during horizontal head rotation and eye movement. J Neurophysiol 41: 764-777.

Maex R, Vos BP, De Schutter E (2000). Weak common parallel fibre synapses explain the loose synchrony observed between rat cerebellar golgi cells. J Physiol 523: 175-192.

Maex R, De Schutter E (1998). Synchronization of golgi and granule cell firing in a detailed network model of the cerebellar granule cell layer. J Neurophysiol 80: 2521-2537.

Miles FA, Fuller JH, Braitman DJ, Dow BM (1980). Long-term adaptive changes in primate vestibuloocular reflex. III. Electrophysiological observations in flocculus of normal monkeys. J Neurophysiol 43: 1437-1476.

Mittmann W, Koch U, Häusser M (2005). Feed-forward inhibition shapes the spike output of cerebellar Purkinje cells. J Physiol 563: 369-78.

Noda H (1986). Mossy fibres sending retinal-slip, eye, and head velocity signals to the flocculus of the monkey. J Physiol 379: 39-60.

Noda H, Warabi T (1987). Responses of Purkinje cells and mossy fibres in the flocculus of the monkey during sinusoidal movements of a visual pattern. J Physiol 387: 611-628.

Palay S, Chan-Palay V (1974). Cerebellar cortex cytology and organization (New York: Springer)

Santamaria F, Tripp PG, Bower JM (2007). Feedforward inhibition controls the spread of granule cell-induced Purkinje cell activity in the cerebellar cortex. J Neurophysiol 97(1):248-63.

Snellman J, Kaur T, Shen Y, Nawy S (2008). Regulation of ON bipolar cell activity. Prog Retin Eye Res 27: 450-463.

Thach WT (1968). Discharge of Purkinje and cerebellar nuclear neurons during rapidly alternating arm movements in the monkey. J Neurophysiol 31: 785-797.

Thach WT, Goodkin HP, Keating JG (1992). The cerebellum and the adaptive coordination of movement. Annu Rev Neurosci 15: 403-442.

Watanabe D, Nakanishi S (2003). mGluR2 postsynaptically senses granule cell inputs at Golgi cell synapses. Neuron 39: 821-829.

Chapter V

Future directions to unravel the roles of cerebellar cortical interneurons in sensori-motor processing

While the title of this dissertation is very general, the work described in the preceding pages was only a first step in an attempt to understand the computations performed by the cerebellar cortex and the role that these computations play in controlling oculomotor behavior. In this chapter I will discuss some ideas for additional experiments to attack the problem.

In this work we focused primarily on the first stage of processing, as information enters the cerebellar cortex. We showed that Golgi cells have highly specific responses, including an exclusive coding of eye movement information and responses within only a fixed range of eye positions (the so-called eye position fields). We argued that these properties would allow the Golgi cells, through their inhibition of granule cells, to restrict the flow of information to subsequent processing stages based on the state of the motor system, and we suggested that this kind of state-specific filtering could be useful for the construction of forward (predictive) models in the oculomotor system. The problem with this interpretation is that it is vague. In fact, most conceptions of forward models suffer from the same problem (see Ghasia et al., 2008 for a critique). As motor physiologists we know that forward models must exist in order to allow animals to predict the consequences of their own movements, and that they must be implemented somehow in the brain, but we seem to have trouble defining what exactly a forward model should look like (Lisberger, 2009). Thus, we have trouble finding evidence for such models in the

central nervous system. However, a couple of recent experiments stand out as examples of the kinds of experiments that should be done to move us in the right direction.

First, Sawtell and Williams (2008) recorded sensory afferents from the electroreceptors and efferent cells in a cerebellum-like structure in the presence and absence of tail movements. The efferent cells resemble the target neurons of Purkinje cells in higher vertebrates. By recording from these two nodes in the processing stream these authors were able to show that sensory information about the tail movements was somehow subtracted out from the afferent signal, using either a central or proprioceptive signal. This is an exciting result because it implies that the consequences of self motion are already removed at the output of the cerebellum and suggests that the cerebellar cortical circuit may be involved in this process. However, the major problem with their experiments, from a motor control perspective, was that the tail movements were passively generated by the investigators rather than self-generated by the fish. Therefore, they may have been missing an important component in the generation of forward models, namely, a motor command.

Another experiment that stands out as push in the right direction, and which is more directly related to the problems addressed in this dissertation, was Ghasia and colleagues (2008), who used a different approach to probe the loci of forward models. These authors utilized the fact that for certain types of eye movements the motor command signal that generates the eye movement is dissociable from the 3D kinematics of the eye. They examined the representation of eye movements at two different nodes in the oculomotor system, a brainstem nucleus that provides a large input to the VPFL (the source of the burst-tonic mossy fibers) and a nucleus that serves as the output of the VPFL. They

argued that neurons representing the output of a forward model should carry signals appropriate to represent the 3D kinematics of the eye rather than the motor command itself. Using this approach, they found that, while input neurons to the VPFL code the oculomotor command signal, the neurons at the output of the VPFL have a signal more consistent with the 3D kinematics. As alluded to in the Introduction to Chapter 3, this suggests that at least some of the processing necessary to generate a forward model of the oculomotor system takes place within the cerebellar cortex.

The promising results from these two sets of experiments suggest a direction for future studies of cerebellar cortical computations within the framework of internal models. First, tasks should be designed that require some degree of prediction of one's movement for successful completion but allow a decoupling of the prediction from the motor response. Electrophysiologists could then put electrodes in the cerebellum to look for signals related to the prediction. This kind of study was already performed by Cerminara and colleagues (2008) and they found that Purkinje cells in the lateral cerebellum of the cat encode a signal related to the predicted trajectory of a target. If this approach could be extended to an area of the cerebellum that has more well-defined inputs and outputs, such as the VPFL, and other cell types in the cerebellar cortex were recorded, tremendous gains could be made. We are currently designing just these kinds of tasks, one of which is already implement in the task control program presented in Chapter 2 (the "target interception" task), and will soon begin recording Purkinje cells while the monkeys perform the tasks.

Another potential avenue to explore this line of inquiry is to see how manipulating different circuit elements in the cerebellar cortex affects an animal's ability to perform

complex predictive tasks. Neurological results from cerebellar patients suggest that lesions of the cerebellum disrupt this ability (Bo et al., 2008), but what about less severe disruptions of the circuit? Because most intracortical processing, besides the main excitatory pathway through granule cells, is mediated by inhibitory interneurons, perhaps the most straightforward way to test this would be to pharmacologically disrupt GABAergic signaling in a particular area of the cerebellar cortex of the monkey, e.g. with large gabazine injections, to see what role intracortical inhibition plays in the ability to perform these complex predictive tasks. Ideally, one would like to dissociate actual motor deficits from deficits of prediction. I performed some preliminary experiments that suggest this can be done. I performed a series of injections of either muscimol or gabazine in the VPFL while untrained monkeys performed an ocular following paradigm similar to pursuit but requiring no prediction (the eye movements are a response to a retinal error signal from whole field motion of a random dot pattern). Following muscimol injection the monkey experienced the hallmark signs of flocculus inactivation, including downbeat nystagmus and a substantial reduction in the ocular following gain. However, there was no detectable deficit in ocular following gain after gabazine injection. My interpretation of these results is that wholesale inactivation of the VPFL with muscimol creates an imbalance in the brainstem pathways mediating eye movement by eliminating tonic inhibition of VPFL target neurons in the vestibular nuclei by Purkinje cells, while the more modest interruption of the cerebellar circuit with gabazine leaves basic oculomotor behaviors intact. If this result holds it could allow us to look for more subtle effects of gabazine on oculomotor behavior, while controlling for overall deficits in eye movement generation.

An even more exciting prospect for selectively manipulating the circuit is offered by the new field of optogenetics (Scanziani and Häusser, 2009). One day in the near future we may be able to selectively silence interneurons belonging to a particular class, e.g. Golgi cells, while leaving the other interneuron networks intact. Golgi cells are an excellent candidate for this approach because gene promoters specific to Golgi cells have already been successfully used to genetically target them for ablation (Watanabe et al., 1998). This kind of manipulation could be done on a large scale to look at the effects on behavior, or on a smaller scale to look at the effects on individual neurons such as Purkinje cells without affecting behavior, similarly to what we did with the multibarrel experiment in Chapter 4.

In the interim, it will be important to expand upon the multibarrel experiments we performed. Many questions still remain about the effects of locally injected gabazine on Purkinje cell responses, such as how does gabazine affect the directional tuning of Purkinje cells? and how does it affect Purkinje cell responses during other oculomotor behaviors such as pursuit and VORS? We will be collecting data to address these questions in the near future. In addition, the multibarrel technique can be employed to test the mechanisms we proposed in Chapter 4 to explain the pauses in Golgi cell firing rates and the apparent antiphasic relationship between Golgi cells and nearby mossy fibers. I have already performed some preliminary experiments to address this question and found evidence favoring the mGluR2 hypothesis. Notably, of two Golgi cells tested with gabazine injections, neither detectably changed their responses to eye movements. However, three Golgi cells were tested with LY-341495, a potent mGluR2 antagonist. Of these, one Golgi cell completely and reversibly stopped modulating during spontaneous

eye movements. Both the on and off responses of the neuron were reduced ten-fold. The other two neurons exhibited responses prior to injection that were uncharacteristic of the greater population of Golgi cells, suggesting that the drug may have been leaking from the barrels before the injection. Injection of LY-341495 did not detectably alter their firing properties. Clearly, more work needs to be done to determine the mechanism behind Golgi cell responses, perhaps using lower concentrations of LY-341495 to compensate for drug leakage during the control period.

Lastly, no discussion of the cerebellum would be complete without mentioning motor learning. The cerebellum is undoubtedly involved in some forms of motor learning, as Purkinje cell responses in the VPFL change when an animal learns a new VOR calibration (Lisberger et al., 1994; Hirata and Highstein, 2001; Blazquez et al., 2003), and ablation of the VPFL disrupts learning (Rambold et al., 2002). Do similar changes occur in the interneurons? To address this question it will be important to record interneurons such as Golgi cells before, during, and after having animals perform learning paradigms that recruit the oculomotor areas of the cerebellum, such as VOR adaptation and pursuit adaptation, to see if and how their responses change. Similarly, it will be important to see how disrupting inhibition of Purkinje cells by molecular layer interneurons affects the changes observed in Purkinje cells following motor learning.

References

Blazquez PM, Hirata Y, Heiney SA, Green AM, Highstein SM (2003). Cerebellar signatures of vestibulo-ocular reflex motor learning. J Neurosci 23: 9742-9751.

Bo J, Block HJ, Clark JE, Bastian AJ (2008). A cerebellar deficit in sensorimotor prediction explains movement timing variability. J Neurophysiol 100(5):2825-32.

Cerminara NL, Apps R, Marple-Horvat DE (2009). An internal model of a moving visual target in the lateral cerebellum. J Physiol 587(Pt 2):429-42.

Ghasia FF, Meng H, Angelaki DE (2008). Neural Correlates of Forward and Inverse Models for Eye Movements: Evidence from Three-Dimensional Kinematics. J Neurosci 28: 5082-5087.

Hirata Y, Highstein SM (2001). Acute adaptation of the vestibuloocular reflex: signal processing by floccular and ventral paraflocculars Purkinje cells. J Neurophysiol 85(5):2267-88.

Lisberger SG, Pavelko Ta, Bronte-Stewart HM, Stone LS (1994). Neural basis for motor learning in the vestibuloocular reflex of primates. II. Changes in the responses of horizontal gaze velocity Purkinje cells in the cerebellar flocculus and ventral paraflocculus. J Neurophysiol 72: 954-73.

Lisberger SG (2009). Internal models of eye movement in the floccular complex of the

monkey cerebellum. Neuroscience 162(3):763-76.

Rambold H, Churchland A, Selig Y, Jasmin L, Lisberger SG (2002). Partial ablations of the flocculus and ventral paraflocculus in monkeys cause linked deficits in smooth

pursuit eye movements and adaptive modification of the VOR. J Neurophysiol 87(2): 912-924.

Sawtell NB, Williams A (2008). Transformations of electrosensory encoding associated with an adaptive filter. J Neurosci 28(7):1598-612.

Scanziani M, Häusser M (2009). Electrophysiology in the age of light. Nature. 461(7266):930-9.

Watanabe D, Inokawa H, Hashimoto K, Suzuki N, Kano M, Shigemoto R, Hirano T, Toyama K, Kaneko S, Yokoi M, Moriyoshi K, Suzuki M, Kobayashi K, Nagatsu T, Kreitman RJ, Pastan I, Nakanishi S (1998). Ablation of cerebellar Golgi cells disrupts synaptic integration involving GABA inhibition and NMDA receptor activation in motor coordination. Cell 95:17-27.